THE MULTIFACETED ROLES OF SERINE/ARGININE REPETITIVE MATRIX 4 IN THE DEVELOPMENT OF NEUROENDOCRINE PROSTATE CANCER

by

AHN RHI LEE

B.Sc. (Hon.), McGill University, 2014

A DISSERTATION SUBMITTED IN PARTIAL FULFILLMENT OF
THE REQUIREMENTS FOR THE DEGREE OF

DOCTOR OF PHILOSOPHY

in

THE FACULTY OF GRADUATE AND POSTDOCTORAL STUDIES

(Reproductive and Developmental Sciences)

THE UNIVERSITY OF BRITISH COLUMBIA

(Vancouver)

April 2019

© Ahn Rhi Lee, 2019

The following individuals certify that they have read, and recommend to the Faculty of Graduate and Postdoctoral Studies for acceptance, the dissertation entitled:

The multifaceted roles of serine/arginine repetitive matrix 4 in the development of neuroendocrine prostate cancer

submitted by	Ahn Rhi Lee	in partial fulfillment of the requirements for
the degree of	Doctor of Philosophy	
in	Reproductive and Developmental Sciences	

Examining Committee:

Xuesen Dong, Urologic Sciences

Supervisor

Ralph Buttyan, Urologic Sciences

Supervisory Committee Member

Supervisory Committee Member

Marianne Sadar, Pathology and Laboratory Medicine

University Examiner

Geoffrey L. Hammond, Cellular and Physiological Sciences

University Examiner

Additional Supervisory Committee Members:

Colin Collins, Urologic Sciences

Supervisory Committee Member

Yuzhuo Wang, Urologic Sciences

Supervisory Committee Member

Abstract

As the clinical burdens of a lethal and therapy-resistant subtype of prostate cancer called treatment-induced neuroendocrine prostate cancer (t-NEPC) are increasing, delineating the molecular underpinnings of t-NEPC will be paramount in developing clinical strategies for this disease course. Recently, t-NEPC-unique RNA-splicing signatures, predominately facilitated by SRRM4, have been characterized. SRRM4 is an RNA-splicing factor that promotes progenitor cell differentiation via neural-specific exon networks essential for functional reprogramming of proteins required for neurogenesis. SRRM4 can transform prostate adenocarcinoma cells into t-NEPC xenografts under castration via a neuroendocrine transdifferentiation mechanism. Given the essential roles of SRRM4 during neurogenesis, we hypothesize that SRRM4 can ultimately promote neuroendocrine reprogramming in different cell types by neural-specific exon networks that contribute to t-NEPC progression.

Given the cellular heterogeneity of prostate tumours, this work investigates the functions of SRRM4 in various prostate adenocarcinoma cell lines. We show that SRRM4 ultimately promotes neural-specific transcriptome and splicing programs across all tested cell lines. We also uncover a novel mechanism whereby SRRM4 facilitates t-NEPC development via a pluripotency gene network in DU145 cells that closely recapitulates the molecular and cellular phenotypes of clinical t-NEPC. Furthermore, we characterize the downstream functional consequences of SRRM4-mediated alternative splicing of t-NEPC-unique *MEAF6* and *GIT1* transcripts. We report a novel facet of SRRM4 in promoting t-NEPC development—invasion and migration via *MEAF6* splicing

and focal adhesion-mediated signaling and stability via *GIT1* splicing. Moreover, we reveal that the t-NEPC-specific MEAF6 isoform promotes cell proliferation and tumorigenesis. These studies demonstrate an important role of SRRM4-mediated RNA alternative splicing of *MEAF6* and *GIT1* in its contributions to the multifaceted processes of t-NEPC development such as cell proliferation, clonal expansion, and invasion/metastasis.

This thesis work adds to an understudied field of alternative splicing and its importance in the t-NEPC disease progression. My findings suggest a role of SRRM4 and SRRM4-mediated splicing signatures (i.e. *MEAF6*/*GIT1*) as potential biomarkers of t-NEPC and support the notion that SRRM4 is an important facilitator of t-NEPC development. Ultimately this knowledge pertains to the clinical implications of SRRM4 and SRRM4-mediated splicing in informing future therapies that will be effective in detecting, preventing, or managing t-NEPC.

Lay Summary

Hormone therapies that treat prostate cancer can promote the development of an aggressive, deadly disease called treatment-induced neuroendocrine prostate cancer (t-NEPC). t-NEPC is becoming a serious clinical threat as it affects nearly one in five men with advanced-stage prostate cancer, with its incidences predicted to rise with the extensive use of anti-hormone therapies. Unfortunately, due to the limited understanding on how t-NEPC develops, there are no effective therapies to treat this growing clinical burden. Our lab has recently discovered a key player in this development called SRRM4 that controls genes that are unique to t-NEPC tumours. This work reports that SRRM4 and the genes SRRM4 regulates work together to promote the emergence, growth, and establishment of a subset of t-NEPC tumours. The broader impact of this work pertains to the clinical implications of SRRM4 in informing future therapies that will be effective in detecting, preventing, or managing t-NEPC.

Preface

All of the work presented henceforth was conducted in the Vancouver Coastal Health Research Institute at the Vancouver Prostate Centre, Jack Bell Research Centre and Robert NH Ho buildings. All projects and associated methods were approved by the University of British Columbia Biosafety Committee (protocol #B13-0187). All animal procedures were performed in accordance with the guidelines and regulations of the Canadian Council on Animal Care and approved by the Institutional Animal Care and Use Committee at the University of British Columbia (protocol #A18-0065).

A version of Chapter 1 and Chapter 6 has been published in Frontiers in Oncology [Lee AR*, Che N*, Lovnicki JM, Dong X. (2018) Development of neuroendocrine prostate cancers by the ser/arg repetitive matrix 4-mediated RNA splicing network. *Front. Oncol*. 8:93. doi: 10.3389/fonc.2018.00093]. I am the corresponding co-first author and contributed to the conception as well as the design of the article and performed the necessary and required literature research to the drafting of the work. NC was involved in the early stages of concept formation as well as the first draft of the article. XD was the supervisory author on this project and was involved throughout the project in concept formation. All authors revised the work critically for important intellectual content, contributed to manuscript revision, and approved the submitted version.

A version of Chapter 2 and 3 has been published in EBioMedicine [Lee AR*, Gan Y*, Tang Y, Dong X. (2018) A novel mechanism of SRRM4 in promoting neuroendocrine prostate cancer development via a pluripotency gene network.

EBioMedicine. 35: 167-177. doi.org/10.1016/j.ebiom.2018.08.011]. I was responsible for the conception of the study as well as the manuscript composition. YG and I were co-first authors responsible for all major areas of data collection and analysis. XD was the supervisory author on this project and was involved throughout the project in concept formation. All authors revised the work critically for important intellectual content, contributed to manuscript revision, and approved the submitted version.

A version of Chapter 2 and 4 has been published in Oncotarget [Lee AR, Li Y, Xie N, Gleave ME, Cox ME, Collins CC, Dong X. (2017) Alternative RNA splicing of the MEAF6 gene facilitates neuroendocrine prostate cancer progression. *Oncotarget*. **8**(17): 27966–27975. doi.org/10.18632/oncotarget.15854]. I was the lead investigator, responsible for all major areas of concept formation, data collection and analysis, as well as the majority of manuscript composition. NX and YL assisted with molecular and cellular biology techniques. CCC provided RNA-seq data and analysis assistance. XD was the supervisory author on this project and was involved throughout the project in concept formation. All authors revised the work critically for important intellectual content, contributed to manuscript revision, and approved the submitted version.

A version of Chapter 2 and 5 has been published in Cancer Science [Lee AR, Gan Y, Xie N, Ramnarine VR, Lovnicki JM, Dong X. (2019) Alternative RNA splicing of the GIT1 gene is associated with neuroendocrine prostate cancer. *Cancer Sci*. 110:245–255. doi.org/10.1111/cas.13869]. I was the corresponding lead investigator, responsible for all major areas of concept formation, data collection and analysis, as well as the manuscript composition. YG aided in the analysis and scoring of RISH and IHC as well as AmpliSeq analysis and GSEA. NX performed the cloning and

construction of overexpression plasmids as well as the RISH assays. VRR analyzed RNA-sequencing data and respective statistics for the VPC 2018 and Beltran cohorts. XD was the supervisory author on this project and was involved throughout the project in concept formation. All authors revised the work critically for important intellectual content, contributed to manuscript revision, and approved the submitted version.

Table of Contents

List of Tables

List of Figures

List of Abbreviations

AdNC	Adenocarcinoma Prostate Cancer with Neuroendocrine Cells
AdPC	Prostate Adenocarcinoma
ADT	Androgen Deprivation Therapies
AR	Androgen Receptor
ARPI	Androgen Receptor Pathway Inhibition
ASD	Autism Spectrum Disorder
ASO	Antisense Oligonucleotides
Bif-1 or SH3GLB1	Bax-Interacting Factor 1
BPH	Benign Prostatic Hyperplasia
BrdU	Bromodeoxyuridine
c-PARP	Cleaved Poly(ADP-Ribose) Polymerase
CI	Confidence Interval
CPT	Camptothecin
CRPC	Castration-Resistant Prostate Cancer
CRPC-Ad	Castration-Resistant Adenocarcinoma
CSS	Charcoal-Stripped Serum
Ctrl or CTL	Control
Cx	Castration
d	Day
DAVID	Database for Annotation, Visualization, And Integrated Discovery
DEGs	Differential Expression Genes
DHT	5α-Dihydrotestosterone
DKO	Double Knock-Out
DMEM	Dulbecco's Modified Eagle Medium
Doce	Docetaxel
DuNE	SRRM4-Transduced DU145 Cell-Derived Neuroendocrine Prostate Cancer Model
E-Cad	E-Cadherin
ECM	Extracellular Matrix
EMT	Epithelial-to-Mesenchymal Transition
EZH2	Enhancer of Zeste 2 Polycomb Repressive Complex 2
FA	Focal Adhesion
FDR	False Discovery Rate
FBS	Fetal Bovine Serum
GEMM	Genetically Engineered Mouse Model
GEO	Gene Expression Omnibus
GO	Gene Ontology
GSEA	Gene Set Enrichment Analysis
HAT	Histone Acetyltransferase

HDAC	Histone Deacetyltransferase
HGPIN	High Grade Prostatic Intraepithelial Neoplasia
HPG	Hypothalamus-Pituitary-Gonad
IF	Immunofluorescence
IHC	Immunohistochemistry
IPA	Ingenuity Pathway Analysis
LE	Luminal Epithelial
LHRH	Luteinizing Hormone Releasing Hormone
LnNE	SRRM4-Transduced LNCaP-Derived Neuroendocrine Prostate Cancer Model
LTL	Living Tumour Laboratory
MEAF6	MYST/Esa1-Associated Factor 6
NE	Neuroendocrine
NEPC	Neuroendocrine Prostate Cancer
NES	Normalized Enrichment Score
OD	Optical Density
PHF21A or BHC80	PHD Finger Protein 21A
PDX	Patient-Derived Xenograft
PSA	Prostate-Specific Antigen
PTEN	Phosphatase and Tensin Homolog
RB1	Retinoblastoma Transcriptional Corepressor 1
REST	RE-1 Silencing Transcription Factor
RISH	RNA *In Situ* Hybridization
RNA-ChIP	RNA-Chromatin Immunoprecipitation
RRM	RNA Recognition Motifs
RS	Arginine/Serine-Rich
RT-qPCR	Real-time Quantitative Polymerase Chain Reaction
SC	Stem Cell
SCLC	Small-Cell Lung Cancer
SCNC	Small-Cell Neuroendocrine Carcinoma or Small-Cell Prostatic Carcinoma
SDS	Sodium Dodecyl Sulfate
SKO	Single Knock-Out
SMI	Small Molecule Inhibitors
SOX2	Sex Determining Region Y-Box 2
SR	Serine/Arginine
SRRM4 or nSR100	Serine/Arginine Repetitive Matrix 4
SSO	Spice-Switching Oligonucleotides
SYP	Synaptophysin
t-NEPC	Treatment-Induced Neuroendocrine Prostate Cancer
TKO	Triple Knock-Out
TMA	Tissue Microarray

TP53	Tumour Protein P53
UGS	Urogenital Sinus
UTR	Untranslated Region
UV	Ultra Violet
VPC	Vancouver Prostate Centre
WB	Western Blot
wk	Week
WT	Wild-Type

Acknowledgements

I'd like to acknowledge my supervisor, Dr. Xuesen Dong, for providing one of the greatest learning opportunities and for all of your direction throughout the milestones of my academic development. And, for your amazing team of intelligent individuals, Ms. Ning Xie, Dr. Yinan Li, Dr. Yu Gan, Dr. Haolong Li, Dr. LiangLiang Liu, Dr. Richard Chen, Ms. Jessica Lovnicki, and Ms. Yue Yu. All your expertise, advice, attention, and smiles have been the driving force and foundation of my academic achievements.

I am eternally grateful to all the members of my supervisory committee, Dr. Colin Collins, Dr. Yuzhuo Wang, Dr. Ralph Buttyan, and Dr. Caigun Du. Thank you for generously offering your time, support, and guidance throughout the preparation and reviews of my graduate work throughout the years.

I wish to express my gratitude to my collaborators and team at the Vancouver Prostate Centre, Dr. Martin Gleave, Dr. Michael Cox, Ms. Mary Bowden, Dr. Ladan Fazli, Ms. Estelle Li, and Mr. Alireza Moeen, for their generous help, knowledge, and expertise.

I would like to also express my utmost gratitude for the support and interest of my funding agencies and sources, Prostate Cancer Foundation British Columbia and the Reproductive and Developmental Sciences program at the University of British Columbia. Your support has ensured not only the success of the proposed projects, but also the development of my professional and academic growth.

To all my graduate peers and colleagues that have given me the most productive (and unproductive) behind-the-scene collaborations and scientific brainstorming: Kevin Tam, Kush Dalal, Daksh Thaper, Mannan Nouri, Rohan Ramnarine, Mani Moniri, Justin

Lardizabal, and Parvin Yenki. Thank you for all the academic support, advice, and for resonating with my feelings about all the absurdity that comes with graduate studies.

To my executive editor, Sahil Kumar: bless you for always editing my manuscripts (and life). To my RDS confidante, Kayleigh Campbell: thank you for the “accountability” meetings (over breakfast). And, to my partner and love, Ron Jovillar: merci for being the artist to the original dissertation drawings and for being my driver to the lab every morning and late night. Thanks for putting up with all my academic (and non-academic) frenzies!

To the special people that I have always aspired to become: my grandfather, Habu, my parents (John and Angela), and the best siblings anyone can wish for, Tommy and Jay. Thank you for all your love and for being the core support and fuel to my very existence. Love you always.

Dedication

계절은 바야흐로 초록의 계절(Evergreen Season)을 맞지하고 있습니다.

만좌에 참석하신 총장님을 비롯하여 각 학과 학장님 신사 숙녀 귀빈 여러분 !

저, 이안이 입니다. 부리티쉬 쿨롬비아대학 비뇨기과 전립선 연구 학업을 졸업 하였습니다.

오늘의 제가 캐나다에서 초등, 중등, 고등, 그리고 대학을 맏치고 부리티쉬 쿨롬비아대학 에서 비뇨기과 전립선 연구을 완료 하였습니다. 그간 저명하신 교수님들의 명강의와 그리고 상급생 여러 학우들과 서로 서로 연구 토론이 일치될 때도 있으나 의견이 다를때 애로가 발생 했다가도 지혜롭게 해결하고 비약 할수있는 Vision 으로 바뀌워 보람된 미래를 설계해 갔습니다. 좋고 유익한 추억을 간직 했습니다. 또한 지도 교수님들에 전폭적인 분석과 과학적인 설명등에 힘입어 저는 최선을 다 하였음으로 앞으로 아름다운 캐나다 국가을 더욱 발전 시킬수 있는 의학 연구를 제 평생에 사명으로 마음속에 새겨두었읍니다. 오늘까지 변함 없이 저를 이끌어 준 그리고 모든 교육과 국민 정신을 빛나게 연마 하여서 제가 받은 훌륭한 지, 성, 미를 아름다운 캐나다 국가 건설에 이바지 하므로써 은혜에 보답하며 고통받는 비뇨기 환자들에게 아픔없는 삶을 살어가도록 최선을 다해 갈것이며 오늘에 영광된 이 날이 있기 까지 물심 양면으로 양육해 주신 부모님과 국민 여러분게 감사 드립니다.

비뇨기 의학 연구 과학과 졸업자 이안이 드림.

Chapter 1 Introduction

According to 2018 GLOBOCAN estimates, the incidence of cancer is increasing in frequency across the world. It is estimated that 18.1 million new cancer cases and 9.2 million cancer deaths will have occurred globally in 2018 (1). Within these cancer statistics, prostate cancer is the most prevalent cancer diagnosed in men not only in North America, but also on a global scale. This emphasizes the heavy economical and clinical burden of prostate cancer. Unfortunately, prostate cancer is not just a singular disease; it is many diseases that are interconnected through molecular, phenotypic, and functional heterogeneity not only between patients but also within the individual. This heterogeneity is one of the greatest challenges in developing therapeutic programs for prostate cancer. The diversity in the tumour cell population gives the ultimate survival advantage of tumour cells when challenged with therapeutics as some cells can gain the ability to escape therapeutics via dormancy, metastasis, and/or resistance. Though great headway has been made in delineating the mechanisms and facilitators of prostate tumour heterogeneity, a deeper understanding of the networks involved as well as its interconnections does not exist. Therefore, to develop more effective, suitable, and personalized treatment regimens for prostate cancer patients, a more comprehensive understanding for the mechanisms involved in facilitating this heterogeneity is fundamental.

1.1 The prostate

1.1.1 Prostate biology

1.1.1.1 The development of the prostate

The rudiments of prostate cancer biology are derived from our knowledge of normal developmental biology. Ultimately, cancer cells highjack tightly controlled and sophisticated biological processes and mechanisms driving embryonic and fetal development such as invasion, proliferation, regulation of cell death, and lineage differentiation. Thus, this subsection of the first chapter will highlight the development, cellular structures and functions, and gross anatomy of the normal prostate to better understand the basic biology of prostate cancers.

The development of secondary male structures, such as the prostate, follows embryonic sex and gonadal differentiation as its development and differentiation is dependent on the androgens produced by a functioning testis. The prostate is derived from the primitive endoderm layer. Following the differentiation of the primitive endoderm (or gut tube) into the foregut, midgut, and hindgut, the caudal end of the gut tube swells to form the cloaca or urogenital sinus (UGS), which will differentiate into the future bladder and urethra (2). By the 10^{th} gestational week, the development of the prostate is initiated by the protrusion and budding of the UGS epithelium cells (Figure 1.1) (3). The induction of this budding process is dependent on the androgen receptor (AR) signaling in the UGS mesenchyme that surrounds the UGS epithelium (2–4). Androgens produced from the fetal testis and converted to 5α-dihydrotestosterone (DHT), a more potent derivative of testosterone, activates the AR in the UGS mesenchymal cells (5–7). Activated AR signaling is believed to promote the secretion of

inductive factors called andromedins (2,5,8,9). Andromedins are then proposed to promote the secretion of growth factors, such as FGF, in a precise temporal and spatial pattern. Growth factors initiate UGS epithelial bud invasion, outgrowth, and branching to definite locations that will develop and differentiate into specific zones of the prostate in the future. During branching and canalization of the UGS epithelial structures (i.e. future prostatic ducts), mesenchymal condensation of the surrounding UGS mesenchymal cells occurs, forming the stromal components of the human prostate zones (Figure 1.1) (2). By week 18 of gestation, cytodifferentiation of the UGS epithelial cells occur where definitive luminal secretory and basal cells of the future prostatic ducts appear and express differentiation markers such as cytokeratins 8/18 and 5/14, respectively (2,10). Though the role of the AR is important in the differentiation of prostate cells, the mechanisms of cytodifferentiation of the developing prostate cells remain elusive. The prostate remains immature and small following fetal development until puberty, when the maturation, growth, and reproductive functions of the prostate is established by AR-signaling.

Figure 1.1

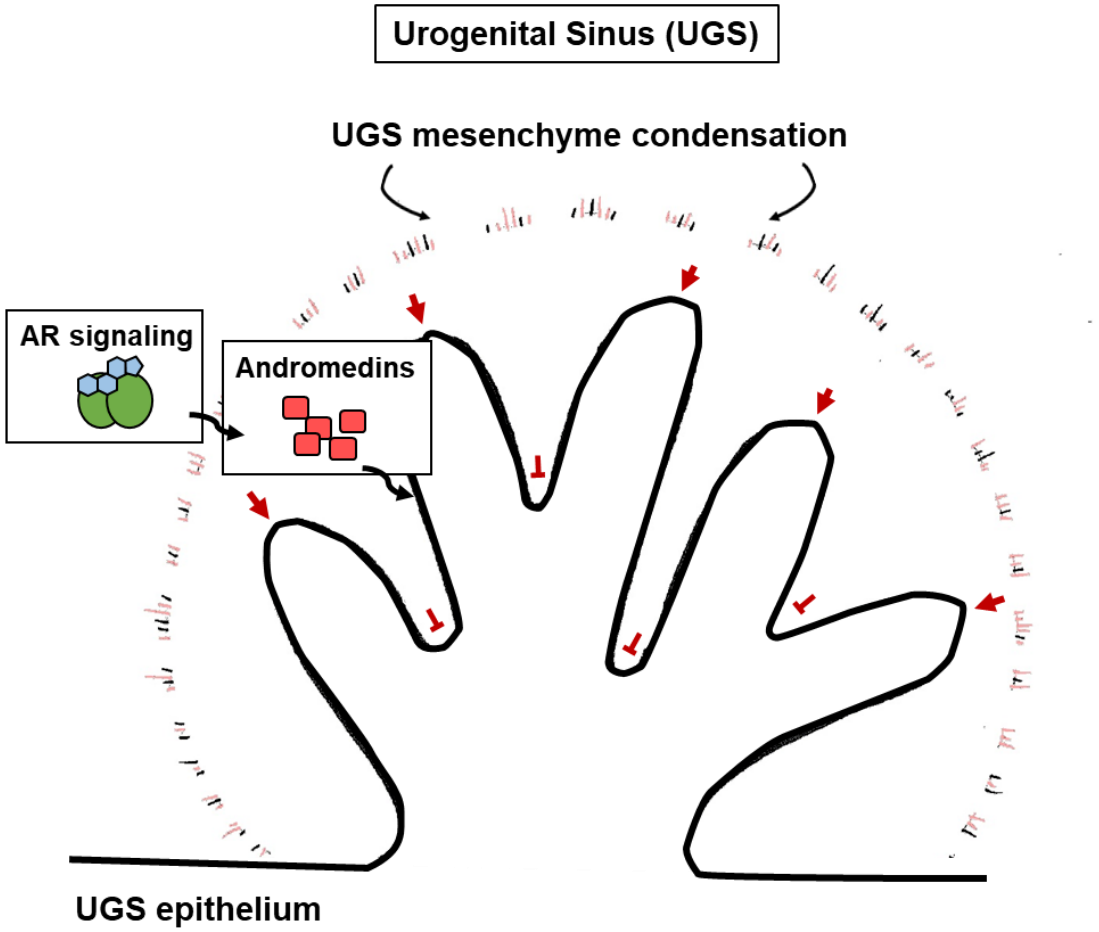

Figure 1.1 The development of the prostate: budding and branching. An outline of a developing prostate. Androgens activate the AR in the UGS mesenchymal cells and is believed to promote the secretion of inductive factors called andromedins. Andromedins are proposed to then initiate UGS epithelial bud invasion, outgrowth, branching, and canalizing via growth factors. Red arrows that are blunted and pointed represent inhibitory and stimulatory signals, respectively, at branching points. AR, androgen receptor; UGS, urogenital sinus. *Original drawing*.

1.1.1.2 The gross anatomy of the prostate

The human adult prostate is a walnut-sized secondary sex organ located underneath the bladder and ventral to the rectum. The gross anatomy of the human prostate is divided into four zones: the transition, central, peripheral, and fibromuscular zone (Figure 1.2). These zones differ in histology, ductal branching patterns, structure, and molecular features. Though the transition zone contains only <5% of the prostate

glandular elements, the central and peripheral zones contain 25% and 75% of the prostatic ducts, respectively (2,11). One of the main functions of this exocrine gland is to produce the prostatic fluid component of a male's ejaculate that protects and mobilizes the sperm (2). The majority of the male ejaculate is produced by the seminal vesicles and is secreted via the ejaculatory duct. This duct empties into the craniodorsal side of the prostate and into the prostatic urethra/duct. Additionally, the muscular features of the prostate are important for providing the necessary robust propulsion of the ejaculate through the prostatic urethra and into the vaginal tract.

Figure 1.2

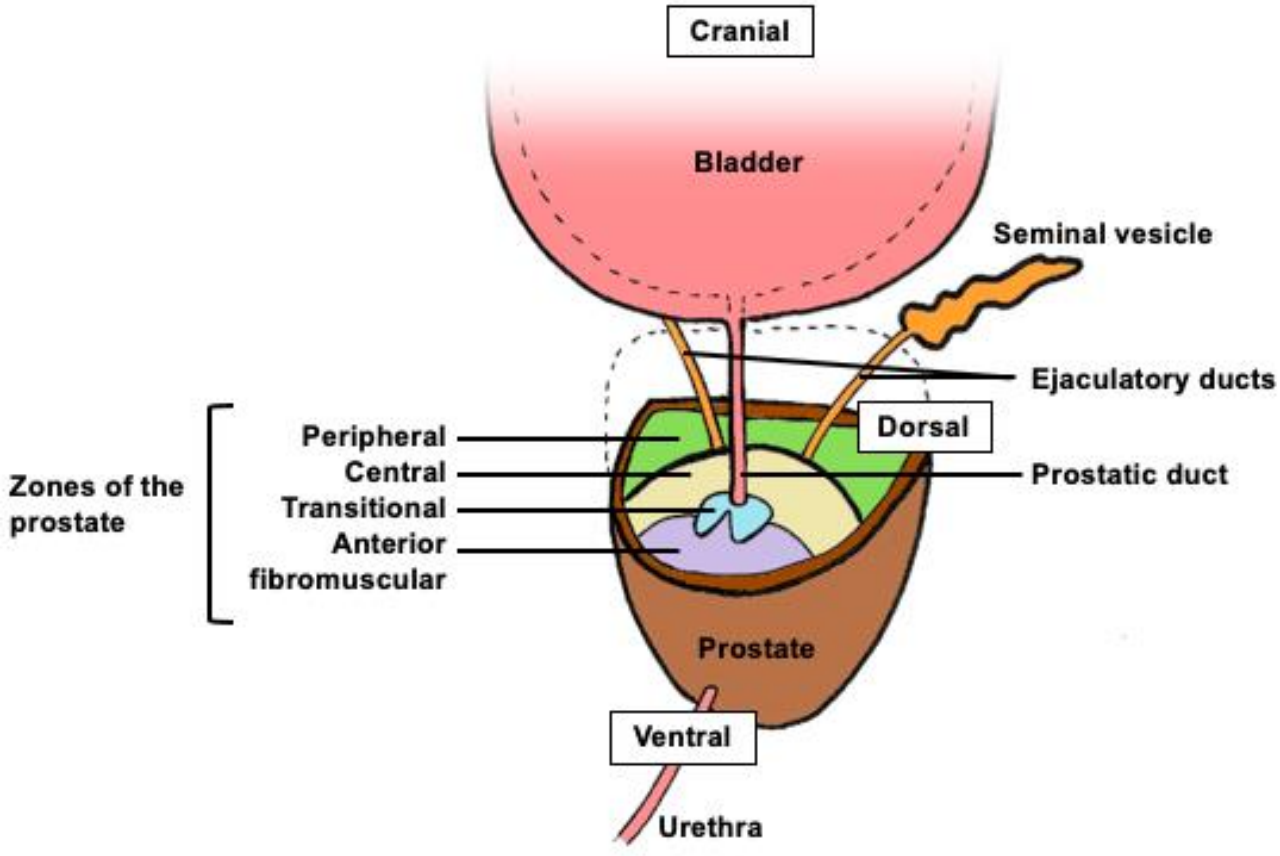

Figure 1.2 The gross anatomy of the adult prostate. Cross section of the prostate to illustrate its position and the locations of its four zones. *Original drawing adapted from Issa M and Marshall F "Contemporary diagnosis and management of disease of the prostate" (2005). 3rd ed. Newtown, Pa: handbooks in healthcare co.*

1.1.1.3 The cellular anatomy of the prostate

At the cellular level of a developed adult prostate, the epithelium compartment of the prostate is composed of luminal, intermediate, basal, neuroendocrine (NE), and stem cells (Figure 1.3). Luminal or secretory epithelial cells constitute the majority of the prostate epithelium layer and encloses the lumen of the prostatic ducts. Luminal epithelial (LE) cells perform the laborious task of producing and secreting the enzymes and proteins that make up the prostatic fluid (2). One of the many proteins secreted by the luminal secretory cells include PSA, which is an enzyme involved in liquefying the ejaculate for sperm mobility. These simple columnar cells maintain the integrity of the epithelium layer and are terminally differentiated with low proliferative activity. Basal cells are located on the basement membrane between the LE cells and make up ~10% of the cell population in the epithelium layer (2). Basal cells have a very low proliferative index of <1% (2,12). Intermediate cells, as the name would suggest, possess characteristics intermediate between the LE and basal cells of the prostate epithelium layer, such as producing both the basal- and secretory-specific cytokeratins (2). Similar to basal cells, prostate NE cells are quiescent, make up a very small population of the epithelium layer, and are wedged between columnar secretory cells on the basement membrane (2). NE cells are terminally differentiated and also reside in the urothelium of the prostatic urethra. Though the origin of NE cells is unknown, NE cells are observed in the UGS epithelium prior to the induction of prostate development and are AR-negative (13). NE cells of the prostate receive neural stimuli via heterotypic interactions with the nerve cells of the prostate stromal layer and, in turn, release hormones and bioactive peptides such as chromogranin and serotonin into the prostatic lumens, circulatory

system, or to the nearby LE or basal cells. These factors released by the NE cells are likely to promote the secretion, growth, and differentiation of the epithelial cells via paracrine signaling (2). Supporting the epithelium layer, the extracellular matrix (ECM) is comprised of collagen, elastin, keratin, laminin, and glycosaminoglycan. The stromal compartment of the prostate is composed of nerve, immune, smooth muscle, fibroblast, and endothelial (capillaries) cells (Figure 1.3). Analogous to the indispensable heterotypic regulation between the UGS epithelial and mesenchymal cells required for prostate development, heterotypic interactions between the epithelium and stromal compartments of the adult prostate are important for the maintenance, differentiation, growth, and function of prostate cells.

Figure 1.3

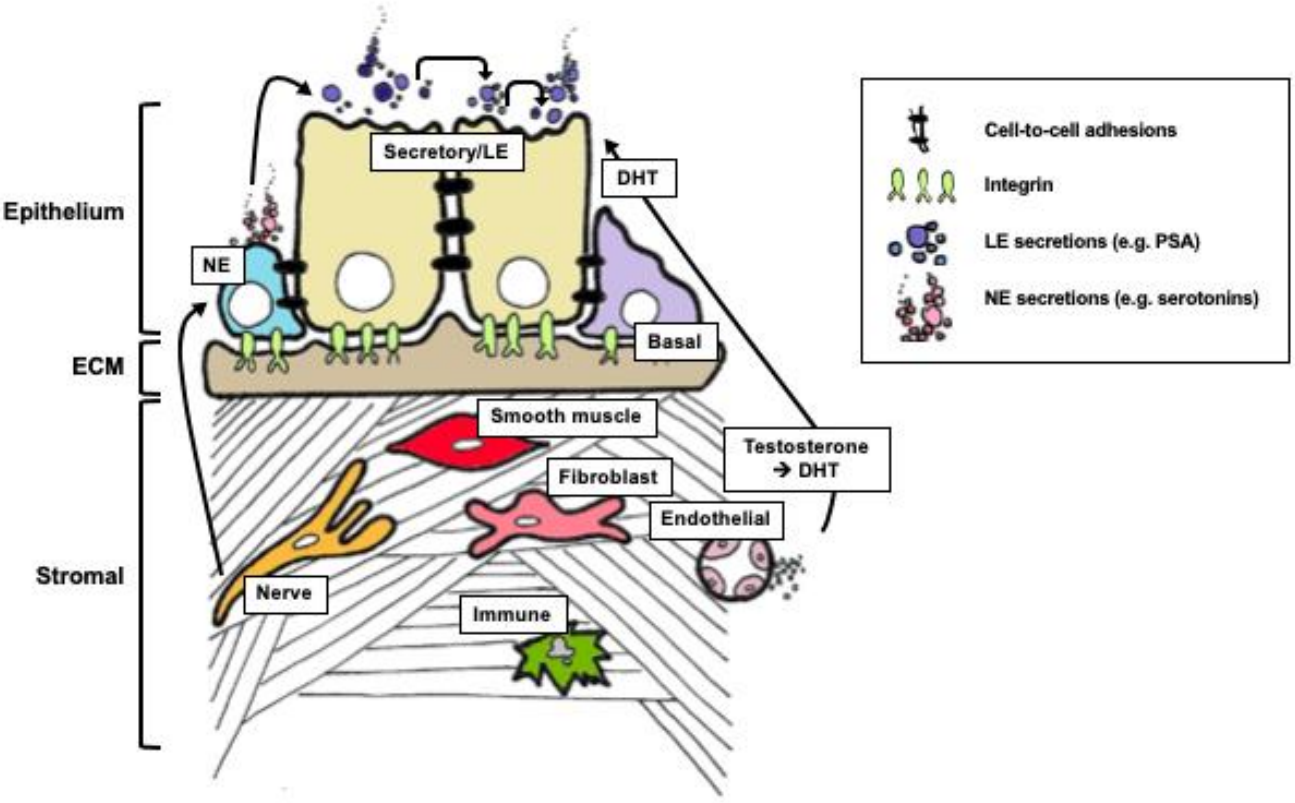

Figure 1.3 The cellular anatomy of the adult prostate. Illustration of the different cell types of the prostate. The arrows indicate some of the heterotypic or homotypic paracrine and autocrine communications that occur between or within the prostate cells. ECM, extracellular matrix ; LE, luminal epithelial; NE, neuroendocrine; DHT, 5α-dihydrotestosterone; PSA, prostate-specific antigen. *Original drawing adapted from Berman DF et al. "Development, Molecular Biology, and Physiology of the Prostate" (2012). 11th ed. Campbell-Walsh Urology (10.1016/B978-1-4160-6911-9.00090-6).*

1.1.1.4 The physiological roles of AR in the prostate

Similar to the aforementioned paracrine communication between the prostate NE and LE or basal cells, long-distance endocrine factors and steroid hormones such as testosterone also regulate prostate epithelium growth, proliferation, and secretion. Unlike the role of androgens during embryonic prostate induction, in the adult prostate, AR-signaling occurs directly in the LE cells (5). Testosterone production in the adult testis is stimulated by the luteinizing hormone releasing hormone (LHRH) via the

hypothalamus-pituitary-gonad (HPG) axis and released through the endocrine system (2). Testosterone is then taken up by prostate stromal cells and predominantly converted to DHT (Figure 1.3). Through heterotypic paracrine communications, DHT will bind to its receptor (i.e. AR) in the cytoplasm of LE cells. Dimerization of the hormone-bound AR will activate and translocate the steroid receptor to the nucleus where it will interact with chromatin remodeling complexes for preparation of transcriptional activation or repression machineries. Following the unwinding of the DNA, activated AR dimers will recruit co-factors and bind to androgen response elements within the enhancer regions of its target genes. This will then activate transcription of AR-target genes (e.g. *KLK3* and *Nkx3.1*) encoding growth factors and secretory proteins (e.g. PSA).

The AR has imperative roles in the development and maintenance of the prostate throughout a male's lifespan. Its activity in the prostate varies during the different stages of development including fetal, puberty, and adulthood. During adulthood, AR-signaling is tightly regulated in the stromal cells to indirectly maintain functional and cellular homeostasis of the prostate epithelial cells (2,5). Consequently, disruption of this homeostasis or dysfunction of the AR can result in benign or malignant diseases.

1.1.2 Prostate pathology

In fact, the prostate gland is vulnerable to pathologies or complications that arise from aging. One of the most common prostate pathologies with a global lifetime prevalence estimated at ~26% is benign prostatic hyperplasia (BPH) (14). BPH is the benign enlargement of the prostate transition zone that surrounds the urethra, resulting

in lower urinary tract complications. Another frequent prostate pathology is high grade prostatic intraepithelial neoplasia (HGPIN). HGPIN is considered to be the precursor of the most common variant of prostate cancer called prostate adenocarcinoma (AdPC) as HGPIN arises from the LE cells of the prostate peripheral zone similar to AdPC (1,2). However, HGPIN preserves normal, intact prostatic ducts and does not present with infiltrative growth into the stromal compartment unlike AdPC (15).

1.1.2.1 Prostate adenocarcinoma (AdPC): the oncogenic roles of AR in the prostate

According to 2018 GLOBOCAN estimates, AdPC is the most prevalent cancer diagnosed in men and the second leading cause of cancer-related deaths not only in North America, but also on a global scale (in incidences) (1). The most significant risks of AdPC are age, ethnicity, and hereditary genetics (16,17). As previously mentioned above, AdPC is the most common form of prostate cancer. The central driving mechanism of AdPC development is dysregulation and hyperactivity of the AR. In the context of cancer, this leads to the oncogenic role of the AR in the uncontrolled proliferation, survival, and invasion of prostatic LE cells. Overproduction of LE lineage-specific differentiation markers, such as cytokeratins 8 and 18, and secretion of excessive PSA ensues with hyperactivity of the AR-signaling pathway. These characteristics or hallmarks of AdPC are exploited for detection and guiding treatment regimens following diagnosis of the disease.

1.1.2.2 Detection, diagnosis, and treatments for AdPC

In the last three decades, PSA has been the choice of biomarker for AdPC detection and surveillance of prostate cancer progression. In addition, physical

castration, chemical androgen deprivation therapies (ADT), or androgen receptor pathway inhibitors (ARPI) have been the first line of therapy for almost a century (18). These methods minimize or block AR activity in order to limit the growth and viability of AdPC tumours (19,20). ADT, such as LHRH antagonists and agonists, ultimately target the regulation of circulating androgens via the HPG axis or androgen biosynthesis (i.e. steroidogenesis) pathway. ARPI (such as AR-antagonist abiraterone acetate, which also inhibits the biosynthesis of androgens) directly target the AR-signaling pathway. More potent next-generation ARPI enzalutamide and apalutamide binds to the ligand-binding domain of the AR. Following initial diagnosis of localized prostate cancer, treatment course can include surgical resection and radiation therapy. Treatments for locally advanced prostate cancer (i.e. the spread of the disease to local structures such as the seminal vesicles) are more aggressive with the combination of ADT and radiation therapy. AdPC with metastasis to distant sites, such as to the bones (the most common site of prostate cancer spread), are treated with a combination of ARPI and chemotherapies such as docetaxel. Docetaxel is a taxane, which is a class of chemotherapy compounds that inhibit the depolymerisation of microtubules and thus the mitosis of cells.

1.1.2.3 Castration-resistant prostate cancer (CRPC)

Though the aforementioned treatments are ultimately effective, 20-30% of cases result in recurrent prostate cancer or castration-resistant prostate cancer (CRPC) within 5 years from diagnosis (21–23). CRPC is treated with potent, next-generation ARPI therapies, such as enzalutamide and abiraterone acetate. Though these treatments have been shown to improve the median overall patient survival to 18.4 or 14.8 months,

respectively, the benefits are short-lived (24,25). Resistance to these therapies and, in turn, progression to a more lethal stage with visceral metastases inevitably occurs (24–26). At this stage, therapies are currently palliative and limited to second-line taxane chemotherapies such as cabazitaxel (20). These different degrees of aggressiveness and predisposition to recurrence demonstrate the heterogeneity of early and late stage prostate cancer. In fact, heterogeneity also extends to the CRPC tumour subtypes and to the cellular/molecular mechanisms by which prostate cancer cells utilize under the selection pressures of ARPI.

1.1.3 Mechanisms of ARPI resistance in CRPC

Overall, there are three main classifications of resistance mechanisms to ARPI and chemo- or radiation therapies that have been demonstrated to date: androgen-dependent AR signaling, receptor-dependent AR signaling, and complete bypass of AR signaling (Figure 1.4). In androgen-dependent AR signaling, tumour cells can restore the AR signaling pathway by either increasing the synthesis of circulating androgens (27–29) or acquiring AR gene overexpression, amplification, and mutations that allow AR activation under attenuated levels of androgens following castration or ARPI (30–34). In contrast, tumour cells can re-gain active AR signaling that is independent of androgen ligand-mediated activation of the AR by means of the following: **(i)** generating constitutively active splice variants of the AR (35–37), **(ii)** altering the mode of actions of the AR in a receptor-dependent manner (38), or **(iii)** relying on the downstream signaling of other hormone receptor pathways, such as the glucocorticoid receptor (39,40). CRPC tumours that restore its AR signaling retain its LE lineage and AdPC

phenotype and are referred to as castration-resistant prostate adenocarcinoma (CRPC-Ad). However, a subset of tumour cells will develop mechanisms that bypass its dependency on AR signaling altogether and progress into AR “indifferent” tumours. One subtype of AR-indifferent CRPC that was recently reported by Bluemn *et al.* is double-negative for AR and NE markers (41). These tumours have hyperactive FGF and MAPK pathways, which have been reported to promote ARPI resistance and facilitate this tumour progression. However, the phenotypes of these double-negative prostate cancer subtypes have yet to be characterized.

1.1.3.1 Treatment-induced neuroendocrine prostate cancer (t-NEPC)

Another subtype of AR-indifferent CRPC, induced by the selection pressures of ARPI, is called treatment-induced neuroendocrine prostate cancer (t-NEPC) (42–46), a subtype of neuroendocrine prostate cancer (NEPC). Generally, NEPC tumours are defined by the expression of NE markers, such as synaptophysin (SYP), chromogranin A (CHGA), and neuron-specific enolase (NSE), and the loss or low expression of LE makers, such as E-cadherin (E-Cad), PSA, and AR (45).

Figure 1.4

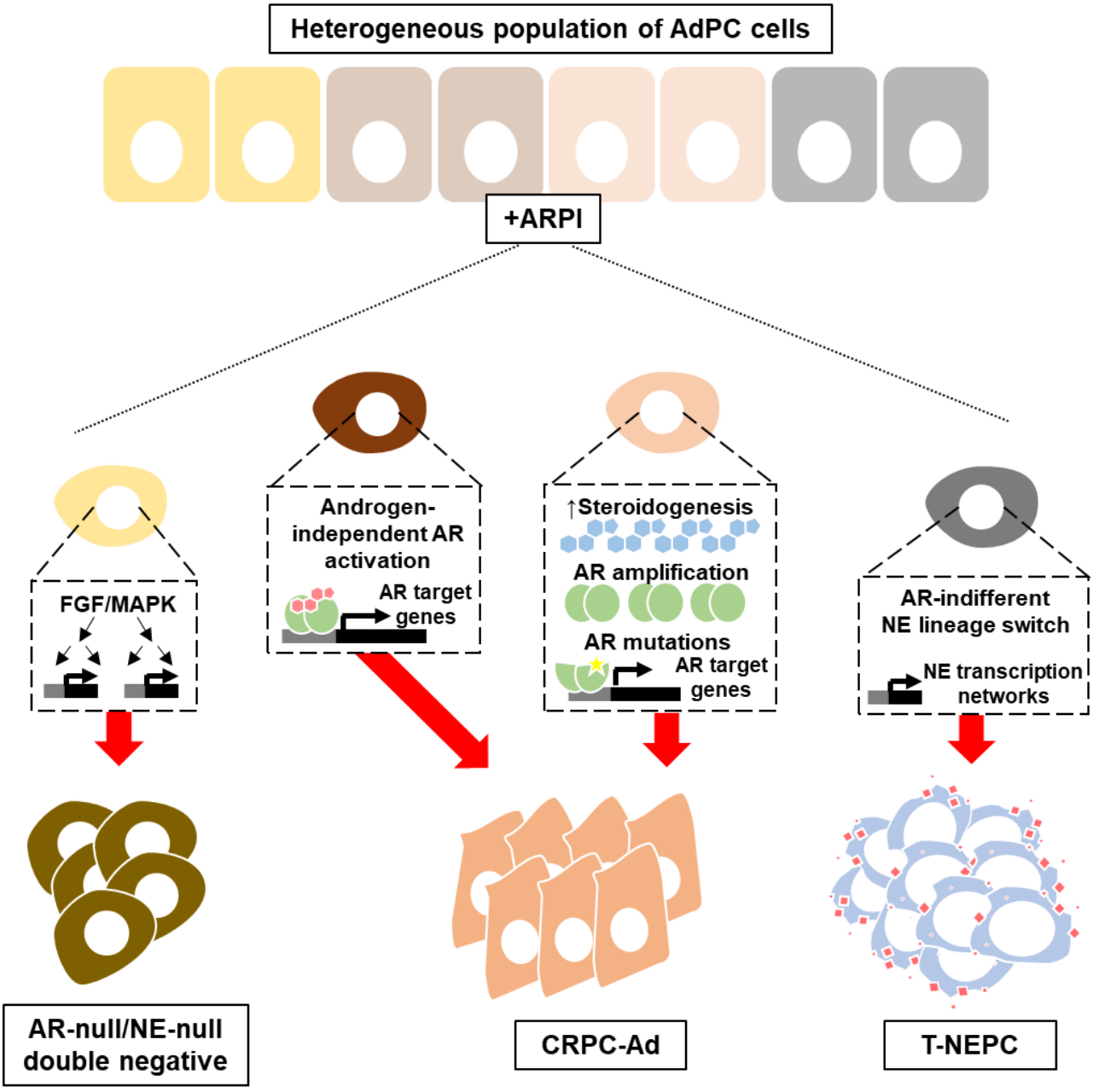

Figure 1.4 Mechanisms of ARPI resistance in CRPC. ARPI and chemo- or radiation therapies promote the emergence of various CRPC subtypes. Whether tumour cells progress to the double-negative, CRPC-Ad, or t-NEPC phenotypes depends on the molecular profiles of the cells within the heterogeneous cell population of the recurrent prostate tumour. This figure illustrates three main classifications of resistance mechanisms that have been demonstrated to date: androgen-dependent AR signaling (via increase in steroidogenesis and/or AR mutations or amplifications), receptor-dependent AR signaling (via androgen-independent AR activation), and complete bypass of AR signaling (via FGF/MAPK pathways or NE lineage switching). AR, androgen receptor; NE, neuroendocrine; T-NEPC, treatment-induced neuroendocrine prostate cancer; CRPC, castration-resistant prostate cancer; CRPC-Ad, castration-resistant prostate adenocarcinoma; AdPC, prostate adenocarcinoma; ARPI, androgen receptor pathway inhibition; NE, neuroendocrine.

1.1.3.2 Heterogeneity of NEPC

The different phenotypes and mechanisms of resistance seen within CRPC subtypes described above represent the molecular heterogeneity of prostate cancer. However, to complicate matters further, CRPC tumours do not exclusively assume one of the three different mechanisms of ARPI resistance. They can exhibit a varied range of AR or NE marker expressions, resulting in a phenotypic, functional, and molecular heterogeneity seen within the tumour (45–48). For example, it has been previously reported by several groups that NE foci are observed in anywhere from 10% to 100% of the examined CRPC-Ad patient tumours (46,49–53). However, these tumours with NE foci/differentiation have not been confirmed to progress to t-NEPC and its associated prognosis is unclear. Moreover, histopathological heterogeneity in the expression levels of AR as well as the expression of different NE and LE markers vary across different t-NEPC patient tumours (54–56).

The degree of histopathological, molecular, and phenotypic heterogeneity is seen not only between CRPC subtypes, but also within individual CRPC subtypes. In fact, heterogeneity extends to the different subtypes of NEPC, which are classified by its histopathological and clinical characteristics (57,58). These NEPC subtypes include AdPC with NE differentiation (AdNC), carcinoid tumours, and small- or large-cell NEPC. Small-cell neuroendocrine carcinoma (SCNC; also known as small-cell prostatic carcinoma) is the most common subtype detected within t-NEPC patients, suggesting its emergence induced by therapies (55,56,59). SCNC tumours grow as solid sheets and exhibit typical NE cell features such as a scant cytoplasm, salt-and-pepper nuclei,

and a high nucleus-to-cytoplasm ratio (57,60,61). As well, a high mitotic index and areas of necrosis are often detected in SCNC.

1.1.3.3 Current clinical challenges in t-NEPC

Though *de novo* NEPC is one of the least common variants of prostate cancer, making up 0.5-2% of all prostate cancer cases (62), t-NEPC now poses a major clinical issue with 16-25% of advanced-stage prostate cancer patients bearing this subtype (41,63). This rate of occurrence is predicted to rise with the widespread use of ARPI. Once diagnosed, patients rapidly succumb to the disease within 7 months to 2 years (64). Similar to CRPC-Ad patients, treatments are palliative and limited to second-line etoposide and platinum-based chemotherapies as there are no current targeted therapies in practice for t-NEPC patients (63,64). Moreover, there is no golden standard in detecting or diagnosing t-NEPC subtypes to meet this growing clinical burden. Presently, SYP, CHGA, and NSE are the three main NE biomarkers used to detect NEPC tumours (45). However, 10–40% of AdPC tumours are positive for these same markers, which demonstrates the relatively poor specificity of these diagnostic biomarkers (65). The gravity of an increasing frequency of an aggressive and fatal disease, whereby no effective detection or therapeutic regimens have been defined, emphasizes a need for the understanding of the etiology and molecular underpinnings of t-NEPC development.

1.2. Mechanisms of lineage plasticity: the emergence of t-NEPC

These mechanisms of therapeutic resistance and tumour cell heterogeneity can be facilitated by cellular processes called lineage plasticity. Lineage plasticity is

described as a reprogramming mechanism whereby AdPC cells can gain the ability to transform into other phenotypes or lineages, such as mesenchymal phenotypes or NE-like lineages. These programs promote the ultimate survival advantage. In fact, recent advances in delineating the etiology of t-NEPC suggest that t-NEPC tumours arise from AdPC cells that have exploited lineage plasticity mechanisms to bypass AR-signaling via phenotypic reprogramming into AR-indifferent NE-like cells (54,63,66). Proposed reprogramming mechanisms in the emergence of t-NEPC include, but are not limited to, dedifferentiation of AdPC to stem-like cells to NE-like cells and direct NE transdifferentiation of AdPC cells to NE-like cells (63). Though the molecular underpinnings of these NE-like cellular reprogramming mechanisms remain unclear, recent studies have demonstrated that genetic, epigenetic, and RNA splicing regulations may facilitate the lineage plasticity of AdPC cells.

1.2.1 Genetic and epigenetic modifications confer plasticity of AdPC cells

Although the overall genomic mutational landscapes (i.e. somatic copy number, point mutations, and polyploidy) of CRPC-Ad and t-NEPC tumours show significant overlap, genetic alterations may contribute to the lineage plasticity of cells in the emergence of t-NEPC (54,63,66). Whole-genome sequencing of CRPC-Ad and t-NEPC tumours has revealed that 55-75% of t-NEPC cases have concurrent functional mutations or deletions of the *RB1* and *TP53* genes, as opposed to the 15-40% of cases seen in CRPC-Ad tumours (54,67). In fact, one of the earliest genetically engineered mouse model (GEMM) of prostate cancer progression called TRAMP reveals the implications of these tumour suppressors in the emergence of t-NEPC tumours (68).

TRAMP GEMMs express the transforming region of SV40 large T antigen, which acts to sequester and inactivate both Trp53 and Rb1. TRAMP mice spontaneously develop prostate cancer that closely resembles the molecular and phenotypic characteristics as well as the progression of hormone-naïve prostate cancer to metastatic CRPC-Ad to t-NEPC under castration conditions. A recent study by Mu *et al.* has reported that knockdown of *RB1* and *TP53* in the human LNCaP AdPC cell line facilitates resistance to ARPI and promotes t-NEPC progression via a pluripotency gene network mediated by SOX2 (69). SOX2 is a putative developmental factor essential for self-renewal and pluripotency of embryonic stem cells. During the same time of that study, Ku *et al.* reports a similar resistance mechanism in their *Pten*/*Rb1*/*Trp53* triple knock-out (TKO) GEMMs (70). Both groups propose a model of lineage plasticity whereby LE cells undergo dedifferentiation reprogramming into a stem-like intermediate cell that can differentiate into NE, basal, or mesenchymal lineages. A separate study has recently reported that NPp53 GEMMs, containing co-inactivation of *Trp53* and *Pten* restricted to the adult prostate LE cells, can progress to highly aggressive and proliferative phenotypes with SCNC histopathology under ARPI (71). Lineage tracing of this progression has revealed that this t-NEPC tumour phenotype emerges from the LE cells via NE differentiation. This group proposes that SOX11, a target of *Trp53* and conserved in t-NEPC patient tumours, promotes this NE differentiation downstream of SOX2. Moreover, they suggest that the SOX family of transcription factors (i.e. SOX2 and SOX11) are temporally regulated to promote lineage plasticity of LE cells to the NE cell lineage fate in the emergence of t-NEPC. However, it is also important to note the well-established functions of p53 and Rb1 as putative tumour suppressors of

proliferation and survival. As its genomic and functional alterations are prevalent in t-NEPC tumours, loss-of-function mutations in these genes may contribute to the high mitotic index observed in clinical t-NEPC tumours (72).

Although there is a large overlap in the genomic mutational landscapes between CRPC-Ad and t-NEPC tumours, there are significant differences in its epigenetic profiles, such as DNA methylation profiles (54,63). It is suggested that this marked difference in the genome-wide DNA methylation status between CRPC-Ad and t-NEPC tumours is primarily facilitated by a histone methyltransferase called EZH2 (54,63,73,74). EZH2 protein and mRNA levels are found to be upregulated in t-NEPC tumours. Recent findings by Dardenne *et al.* have reported that N-Myc and EZH2 signaling activity is tightly coupled to induce a t-NEPC molecular program (75). *MYCN* (encoding the N-Myc protein, a neural-specific oncogenic transcription factor) is amplified in ~40% of t-NEPC tumours (73,75). Dardenne *et al.* have also demonstrated that the overexpression of N-Myc increases EZH2 activity, which, in turn, represses AR signaling to facilitate t-NEPC development (75). Although further studies are required, these results suggest a potential mechanism by which N-Myc can promote an EZH2-mediated reprogramming of the epigenome to promote t-NEPC development. In addition, Ku *et al.* suggests that the NE lineage transition and ARPI resistance seen in their TKO GEMMs is induced by EZH2, whereas EZH2 inhibitor treatments can reverse this phenomenon (70). Though the interplay of genetic alterations and epigenetic modifications have been shown to promote lineage plasticity, and, in turn, the emergence of t-NEPC, these epigenetic mechanisms and signatures remain elusive and require further investigation.

While these studies propose that functional inactivation of *TP53* and *RB1* and/or neural-specific epigenetic reprogramming confer AdPC lineage plasticity under ARPI in the emergence of t-NEPC, other factors may be required to facilitate t-NEPC development. A prime example is brain metastasis-derived DU145 AdPC cell lines which contain inactivated mutations in *TP53* and *RB1* as well as an AR-null profile but present typical AdPC phenotypes (76–78). As these cells have had the ability to reside and colonize in a neuronal niche (presumably for a long time), it would not be outrageous to assume that these cells have been exposed to some degree of neural-specific epigenetic reprogramming induced by its neural niche (78–80). Though DU145 cells exhibit some stem-like characteristics and markers (81,82), they present typical AdPC phenotypes *in vivo* (76–78). In addition, DU145 cell-derived xenografts present typical LE markers (such as cytokeratins 8/18) and little to no expression of NE markers. These characteristics of DU145 cells suggest that, although genetic and epigenetic alterations may be important in lineage plasticity mechanisms, other factors may be required in the emergence of t-NEPC.

1.2.2 Alternative RNA splicing confers plasticity of AdPC cells

Alternative RNA splicing processes are exploited by prostate cancer cells to facilitate cellular plasticity, growth, proliferation, differentiation, and treatment resistance (83). For example, in the emergence of CRPC-Ad, AR splice variants, such as ARv7 (the most frequent variant of AR observed in prostate cancers), have been shown to promote resistance to ARPI and proliferation of various cell models in a ligand-independent, constitutively active manner (84–88). In the context of t-NEPC, increased

mRNA expression of serine/arginine repetitive matrix 4 (SRRM4 or nsr100), a neural-specific RNA splicing factor, is uniquely seen in t-NEPC patient tumours (89–92). Importantly, our team at the Vancouver Prostate Centre has recently identified a t-NEPC-unique RNA splicing signature that is predominately facilitated by SRRM4 (90). Overexpression of SRRM4 in LNCaP AdPC cells facilitates the transformation of these cells into t-NEPC xenografts in castrated mice. Following this study, our lab has generated a series of five t-NEPC xenograft models called LnNE via long-term serial passaging from mouse to mouse (93). These LnNE tumour series reveal a model of AdPC-to-t-NEPC progression whereby the later generations/passages of the tumours present increasing expressions of NE markers and decreasing to no expression of PSA. Furthermore, we have recently found that increased expression of *SRRM4* is highly correlated with therapeutic interventions such as ARPI in clinical prostate cancer tumours, suggesting its role as a mechanism of therapeutic resistance (91). Altogether, these findings propose that SRRM4 transforms AdPC cells to t-NEPC tumours via direct NE transdifferentiation to escape therapeutics in the emergence of t-NEPC. Following studies on the downstream mechanisms of SRRM4 suggest that SRRM4 facilitates t-NEPC development via reprogramming of alternative RNA splicing networks that are required for NE transdifferentiation and therapy resistance (90,94). In fact, SRRM4 and SRRM4-mediated alternative RNA splicing networks plays an essential role in the development of neural systems as well as neural-related diseases. Particularly, SRRM4-mediated splicing has been shown to be critical in reprogramming the overall function of the proteins required for neurogenesis. The resulting neural-specific protein networks are essential for facilitating neural differentiation (i.e. morphological and

phenotypical), neural-specific cell processes/functions (e.g. cell migration, growth, evasion of apoptosis, and proliferation during neurite development and network formations), neuronal transcription networks, and neural-specific epigenetic networks (95–100). These functions of splicing are of particular interest as AdPC to t-NEPC development also involves multifaceted, interconnected mechanisms and cellular processes of the following (Figure 1.5):

i. Lineage plasticity of AdPC cells to ultimately differentiate into NE-like cell lineages, which may be facilitated by neural-specific epigenetic, transcriptional, and/or protein networks. Mechanisms of lineage plasticity may involve dedifferentiation of AdPC to stem-like cells to NE-like cells, NE differentiation via a pluripotency network, and direct NE transdifferentiation of AdPC cells to NE-like cells.

ii. Evasion of apoptosis mediated by ARPI or chemotherapies.

iii. Expansion of the differentiated NE cell lineages and establishment of a t-NEPC tumour.

Figure 1.5

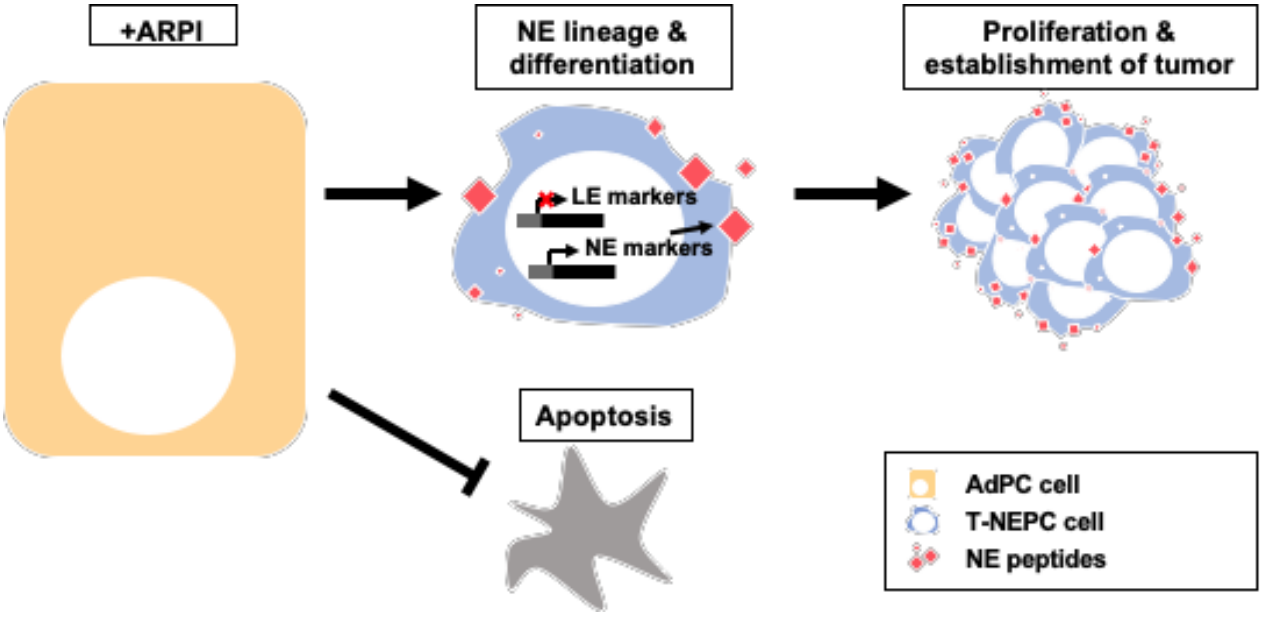

Figure 1.5 The multifaceted, interconnected mechanisms of t-NEPC development. Progression from AdPC to t-NEPC requires mechanisms of apoptosis evasion to bypass and survive ARPI or chemotherapies as well as mechanisms of lineage plasticity (e.g. neural-specific transcriptional networks) to ultimately differentiate into NE-like cell lineages. In addition, cell proliferation and clonal expansion of the NE lineage cells is also required in the emergence of t-NEPC tumours. AdPC, prostate adenocarcinoma; T-NEPC, treatment-induced neuroendocrine prostate cancer; LE, luminal epithelial; NE, neuroendocrine; ARPI, androgen receptor pathway inhibitors.

1.3 Ser/Arg Repetitive Matrix 4 (SRRM4)

1.3.1 The SR family and SR-related family of proteins

It has been predicted that 90–98% of the genes in the human genome have alternative splice variants, which highlights a critical role of alternative splicing processes and different mRNA or protein variants in normal cellular functions (101,102). One of the essential families of splicing factors are the serine/arginine (SR) family of proteins, such as ASF/SF2 (103,104). Members of this family contain one or two conserved RNA recognition motifs (RRM) at the N-terminus that are essential for RNA-binding specificity (103–106). In addition, SR family members contain an RS domain of

varying sizes at the C-terminal end, which is important for protein-protein interactions and recruitment of the spliceosome complex (103–106). The SR family of proteins has diverse functions in regulating not only constitutive and alternative pre-mRNA splicing, but also post-splicing events including exportation of mRNA, nonsense-mediated mRNA decay, and translation of mRNA. On the other hand, SR-related proteins contain an RS domain, but may or may not contain a defined RRM (107). Similar to SR family of proteins, SR-related proteins are found to play a role in not only splicing, but also other fundamental cellular processes, such as chromatin remodeling, cell cycle progression, and transcription (108). Though these proteins have a diverse range of functions, its fundamental role is in the regulation of RNA splicing (95,99,109). Splicing processes can have dramatic effects on the function, localization, stability, and/or expression of the mRNA splice variants or of its resulting translated protein isoform (95,99,109). The factors essential for orchestrating splicing programs include RNA-binding domain-containing small nuclear ribonucleoproteins (snRNP), such as U1, U2, U4, U5, and U6, and SR and SR-related family of proteins (110,111). These components make up a macromolecular complex called the spliceosome. The spliceosome interacts with *cis*- and *trans*-acting factors to regulate the repression or activation of splicing (i.e. the inclusion or exclusion of exons) and to ensure correct splice-site selections. The regulation of SR and SR-related protein splicing activity and its subcellular localizations depend, in part, on the dynamic cycle of phosphorylation and de-phosphorylation of the serine residues in the RS domain (112). Phosphorylation results in protein conformational changes, whereby altering protein-protein or protein-RNA interactions. Therefore, the phosphorylation status of RS proteins have a diverse effect in mediating

the regulation of spliceosome complex assembly, recruitment, splicing activation, and splice-site selection (113–115).

SRRM4 is particularly interesting as it has been suggested to be the source of proteomic diversity and functional complexity within the vertebrate nervous system—although its evolutionary origin is unclear (116). SRRM4 belongs to the family of SR-related proteins. It is a neural tissue- and vertebrate-restricted SR protein involved in complex alternative splicing of neural-specific exons—by binding to its conserved putative intronic 3’ UGC motif upstream of the neural-specific exon—which are essential for vertebrate nervous system development and neural cell fate differentiation of neural progenitor cells (116). In addition, SRRM4 is uncharacteristically heavy (when compared to the other members of the SR-related protein family) with a molecular weight of 100 kDa, which is likely a result of the large RS region in the protein (100,116). The presence of large RS domains makes SRRM4 more phosphorylated than its family members, which is an important characteristic of splice-site selection as mentioned above. Furthermore, the RS-rich domains of SRRM4 have also been predicted to be responsible for protein-protein and/or protein-RNA interactions required for spliceosome complex assembly to promote alternative splicing (98,100,106,117). SRRM4-mediated alternative splicing regulates the inclusion of brain-specific exons associated with neuronal development. This brain-specific exon network mediated by RNA splicing mechanisms has been proposed to be essential for neural function and development (118,119).

1.3.2 SRRM4 in normal development

Raj *et al.* has recently demonstrated that, by knocking down or overexpressing SRRM4 *in vivo*, SRRM4 mediates the inclusion of 30-50% of conserved mouse and human brain-specific exons that manifests a unique neural splicing program (98). Additionally, *in utero* SRRM4 knockdown studies (i.e. knockdown of SRRM4 in embryonic stem cells) in mice has reported diminished differentiation of neural progenitor cells and neurodevelopmental defects that resulted in postnatal mortality of the mice (96). Furthermore, knockdown of SRRM4 in neural cells and in zebrafish impairs neurite morphogenesis and branching (116). Collectively, these studies propose that SRRM4-mediated neural-specific exon networks are essential in reprogramming the functions of the resulting protein isoform (Figure 1.6). Functional reprogramming ultimately alters protein-protein interaction networks that facilitate neurogenesis, promotes neuronal transcription networks, and mediates neural-specific functions and morphological processes. For example, several transcripts regulated by SRRM4-mediated alternative RNA splicing encode neuronal GTPases that are required for cytoskeletal remodeling and dendritic growth and branching (116). Though studies on the functional significance SRRM4-targeted neural-specific exons are currently limited, findings thus far have suggested that splicing-mediated functional reprogramming of the resulting protein isoforms are required to facilitate neuronal cell differentiation and functions.

Figure 1.6

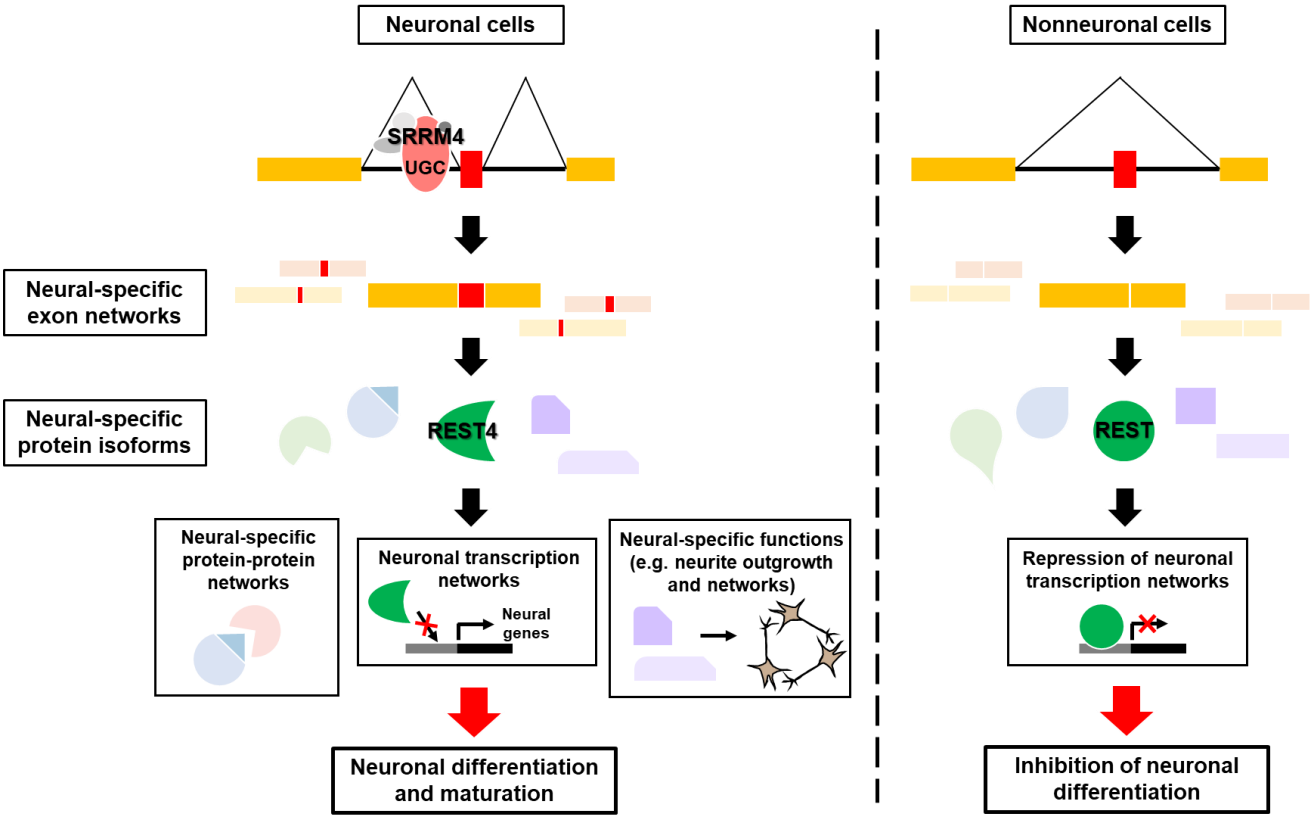

Figure 1.6 SRRM4 promotes neural-specific exon networks that are essential for neuronal cell differentiation during neurogenesis. In neuronal cells, SRRM4 mediates the inclusion of neural-specific exon networks by binding to its putative UGC motif site. Translation of these neural-specific splice isoforms results in functionally significant neural-specific protein isoforms that are required for neuronal specific protein-protein networks, neuronal transcription networks (e.g. mediated by the truncated, dominant-negative REST4 splice isoform), and neural-specific functions (such as neurite outgrowth and networks). Ultimately, this neural-specific exon reprogramming will promote neuronal cell differentiation and maturation.

1.3.2.1 SRRM4-mediated alternative splicing confers neuronal cell differentiation and function

One of the well-studied key mechanisms by which SRRM4 and SRRM4-mediated alterative splicing promotes neurogenesis and facilitates neural differentiation of neural progenitor cells is via the cross-regulation of RE-1 silencing transcription factor, REST (96,98,116,120) (Figure 1.6). REST is a transcriptional repressor of neuronal genes that binds to the RE-1 site in the regulatory region upstream of its target

gene. It inhibits the transcriptional activity of neuronal genes by facilitating repressive histone modifications via the recruitment of co-repressors and factors, such as HDAC1/2, coREST, and Sin3A, to the promoter region of the gene. REST and SRRM4 antagonistically regulate neurogenesis. Specifically, REST represses the transcription of genes that are important for promoting the neuronal phenotype as well as directly inhibits SRRM4 expression to prevent neurogenesis in nonneuronal cells (96). Conversely, SRRM4 facilitates the alternative splicing of the *REST* transcript into a splice variant called *REST4* in neuronal cells. REST4 is a truncated isoform of the REST protein with reduced DNA-binding function, resulting in the liberation of the transcriptional activity of REST-repressed target genes. Moreover, it has been shown that REST4 isoforms can directly bind to REST to inhibit its function (120). In summary, to achieve neuronal cell differentiation, SRRM4-mediated alternative splicing promotes the expression of the dominant-negative isoform REST4, which compromises its canonical function in the repression of neuronal transcription networks.

1.3.3 SRRM4 in pathogenesis

Based on the fundamental role of SRRM4 and its alternative splicing functions in fostering and facilitating normal neural development, it is clear that aberrant SRRM4 expression or function may promote pathogenesis. Aberrant RNA splicing has been demonstrated as a mechanism exploited by cells to promote the progression of many neurological diseases or disorders and neural-related cancers (83,95,97,100,101,121–123). For example, autism spectrum disorder (ASD) has been associated with aberrant SRRM4 expression and alternative splicing function (95). In this study, Irimia *et al.*

observes a reduced expression of SRRM4 in ASD and a distortion in the highly conserved SRRM4-mediated splicing program (primarily its regulation in the splicing of “microexons,” which are exons composed of 3-27 nucleotides) (95). They reveal that the positions of these SRRM4-mediated microexons are in regions of conserved domains and motifs that are important for essential protein–protein interactions required for neural development and differentiation. This suggests the importance of microexons in the reprogramming of protein interaction networks during neurogenesis. Moreover, altered increased expression and splicing function of SRRM4 have been associated with the progression of small cell lung cancer (SCLC), a NE cancer of the lung (123). These and other studied neurological-related diseases highlight the importance of SRRM4 and SRRM4 function in its regulation of splicing programs during disease progression. Therefore, studying the altered splicing profiles of diseases mediated by SRRM4 may provide a new avenue in investigating the molecular mechanisms and outcomes of splicing during disease progression.

As previously mentioned, our recent studies have demonstrated that SRRM4 facilitates a unique RNA splicing profile within two t-NEPC patient cohorts, whereby, 24 genes are commonly spliced in all the studied t-NEPC tumours. Within the 24 genes, 21 are predicted to be regulated by SRRM4 (90). In fact, 16 of the 21 genes are known targets of SRRM4 during normal neural development and suggested to be highly enriched with neuronal functions (90,98). In fact, these alternative splice transcripts encode kinases that can activate major signaling cascades/pathways, GTPases that can promote NE-specific morphogenesis, epigenetic regulators, cell survival regulators, and neural differentiation fate factors. These processes are of particular interest as the

AdPC to t-NEPC progression involves the aforementioned multifaceted, interconnected mechanisms involving NE lineage differentiation, evasion of apoptosis, and clonal expansion of the newly differentiated cell populations. Therefore, characterizing the functional significance of alternative RNA splicing of these t-NEPC-unique transcripts may provide further insight on the molecular mechanisms of SRRM4-facilitated t-NEPC development.

1.4 The multifaceted roles of SRRM4 in t-NEPC development

While there is limited knowledge on the function of SRRM4 in t-NEPC development (as the first study was reported just last year), our studies have thus far shown that SRRM4 facilitates 2D and 3D cell growth/proliferation, evasion of apoptosis, colony formation, NE cellular morphological alterations, and t-NEPC tumour development *in vitro* (90,94)—with other possible cellular or molecular functions of SRRM4 still waiting to be defined. These functions of SRRM4 have been suggested to be mediated by neural-specific transcription networks. Exploration of the downstream spliced targets of SRRM4 may uncover the molecular mechanisms by which SRRM4 orchestrates these cellular processes as well as discover novel facets of SRRM4 function in t-NEPC development and progression.

1.4.1 The multifaceted roles of SRRM4 in t-NEPC development is mediated by downstream neural-specific exon networks

Within the 16 t-NEPC-unique spliced genes facilitated by SRRM4, the functional consequences of alternative splicing of only 8 of these genes have previously been characterized (Table 1.1). Of the 8, the role of alternative RNA splicing of only the *REST*

and *Bif-1* transcripts have been studied in the context of t-NEPC development. Characterization of the alternative RNA splicing of *REST* and *Bif-1* genes has revealed that its t-NEPC-unique splice variants are important in contributing to the development of t-NEPC via promoting NE lineage differentiation and evading apoptosis, respectively (Figure 1.7) (90,94). Though further studies are essential in fully understanding the molecular mechanisms involved in t-NEPC progression via SRRM4-mediated alternative splicing events, splicing of the other SRRM4-targeted transcripts may also be important in contributing to the other facets of t-NEPC development such as NE cell proliferation, clonal expansion, and regulation of a t-NEPC-specific epigenome. Excitingly, the literature reveals that several of these t-NEPC-uniquely spliced target genes have putative roles in neural-related functions such as neuronal cell differentiation, neurite branching, and synaptic signaling. Characterizing the functional significance of alternative splicing will be crucial in elucidating how splicing mechanisms contribute to the development of t-NEPC.

Table 1.1 16 t-NEPC-unique genes spliced by SRRM4

Gene name	Proposed functions	Previous literature on splice isoforms
ABI1	Regulation of micropinocytosis and neuronal differentiation via cytoskeletal remodeling	PMID: 20479892
ATL2	GTPase involved in Golgi and endoplasmic reticulum morphogenesis and polarity in motor neurons	N/A
Bif-1 (SH3GLB1)	Regulator of apoptosis	PMID: 29759485
PHF21A (BHC80)	Component of the BRAF-HDAC complex involved in regulation/repression of transcription via deacetylation of histones	PMID: 15325272
CAMTA2	Transcription activator/regulator of genes involved in cardiac cell growth	N/A
ERGIC3	Regulator of endoplasmic reticulum-to-Golgi trafficking	N/A
GIT1	GTPase-activating protein via GPCR-mediated signal transduction important in regulating the dynamics of cytoskeleton	N/A
MEAF6	Component of HAT complexes involved in regulation of transcription via acetylation of histones	N/A
MEF2D	Transcription activator/regulator to promote myoblast cell fusion during myogenesis and neuronal cell differentiation	PMID: 25087874
MON2	Regulator of Golgi-to-endosome trafficking	N/A
NSMF (NELF)	Regulation of neuronal migration	PMID: 24316376
PTK2 (FAK1)	Tyrosine kinase involved in regulation of integrin-mediated spreading, migration, and signal transduction pathways as well as regulation of synaptic functions	PMID: 12391143
PTPRF	Tyrosine phosphatase receptor involved in regulation of neuronal cell growth and neurite outgrowth	PMID: 12716943
REST	Transcriptional regulator/repressor of NE genes	PMID: 21884984
SH3GLB2	Regulator of autophagy and endocytosis	N/A
SPTAN1	Filamentous cytoskeletal protein to provide cell strength and structural rigidity	N/A

Figure 1.7

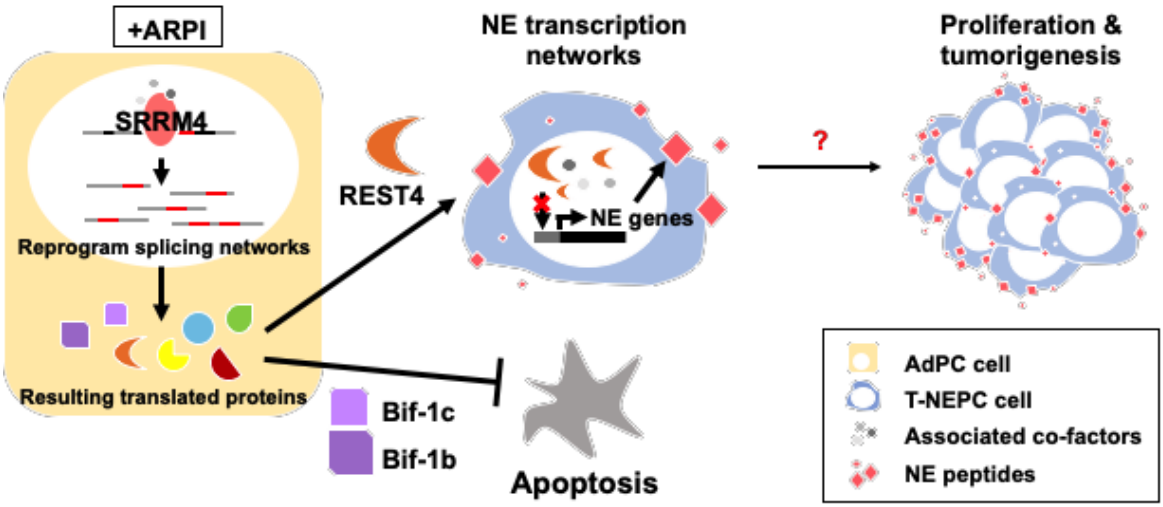

Figure 1.7 The multifaceted roles of SRRM4 in t-NEPC development is mediated by downstream neural-specific exon networks

1.4.1.1 SRRM4-mediated alternative RNA splicing of the *REST* gene facilitates NE differentiation of AdPC cells

The mechanism of neuronal cell differentiation involving SRRM4-mediated alternative RNA splicing of the *REST* gene to its truncated REST4 splice isoform during neurogenesis is exploited in AdPC cells to promote the NE lineage cell fate during NEPC development (90,92). A recent study by Zhang *et al.* has revealed a positive correlation of increased SRRM4 expression, decreased REST expression, and increased *REST* splicing with the NE phenotype in CRPC patient tumours and patient-derived xenograft (PDX) models (89). These observations were also seen in SCLC (123). In fact, our recent report demonstrates that SRRM4 directly splices the *REST* transcript to facilitate NE transdifferentiation of LNCaP AdPC cells (90). These results establish a critical role of SRRM4-mediated functional reprogramming of REST in the emergence of t-NEPC, where the loss of REST-mediated transcriptional repression of

neuronal genes is important in facilitating neural-specific transcription networks. However, one major difference between the roles of REST and SRRM4 during neurogenesis and t-NEPC development is that REST does not regulate SRRM4 expression under the context of prostate cancer cells (90).

1.4.1.2 SRRM4-mediated alternative RNA splicing of the *Bif-1* gene facilitates evasion of apoptosis

Like any other cancer, t-NEPC requires more than just differentiation to develop—resistance to cell death induced by ARPI, radiation, or chemotherapies is a prerequisite condition for t-NEPC to develop. In fact, our lab has recently reported that the role of SRRM4 in the evasion of apoptosis is through the alternative RNA splicing of the Bax-interacting factor 1 (*Bif-1* or *SH3GLB1*) gene, an endophilin protein involved in apoptosis, autophagy, and mitochondrial functions (94). Specifically, *Bif-1* is directly spliced by SRRM4 into two t-NEPC-unique splice variants Bif-1b and Bif-1c. These neural-specific variants have demonstrated resistance to apoptosis in prostate cancer cells. In contrast, the constitutive isoform, Bif-1a, which is highly represented in AdPC tumours, has pro-apoptotic functions when challenged with UV radiation and chemotherapy drugs. Interestingly, the inclusion of neural-specific exons in the *Bif-1b* and *Bif-1c* transcripts lays within the N-BAR domain of Bif-1 required for the activation of the intrinsic apoptosis pathway (124). This suggests that the inclusion of the exon may perturb protein-protein interactions or other related functions of the N-BAR domain, which may describe the altered functions of the Bif-1b and Bif-1c splice variants in apoptosis regulation. However, further characterization of the three Bif-1 splice variants and its associated protein networks and pathways is needed.

1.4.1.3 SRRM4-mediated alternative RNA splicing of putative epigenetic modifiers

Of the 16 t-NEPC-unique target transcripts, the *PHF21A* and *MEAF6* transcripts encode putative epigenetic modifiers of histone deacetylation/demethylase or acetylation, respectively. PHD finger protein 21A (PHF21A) is a component of histone deacetylase (HDAC) complexes associated with HDAC1/2 as well as histone demethylase complexes containing LSD1 and coREST that recognize and methylate unmethylated histone 3 lysine 4 (H3K4) residues to ultimately activate transcription (125). These complexes containing PHF21A mediate REST-dependent transcriptional repression of neuronal genes (125–127). It has also previously been shown that PHF21A functions as a negative modulator of REST-mediated repression of neuronal genes required for neurosecretion and neurotransmission via inhibitory binding to the REST protein (121,127). Previously, Iwase *et al.* has demonstrated that alternative RNA splicing of the *PHF21A* transcript can re-program the function of the PHF21A protein by altering its protein-protein interaction networks (such as enhanced binding to coREST and LSD1) that can facilitate a neural-specific transcription network (128). Furthermore, LSD and coREST function is important in the proliferation and population of neuronal cells during neurogenesis (129). On the other hand, the functional significance of alternatively spliced isoforms of MYST/esa1-associated factor 6 (*MEAF6*) has never been studied. However, *MEAF6* is evolutionarily conserved from yeast to humans, suggesting the functional importance of this gene (130–132). MEAF6 is a component of 4 of the 5 MYST family of histone acetyltransferase (HAT) complexes (130–134). HAT complexes have putative roles in key fundamental nuclear processes (i.e. transcription, DNA repair, and replication) via post-translational modifications of histones and

transcriptional regulators, such as p53. The MYST family of HAT complexes have also been implicated in neurogenesis, where depletion of these HATs results in reduction of neuronal cell differentiation and population number (135). Though the functional significance of alternative RNA splicing of these two putative epigenetic modifiers remains to be elucidated, these findings suggest that alternative RNA splicing of these transcripts may facilitate a neural-specific epigenetic, transcriptomic, and/or protein-protein network to promote NE differentiation and proliferation of prostate cancer cells.

1.4.1.4 SRRM4-mediated alternative RNA splicing of GTPases

As previously mentioned, GTPases are required for neuronal cell differentiation during neurogenesis. GTPases regulate cytoskeletal dynamics, whereby remodeling of the cytoskeleton promotes migration, dendritic growth, and neurite outgrowth in neuronal cells (116). In fact, within the 16 t-NEPC-unique spliced genes, 5 have putative roles in regulating these processes required for neuronal cell differentiation and function. Of the 5 genes, the G-protein-coupled receptor kinase-interacting protein 1 (*GIT1*) gene contains a GTPase-activating domain. In neural systems, GIT1 has been shown to activate signaling cascades important for regulating spine morphogenesis, neuronal cell-cell communication, and stability of synapses (136,137). Though, the functional significance of alternative splice isoforms of *GIT1* has yet to be characterized, GIT1 may be important in the NE differentiation (i.e. morphological differentiation) of prostate cancer cells.

1.5 Objectives, hypotheses, and specific aims

1.5.1 Overall thesis rationale and objective

Though we have limited knowledge on the role of SRRM4-mediated alternative splicing in t-NEPC, great progress in the investigation of this t-NEPC-unique splicing program has been made since its discovery in 2017. Excitingly, our lab has been the leading investigators in this field of unraveling the downstream functional significance of SRRM4-mediated alternative splicing in the contribution to t-NEPC development. Many ongoing investigations on the role of SRRM4-mediated alternative RNA splicing of the *PTK2* and *PHF21A* transcripts are currently happening in our lab. A deeper investigation of the role of SRRM4 and SRRM4-mediated alternative splicing will provide a more comprehensive understanding of the molecular events of t-NEPC development. Furthermore, exploration of these mechanisms may uncover novel facets of the processes involved in t-NEPC development. As the incidences and clinical burden of t-NEPC are increasing, delineating the molecular underpinnings of t-NEPC will be paramount in developing diagnostic or therapeutic strategies that may prevent or mitigate the disease course. Therefore, the overarching **objective of my thesis work is to understand the role of SRRM4 and SRRM4-mediated alternative splicing in promoting t-NEPC development and progression.**

1.5.2 Overall hypothesis and aims

SRRM4 is a key facilitator of neural-specific exon networks containing kinases, GTPases, epigenetic modifiers, cell survival regulators, and NE differentiation fate factors. This neural-specific exon network has been shown to be required for the

differentiation and function of neural progenitor and neuronal cells during neurogenesis. Therefore, **we hypothesize that SRRM4 can ultimately promote NEPC programming in different AdPC cell models, whereby SRRM4-mediated neural-specific exon networks contribute to the multifaceted processes of t-NEPC development**. To test this hypothesis, the following aims have been designed:

> **Aim 1:** To delineate the role of SRRM4 in promoting t-NEPC development in various prostate cancer cell models.
>
> **Aim 2:** To investigate the functional significance of SRRM4-mediated alternative RNA splicing of the *MEAF6* gene unique to t-NEPC tumours.
>
> **Aim 3:** To characterize the functional significance of SRRM4-mediated alternative RNA splicing of the *GIT1* gene unique to t-NEPC tumours.

The specific hypotheses and aims will be discussed in the next sections.

1.5.3 Specific hypotheses and aims

1.5.3.1 Aim 1 hypothesis and aims

Given the heterogeneous cellular nature of prostate tumours seen in the clinic, studying the role of SRRM4-mediated NE differentiation in a heterogeneous population of cell types would be of significant interest. Since SRRM4 is essential for the neuronal differentiation of neural progenitor and neuronal cells, **we hypothesize that SRRM4 can ultimately promote a NEPC program in a panel of different cell types**. To test this hypothesis, the following aims have been designed:

Specific aim 1: To determine the function of SRRM4 in promoting a NEPC-specific transcriptome and splicing program *in vitro*.

Specific aim 2: To investigate the function of SRRM4 in reprogramming various AdPC cell models into NEPC xenografts *in vivo*.

Specific aim 3: To study the cellular functions of SRRM4-transduced cell models.

Specific aim 4: To profile the transcriptome of the SRRM4-overexpressing cell models.

1.5.3.2 Aim 2 hypothesis and aims

Since t-NEPC development requires epigenetic reprogramming and SRRM4-regulated putative epigenetic modifiers have previously been shown to regulate cell proliferation and population during neurogenesis, **we hypothesize that the SRRM4-mediated alternative RNA splicing of the *MEAF6* gene will contribute to the proliferation and tumorigenesis of prostate cancer cells**. To test this hypothesis, the following aims have been designed:

Specific aim 1: To characterize the expressions of the *MEAF6* splice variants in patient tumours, xenograft models, and cell models.

Specific aim 2: To study the functional significance of alternative RNA splicing of *MEAF6* using prostate cancer cell models and its derived xenografts.

Specific aim 3: To investigate the transcriptome and signaling pathways regulated by the MEAF6 splice variants.

1.5.3.3 Aim 3 hypothesis and aims

Given that GTPases are required in the stability of morphological differentiations and migration of neuronal cells during neurogenesis, **we hypothesize that the SRRM4-mediated alternative splicing of the *GIT1* gene will contribute to the NE differentiation and migration of prostate cancer cells**. To test this hypothesis, the following aims have been designed:

Specific aim 1: To characterize the expressions of the *GIT1* splice variants in patient tumours, xenograft models, and cell models.

Specific aim 2: To define the association, specificity, and sensitivity of *GIT1* expression with the NEPC phenotype in CRPC patient tumours.

Specific aim 3: To investigate the transcriptome and signaling pathways regulated by the GIT1 splice variants.

Chapter 2 Materials and Methods

2.1 Cell lines and culture

22Rv1, C4-2, DU145, LNCaP, PC-3, VCaP, WPMY-1, and NCI-H660 cell lines were purchased from American Type Culture Collection (Manassas, VA, USA). LNCaP95 (LN95) cells were kindly provided by Dr. Alan Meeker (Johns Hopkins University, MD, USA). The BPH-1 and hTERT-Myo cell lines were provided by Dr. Simon Hayward (Vanderbilt University, TN, USA) and Dr. Jennifer Condon (Wayne State University, MI, USA), respectively. RWPE-1 and 293T cells were generously provided by Dr. Michael Cox and Dr. Ralph Buttyan, respectively, from the Vancouver Prostate Centre (VPC; Vancouver, BC, Canada). Small cell lung cancer (SCLC) cell lines NCI-H69 and NCI-H82 was kindly provided by Dr. Yuzhuo Wang from the VPC. The LnNE and DuNE cell models, along with its control cells, were established by our group (90,93,138).

VCaP, PC-3, DU145, WPMY-1, and 293T cells were cultured in Dulbecco Modified Eagle Medium/High Glucose (DMEM; Hyclone; Logan, UT, USA) with 10% fetal bovine serum (FBS; Gibco; Waltham, MA, USA), whereas LNCaP, BPH-1, and 22Rv1 cells were cultured in RPMI-1640 medium (Hyclone) with 10% FBS. LN95 cells was maintained in phenol red-free RPMI-1640 medium with 10% charcoal-stripped serum (CSS; Hyclone). Under experimental conditions in Chapter 3, LNCaP cells were cultured in 5% CSS and phenol red-free RPMI-1640 medium. WPMY-1 cells were maintained in DMEM medium containing 10% FBS and 1% penicillin-streptomycin (Hyclone). NCI-H660 was cultured in HITES medium (RPMI-1640 medium containing

0.005 mg/ml insulin, 0.01 mg/ml transferrin, 30 nM sodium selenite, 10 nM hydrocortisone, 10 nM ß-estradiol, and 2 mM L-glutamine) with 10% FBS. NCI-H69 and NCI-H82 suspension cells were maintained with RPMI-1640 medium supplemented with 10% FBS, 100 μg/ml streptomycin, and 100 units/ml penicillin. RWPE-1 cells were grown in Keratinocyte-SFM (1X) media with human recombinant epidermal growth factor 1-53 and bovine pituitary extract supplements (Gibco). Cells were all incubated in 5% CO_2 at 37°C. All cell lines used were tested negative for mycoplasma contamination and authenticated by short tandem repeat assays.

2.2 DNA and siRNA transfections

Cloning and construction of the MEAF6 and GIT1-specific DNA plasmids were performed by Ms. Ning Xie (VPC). To construct Flag-MEAF6-1 (pCMV1 promoter), *MEAF6-1* gBlock was purchased from Integrated DNA Technologies (Coralville, IA, USA) and was used as a template for PCR amplification using the Platinum® Taq DNA Polymerase High Fidelity kit (Invitrogen; Waltham, MA, USA). PCR amplification conditions were as followed: 2 min at 94°C, followed by 35 cycles of 15 sec at 94°C, 30 sec at 45°C-60°C, and 2 min at 65°C, then by 5 min at 68°C, and lastly at 10°C. pCMV1 vector and amplified cDNA was digested with BamHI and EcoRI, followed by a T4 DNA ligation reaction. The Flag-MEAF6-2 construct was generated with the Q5® Site-Directed Mutagenesis kit (New England Biolabs; Ipswich, MA, USA) using Flag-MEAF6-1 as a template and following manufacturer's protocol. The Flag-GIT1-A plasmid (#15225) was purchased from Addgene (Cambridge, MA, USA) and was used as a template to generate the Flag-GIT1-C plasmid using the Q5® Site-Directed

Mutagenesis kit (New England Biolabs) following manufacturer's protocol. Primers used for cloning and site-directed mutagenesis are listed in Table 2.1. The fidelity of all PCR-generated fragments and expression plasmids were confirmed by Sanger sequencing.

All transfections were carried out using Lipofectamine® 3000 (Invitrogen) according to the manufacturer's protocols. Detailed information on expression plasmids and siRNA targets is listed in Table 2.2

Table 2.1 Primers for cloning and site-directed mutagenesis

Primer Name	Forward Primer Sequence	Reverse Primer Sequence
*MEAF6-1*_EcoRI	AAC GAA TTC ATG GCG ATG CAC AAC AAG GCG	
*MEAF6-1*_BamHI	CGC GGA TCC CTA ATA GTC AGC TCG TGG TTT	
*MEAF6-2*_Cloning	GAT TGA TCT GAA GTT AAA CAA AAA ACC ACG	CTGTGCCGGTTTTTATTCTTTCGCTTTTTA TGGC
*GIT1-C*_Cloning	CCTTGACTTATCCGAATTGGCCAAAG	CTGTCAGCCATCTGTGGGATGATG

Table 2.2 siRNA and plasmid information

Reagent	Provider	Catalogue #
Negative control siRNA	Dharmacon, Lafayette, CO, USA	D-001210-01-20
ON-TARGETplus SMARTpool™ siRNA targeting *SRRM4*	Dharmacon	J-058651-10
ON-TARGETplus SMARTpool™ siRNA targeting *SOX2*	Dharmacon	L-011778-00-0005
Silencer® Select Negative Control No. 1 siRNA	ThermoFisher Scientific	4390843
Silencer® Select siRNA targeting *MEAF6*	ThermoFisher Scientific	4392420
Silencer® Select siRNA targeting *ID1*	ThermoFisher Scientific	s7106
Silencer® Select siRNA targeting *ID3*	ThermoFisher Scientific	s7110
Flag-SRRM4 plasmid	Dr. Xuesen Dong (VPC)	
Flag-U2AF65 plasmid	Dr. James Manley (Columbia University)	
Flag-ASF/SF2 plasmid	Dr. Gourisankar Ghosh (UC San Diego)	
Flag-hnRNP I plasmid	Dr. Allain Frédéric (Institute for Molecular Biology and Biophysics Eidgenössiche Technische Hochshule, Switzerland)	
Flag-U1A plasmid	Dr. Xuesen Dong	
Flag-PSF plasmid	Dr. Xuesen Dong	
Flag-p54nrb plasmid	Dr. Benjamin Blencowe (University of Toronto)	

2.3 Construction of cell models by lentiviral approaches

Lentiviral expression vectors (pFUGWBW backbone) encoding Flag-SRRM4 and empty vector (Ctrl or CTL) were provided by Dr. Xuesen Dong from the VPC (90). Flag-MEAF6-1, Flag-MEAF6-2, Flag-GIT1-A, and Flag-GIT1-C plasmids were used as a template to amplify and clone the genes-of-interest into Gateway® pDONR™201 and pFUGWBW vectors using the Platinum® Taq DNA Polymerase High Fidelity kit

(Invitrogen) and Gateway® Technology (Invitrogen), respectively, according to manufacturer's protocol. Primers used for lentiviral vector cloning is listed in Table 2.3. The fidelity of all PCR-generated fragments and lentiviral expression plasmids (pDONR^{TM}201 and pFUGWBW) were confirmed by Sanger sequencing and expressed proteins were validated using anti-flag antibody before and after application.

Table 2.3 Primers used for lentiviral vector cloning

Primer Name	Forward Primer Sequence	Reverse Primer Sequence
*MEAF6*_Lenti	GGG GAC AAG TTT GTA CAA AAA AGC AGG CTT CAC CAT GGA TTA TAA AGA TGA TGA TGA TAA AGC GAT GCA CAA CAA GGC GGC GCC G	GGG GAC CAC TTT GTA CAA GAA AGC TGG GTC CTA ATA GTC AGC TCG TGG TTT
*GIT1*_Lenti	GGGGACAAGTTTGTACAAAAAAGCAG GCTTCACCATGGATTATAAAGATGATG ATGATAAAATGTCCCGAAAGGGGCCG CGAGCG	GGGGACCACTTTGTACAAGAAAGCTG GGTTCACTGCTTCTTCTCTCGGGTGGT GAT

To package lentivirus, lentiviral expression vectors, together with the 2nd Generation Packaging Mix (Applied Biological Materials; Richmond, BC, Canada) were transfected into 293T cells. Media was changed 24 hrs post-transfection. Lentiviral particles were harvested and filtered 30 hrs later and used to transduce target cells. Transduced cells were selected by and cultured under blasticidin (Gibco) with the respective concentrations for the following cells: RWPE-1, 2 µg/ml; BPH-1, 2.5 µg/ml; LNCaP, 22Rv1, and DU 145, 5 µg/ml; PC-3, WPMY-1, and hTERT-Myo, 10 µg/ml.

Exogeneous expressions of SRRM4, MEAF6-1 or MEAF6-2, and GIT1-A or GIT1-C were confirmed by RT-qPCR and immunoblotting assays as shown in Appendix Di, Appendix K, and Figure 5.4A, respectively. Nomenclature of the cell models used is shown in Table 2.4.

Table 2.4 Nomenclature of cell models used

Used in Chapter	Name	Description
3	LNCaP(SRRM4)	Stable overexpression of SRRM4 in LNCaP cells
	LNCaP(Ctrl)	Stable overexpression of empty vector in LNCaP cells
	22Rv1(SRRM4)	Stable overexpression of SRRM4 in 22Rv1 cells
	22Rv1(Ctrl)	Stable overexpression of empty vector in 22Rv1 cells
	DU145(SRRM4)	Stable overexpression of SRRM4 in DU145 cells
	DU145(Ctrl)	Stable overexpression of empty vector in DU145 cells
	PC-3(SRRM4)	Stable overexpression of SRRM4 in PC-3 cells
	PC-3(Ctrl)	Stable overexpression of empty vector in PC-3 cells
4	PC-3(MEAF6-1)	Stable overexpression of MEAF6-1 in PC-3 cells
	PC-3(MEAF6-2)	Stable overexpression of MEAF6-2 in PC-3 cells
	PC-3(CTL)	Stable overexpression of empty vector in PC-3 cells
	LNCaP(MEAF6-1)	Stable overexpression of MEAF6-1 in LNCaP cells
	LNCaP(MEAF6-2)	Stable overexpression of MEAF6-2 in LNCaP cells
	LNCaP(CTL)	Stable overexpression of empty vector in LNCaP cells
5	DU145(GIT1-A)	Stable overexpression of GIT1-A in DU145 cells
	DU145(GIT1-C)	Stable overexpression of GIT1-C in DU145 cells
	DU145(Ctrl)	Stable overexpression of empty vector in DU145 cells

2.4 RT-qPCR and immunoblotting (western blot) assays

Expression of mRNA was assessed by real-time quantitative polymerase chain reactions (RT-qPCR). Total RNA was extracted using TRIzol® (Ambion; Waltham, MA, USA) according to manufacturer's protocol. 2 μg of RNA was reverse-transcribed using random hexamers and Superscript II™ Reverse Transcriptase (Invitrogen) according to manufacturer's instructions. Reactions were prepared using SYBR® Green reaction mix (Roche; Basel, Switzerland) and run on the ABI ViiA7 machine (Applied Biosystems; Burlington, ON, Canada) using their default cycle settings: 2 min at 50°C and 10 min at 95°C, followed by 45 cycles of 15 sec at 95°C and 1 min at 60°C. Relative quantification of mRNA expression was measured by calculating and comparing the ΔΔCt values of

housekeeping genes *GAPDH* or *18S* to our gene-of-interest. RT-qPCR assays were carried out using three technical replicates and three independent biological replicates. Heatmaps in Chapters 3 and 5 were constructed based on the results of the qPCR. Primer information is listed in Appendix A.

For immunoblotting assays, cell lysates were prepared in 50 mM Tris-HCl (pH 8.0), 150 mM NaCl, 1% NP40, 0.5% sodium deoxycholate, and 0.1% sodium dodecyl sulfate (SDS) with cOmplete™ *EASYpack* proteinase and PhosSTOP™ phosphatase inhibitors (Roche) followed by brief sonication to extract protein lysates. Protein concentrations were measured with the Pierce BCA Protein Assay Kit (ThermoFisher Scientific; Waltham, MA, USA) according to the manufacturer's protocol. Equal weight of total protein (40-60 µg) were then mixed with and denatured by SDS and boiled for 5 min at 95°C. Prepared protein samples were separated by electrophoresis on an 8%-15% SDS polyacrylamide gel and transferred onto polyvinylidene difluoride membrane (Millipore; Bedford, MA, USA). Transfers were performed using the semi-dry transfer method: 40-60 min at 25 V at room temperature with the Trans-Blot® SD Semi-Dry Transfer Cell (Bio-Rad; Hercules, CA, USA). Immunoblots were probed by Pierce ECL Western Blotting Substrate (ThermoFisher Scientific) and visualized using autoradiography films via a film processor (EL-RAD; Vancouver, BC, Canada). Densitometry was performed to quantify protein expression. All immunoblotting assays were repeated in three independent experiments with one representative blot shown. β-actin or vinculin served as loading controls. Antibody information is listed in Appendix B.

For RNA and protein extraction of xenograft tumours (performed in Chapter 4), tissues lysates were prepared in TRIzol® or lysis buffer, respectively, with beads and homogenized using the Precellys Homogenizer (Bertin Instruments, France). The supernatant was then collected and further processed for protein or RNA extraction following the standard protocols mentioned above.

2.5 RNA-ChIP assays

RNA-chromatin immunoprecipitation (RNA-ChIP) assays were performed by Ms. Ning Xie and Dr. Yinan Li from the VPC as previously described (91,94). Briefly, cells were transfected with empty vector or Flag-SRRM4 plasmid. 48 hrs post-transfection, RNA-protein complexes were cross-linked with 1% formaldehyde for 10 min at 37°C and sonicated in lysis buffer containing 1% SDS, 10 mM ethylenediaminetetraacetic acid (EDTA), 50 mM Tris (pH 8.0), and protease inhibitor. 2% of the supernatant was used as input, and the remaining lysate was immunoprecipitated with the anti-Flag antibody listed in Appendix B. Eluted RNA fragments were used as templates for RT-qPCR. Primer sequences complimentary to the intron region up to 150 bp upstream of the alternatively spliced exon were designed and listed in Appendix A. Data was calculated as a percentage of input and plotted as fold changes relative to its respective control IgG.

2.6 Cell morphology, cell proliferation, cell invasion and migration, colony formation, and apoptosis assays

The morphology of the cells was imaged by Zeiss AxioObserver Z1 light microscopy (Carl Zeiss AG; Oberkochen, Germany) at 32X magnification, or the cells were fixed with 4% paraformaldehyde, treated in 0.25% Triton X-100 for 15 min, incubated with anti-F-actin conjugated to Phalloidin-iFluor™ 488 (Abcam; Cambridge, UK), and mounted with DAPI staining mount (Vector Labs; Burlingame, CA, USA). Cells were then imaged by Zeiss LSM780 confocal microscopy (Carl Zeiss AG) at 63X magnification. To calculate the length of the cell bodies, 50 cells were randomly selected, and the length was quantified by the Image J program (139). Three independent biological replicates were performed.

For 2D and 3D bromodeoxyuridine (BrdU) cell proliferation, cells were measured with the BrdU cell proliferation assay kit (Millipore) according to manufacturer's protocol. Cells were seeded in Matrigel® (Corning; New York, NY, USA) for 3D BrdU proliferation assays. 2D-proliferation rates were measured every other day for 5 days post-seeding and 3D-proliferation rates measured 24 hrs post BrdU treatment. Optical density (OD) was measured at 450 nm. 2D-proliferation rates were also measured with the CellTitre® 96 AqueousOne kit (Promega; Madison, WI, USA) according to manufacturer's protocol. 2D-proliferation rates were measured at OD of 490 nm every other day for 5 days post-seeding. Each experiment contained six technical replicates, and three independent experiments were performed.

For wound-healing (migration) assays, a monolayer wound was created when cells reached 100% confluency. Cell migration was subsequently captured at time point 0- and 20-hrs after wound scratch. Migration ability of cells was calculated as the migration distance from the two time points by the Image J Program. Three technical replicates and three independent biological replicates were performed.

Cell invasion assays were carried out by using BD BioCoat™ Matrigel® Invasion chambers (BD Biosciences; Franklin Lakes, NJ, USA) according to manufacturer's protocol. Briefly, $1x10^5$ cells were seeded in the chambers containing serum-free media and incubated in serum containing wells. The membrane insert was then mounted 24 hrs later with DAPI staining mount onto microscope slides and imaged with Zeiss AxioObserver Z1 microscope (Carl Zeiss AG). Cells were quantified by the Image J program (139), and invasion rates were calculated as the percentage of cell invasion. Two technical replicates and three independent biological replicates were performed.

For colony formation assays, cells were seeded in 0.7% soft agar with a 1% soft agar bottom base coating. The wells containing cell colonies were stained with crystal violet after 10-14 days. The entire well was imaged by stitching 5X field images together, a feature on the Zeiss AxioObserver Z1 microscope. Colony numbers were counted according to its diameter (>100 µm or 100–300 µm and >300 µm). Three technical replicates and three independent biological replicates were performed.

Apoptosis assay methods were as followed: cells were treated with either docetaxel (Doce), camptothecin (CPT), UV irradiation, or vehicle (100% ethanol). 48 hrs following treatment, protein lysates were extracted for immunoblotting following the

aforementioned standard protocol. Two technical replicates and three independent biological replicates were performed.

2.7 FA assays

For focal adhesion (FA) assays, cells were seeded on coverslips and serum-starved the next day. Following serum-starvation, cells were treated with 10 µM of nocodazole (Sigma-Aldrich; St. Louis, MO, USA) for 4 hrs, subsequently washed away, and replenished with serum-containing medium. Cells were fixed at 0- or 120-min after the washout for IF, co-stained against GIT1 (Alexa Fluor-594; Invitrogen) and vinculin (Alexa Fluor-488; Invitrogen), and then mounted with DAPI (Vector Labs). Antibody information is listed in Appendix B. Five quadrants of the coverslip were imaged using the Zeiss AxioObserver Z1 (Carl Zeiss AG) microscope, and the ZEN program profiled the overlapping GIT1 and vinculin signals in the FA complexes. Three biological repeats were performed for each experiment and the most representative images were shown.

2.8 CRPC TMA

The CRPC tissue microarray (TMA) containing 64 tissue cores from 32 patients that had undergone hormonal therapy, chemotherapy, or radiotherapy was obtained from the tissue bank at VPC. This TMA was used for Chapters 3 and 5. The histopathology of the tumour cores has previously been described by Li *et al.* (91). In summary, the histology is classified as typical AdPC (n=52), AdNC (atypical AdPC with ≥10% NE cells; n=6), or SCNC (small-cell NEPC with only NE cells; n=6). Typical AdPC is classified by the presence of compact and homogenous glandular structures, large

cells with prominent nucleoli, and no NE cells. Next, SCNC tumours contain only NE cell populations, grow as solid sheets, and exhibit typical NE cell features, such as scant cytoplasm, salt-and-pepper nuclei, and a high nucleus-to-cytoplasm ratio. Areas of necrosis are often present in SCNC. Finally, AdNC subtypes are histologically similar to AdPC, however, they are atypical tumours comprised of a mixed-cell population containing ≥10% NE cells and are positive for at least two NE markers.

2.9 Human prostate cancer xenografts

All animal procedures were performed in accordance with the guidelines and regulations of the Canadian Council on Animal Care and approved by the Institutional Animal Care and Use Committee at the University of British Columbia. To construct xenografts in Chapter 3, 1×10^6 cells of the established DU145, PC-3, LNCaP, or 22Rv1 cell models overexpressing SRRM4 or empty vector were implanted subcutaneously 1:1 with Matrigel® Matrix (Corning) in bilateral flanks of 6-8-wk old male nude (Nu/Nu) mice. All mice were surgically castrated prior to tumour implantation. NCI-H660 xenografts were previously established (91). To construct PC-3 xenografts in Chapter 4, 1×10^6 PC-3(MEAF6-1) or PC-3(CTL) cells were implanted subcutaneously with Matrigel® (1:1) in bilateral flanks of 6-8-wk old male Nu/Nu mice. Tumour volume (V = length × width × height × 0.5236) was measured three times a week and were harvested for RNA extraction, protein extraction, or paraffin embedding when tumours reached experimental endpoints (V = 1500 mm^3).

2.10 RISH and IHC assays

Xenograft tumours were fixed in 10% paraformaldehyde, paraffin embedded, and processed for RNA *in situ* hybridization (RISH) or immunohistochemistry (IHC). RISH probes targeting *SRRM4* (NM_194286.3; targeting 496-835 bp), *GIT1-A* (NM_001085454.1; targeting 944-985 bp), *GIT1-C* (NM_014030.3; targeting 941-983 bp), and negative control probe (targeting the *dapB* gene from bacteria) were designed by Advanced Cell Diagnostic (Hayward, CA, USA). RISH assays were performed by technician Ms. Ning Xie and Dr. Yinan Li from the VPC using the BaseScope™ assay kit (Advanced Cell Diagnostic) following manufacturer's instructions. IHC staining was conducted with the Discovery XT autostainer (Ventana Medical Systems; Oro Valley, AZ, USA) and examined with their UltraMap™ DAB kit (Ventana Medical Systems). Antibodies used for IHC are listed in Appendix B.

RISH and IHC scoring methods have previously been characterized by Li *et al.* (91). Briefly, positive RISH signals were presented as red dots under 10X and 40X magnifications. RISH scores of 0, 1, and 2 indicate no positive signal, <20% of all cells with positive signal, and ≥20% of all cells with positive signal within a tissue core, respectively. IHC scores were calculated by the signal intensity (no, low, medium, and high as 0-3, respectively) multiplied by the percentage of positive cells. IHC scores of ≥0.3 were considered to be strongly positive.

2.11 Digital image analysis and Ki-67 scoring

All stained slides were digitalized with the SL801 autoloader and Leica SCN400 scanning system (Leica Microsystems; Wetzlar, Germany) at a magnification equivalent to 40X (scale bar, 100 µm). The images were subsequently stored in the SlidePath digital imaging hub (Leica Microsystems) of the VPC. For the Ki-67 scoring performed in Chapter 3, the Aperio Image Analysis IHC menu (Leica Biosystems; Wetzlar, Germany) was used. We selected five areas of interest within the same core, defined the parameter, optimized the level of intensity, and selected positive pixel Count Algorithm for Ki-67.

2.12 Ion AmpliSeq transcriptome sequencing and GSEA

For Chapters 3 and 5, DU145(Ctrl) and DU145(SRRM4) cell models or DU145(Ctrl), DU145(GIT1-A), and DU145(GIT1-C) were extracted using the mirVana™ RNA Isolation Kit (Ambion) according to the manufacturer's protocol. The quality of the RNA samples was assessed by Nanodrop™ 2000 and 2100 Bioanalyzer (Caliper Life Sciences; Hopkinton, MA, USA). Samples were then sent for Ion AmpliSeq Transcriptome Sequencing. Ion AmpliSeq transcriptome library preparation, sequencing, and primary analyses were completed by the UBC-DMCBH Next Generation Sequencing Centre (Vancouver, BC, Canada) following the protocol detailed by Li *et al.* (140). In summary, cDNA was synthesized from 100 ng of total RNA using the SuperScript® VILOTM cDNA Synthesis kit (Invitrogen) and amplified with Ion AmpliSeq™ technology (ThermoFisher Scientific). cDNA libraries were diluted to 100 pM and amplified on Ion Torren OneTouch™ 2 instrument (ThermoFisher Scientific)

using emulsion PCR. Template libraries were then subjected for sequencing of >20,000 RefSeq transcripts using the Ion Torrent Proton™ sequencing system (ThermoFisher Scientific). Transcriptome data from Chapter 3 is accessible under the accession number GSE118104 in the Gene Expression Omnibus (GEO) database. Transcriptome data from Chapter 5 is available at https://onlinelibrary.wiley.com/action/downloadSupplement?doi=10.1111%2Fcas.13869&file=cas13869-sup-0006-TableS4.xlsx.

Gene Set Enrichment Analysis (GSEA; http://www.broadinstitute.org/gsea/index.jsp) for Chapter 3 was carried out to determine whether a defined set of genes showed concordant enrichment between two samples groups (e.g. SRRM4 vs Ctrl) or two clinical phenotypes (e.g. t-NEPC with high vs low *SOX2* expression). The analyses in Chapters 3 and 5 were performed using the latest MSigDB database for each gene set collection or using gene sets curated based on published data. Heatmaps were constructed based on the results of the AmpliSeq data. GSEA analyses in Chapter 3 used whole transcriptomic data with the p-value cut-off as 0.01.

2.13 Gene microarray

Gene microarray (used in Chapter 4) was performed by the Laboratory for Advanced Genome Analysis (VPC) and have previously been described in detail (141). In summary, two independent biological repeats of LNCaP(CTL) and three independent biological repeats of LNCaP(MEAF6-1) and LNCaP(MEAF6-2) cells were extracted for total RNA using the mirVana™ RNA Isolation Kit (Ambion) according to manufacturer's

protocol and subsequently hybridized to human GE 8×60 K gene expression microarray (Agilent; Santa Clara, CA, USA). The resulting data was processed by the Agilent Feature Extraction software. For statistical analyses, comparisons were performed between RNA samples with LNCaP(MEAF6-1) vs LNCaP(CTL), LNCaP(CTL) vs LNCaP(MEAF6-2), and LNCaP(MEAF6-1) vs LNCaP(MEAF6-2). Unpaired *t*-test with p-value cut-off of 0.05, a fold change cut-off of 1.5, and Benjamini-Hochberg multiple testing correction were applied. LNCaP(MEAF6-1) vs LNCaP(CTL) transcriptomes were then uploaded and analyzed in IPA (Ingenuity Pathway Analysis) for pathway prediction algorithms.

2.14 Clinical, PDX, and GEMM datasets

Clinical cohorts used in Chapter 3 includes the following: RNA-seq data for the Beltran 2016 cohort (CRPC-Ad, n=34; t-NEPC, n=15) was from Weill Medical College of Cornell University (New York, NY, USA) (54); RNA-seq data for the Robinson 2015 cohort (CRPC, n=118) (142) and microarray and clinical data for the Grasso 2012 cohort (CRPC, n=31) (143) were accessed through cBioPortal (144,145); microarray data for both the Varambally 2005 (CRPC, n=6) (146) and Kumar 2016 cohorts (CRPC, n=169) (147) were accessed from the GEO database, GSE3325 and GSE77930, respectively. Microarray data from the Living Tumour Laboratory (LTL) 331-7 and 331-7-R castration time-series patient-derived xenograft (PDX) models were accessed by GSE59986 (148). Sequencing data for the genetically engineered mouse models (GEMMs) including the Ku *et al.* (WT, wild-type, SKO, single knock-out, DKO, double knock-out, TKO, triple knock-out) (70) and Zou *et al.* (NPp53) cohorts (71) were

accessed from GSE90891 and GSE92721, respectively. RNA-seq dataset of the LnNE cell model was previously reported by our lab (93).

RNA-seq datasets from the Beltran 2011 (73) and VPC 2011 (92) clinical cohorts were also used in Chapter 4. Cohort composition for the Beltran 2011 and VPC 2011 were 7 NEPC and 30 AdPC and 5 NEPC and 8 AdPC, respectively. Chapter 5 includes the VPC 2018 (NEPC, n=5, and AdPC, n=24) (149) cohort rather than the VPC 2011 cohort. cDNA samples from the LTL PDX models were shared by Dr. Yuzhuo Wang from the VPC. All specimen collection and RNA extraction protocols for these datasets are described in their associated publications.

2.15 RNA-Seq analysis pipeline

Implemented in-house and published with the VPC 2018 cohort, the RNA-seq analysis pipeline and algorithms used in Chapter 5 were performed by Dr. Varune R Ramnarine (VPC) and was previously described by Ramnarine *et al.* (149). However, in this study, the pipeline was updated to use the Hg38 human genome build and Ensembl GRCh38.86 gene tracks. Cufflinks were also used to identify and quantify alternative splice variants present within all annotated genes.

2.16 Statistics

For Chapters 3 and 4, all results are expressed as the mean ±SD, unless otherwise stated. Statistical analyses were done using GraphPad Prism version 7.00 for Windows (GraphPad Software; La Jolla, CA, USA). One-way ANOVA or Student 2-tailed *t*-tests were carried out to determine differences between groups. Correlation

between two expression groups were computed with Pearson's *r* correlation, and overall survival was estimated by Kaplan-Meier. The levels of significance were set at a p-value of 0.05, 0.01, and 0.001, denoted as *, **, and ***, respectively.

For VPC and Beltran cohorts in Chapter 5, all values were log2-transformed prior to statistical testing (Figure 5.1B). All clinical group-wise comparisons were calculated using a standard Student's 2-tailed *t*-test. Multiple test corrections were applied to p-values using the Bonferroni and Hochberg correction method to minimize false discovery rate. Analyses between two groups were compared via unpaired Student's 2-tailed *t*-test. Pearson's χ^2 test was performed to compare *GIT1-A* and *GIT1-C* RISH scores to the different tumour groups (Figure 5.2B). One-way ANOVA and Newman-Keuls multiple comparison test were performed to compare between multiple groups (Figure 5.2C and Figure 5.3D). Pearson's *r* correlation analyses were performed to compare between RISH scores and the expression of NE positive markers (Figure 5.2D), as well as *GIT1-A* or *GIT1-C* expression with NEPC and AdPC marker expression (Table 5.1) or *SRRM4* expression (Table 5.2). Fisher's exact test was used to calculate the sensitivity and specificity of *GIT1-A* to predict the NEPC phenotype (Table 5.3). The levels of significance were set at a p-value of 0.05, 0.01, and 0.001, denoted as *, **, and ***, respectively.

Chapter 3 SRRM4 promotes neuroendocrine prostate cancer development via a pluripotency gene network

3.1 INTRODUCTION

Tumour cell plasticity and heterogeneity creates many challenges for prostate cancer disease management. To counteract ARPI therapies and become CRPC tumours, AdPC cells can either enhance AR signaling in the presence of castration levels of androgens and progress into CRPC-Ad tumours or, alternatively, become AR-indifferent or AR-negative and progress into t-NEPC (46,63,150,151). While the molecular mechanisms by which AdPC cells transform into t-NEPC remain elusive, recent studies have shown that the combination of AR-inhibition with genomic inactivation of *TP53*, *RB1*, and *PTEN* confers AdPC cells lineage plasticity to gain basal, mesenchymal, or neuroendocrine (NE) phenotypes and subsequently the development of t-NEPC tumours (69,70). These studies demonstrate that this transition from AdPC to t-NEPC can be through an intermediate pluripotent stem cell (SC)-like state. During this state, there are elevated expressions of a network of pluripotency genes including the SOX family members such as SOX2 and SOX11 which are well known for its roles in early embryogenesis, embryonic SC pluripotency, and neurogenesis (69–71,152). Given the genomic heterogeneity of prostate tumour cells, these findings highlight that AdPC cells containing certain genomic features may be prone to undergo this lineage switching to develop into t-NEPC via a pluripotency gene network.

However, whole-exome sequencing has revealed that patient t-NEPC and AdPC tumours have similar gene mutation landscapes (54). *In vitro*, AdPC cell models have been shown to undergo a LE-to-NE cell lineage switch through a transdifferentiation mechanism to initiate t-NEPC development. This NE transdifferentiation process is shown to be mediated by dysregulations of a key transcriptional repressor of neuronal genes, REST (89,153,154), epigenetic modulators, such as EZH2 (54,74,75), and microenvironment factors (e.g. cAMP, IL-6, and hypoxia) (154–157). These results emphasize that multiple non-genomic factors also play important roles during t-NEPC establishment.

In fact, we have recently shown that RNA splicing mechanisms, mediated by the RNA splicing factor SRRM4, promote this NE transdifferentiation mechanism of lineage plasticity in the development of t-NEPC tumours (90). The upregulation of SRRM4 is associated with t-NEPC and predominately establishes a t-NEPC-unique RNA splicing program when compared to AdPC tumours (90). SRRM4 can transform LNCaP AdPC cells, which express functional p53 and Rb1, into t-NEPC xenografts under androgen-deprived conditions. These SRRM4-transduced LNCaP cells also exhibit global transcriptome and RNA splicing signatures similar to that of t-NEPC tumours in patients. Through inoculating these cells into castrated nude mice and serially passaging the tumours for five generations over 18 months, we have reported the establishment of a series of t-NEPC models, called LnNE (93). LnNE tumours strongly express NE markers and present a NEPC morphology. Tumours at later passages grow more aggressively and become androgen-insensitive and PSA-negative. These features mimic AdPC progression to t-NEPC in patients. Further dissection of SRRM4-mediated

signaling has revealed that SRRM4 can not only compromise the functions of REST to promote NE transdifferentiation (90,158,159), but also regulate RNA splicing of other transcripts such as *Bif-1* to promote the evasion of apoptosis (94). Altogether, these findings indicate that SRRM4 is a facilitator of t-NEPC through the NE transdifferentiation mechanism.

SRRM4 is a key regulator of neural-specific exon networks that are required for the differentiation of neural progenitor and neuronal cells during embryonic development (95,96,98–100,108,118). It exerts its actions by promoting the inclusion of neural-specific exons, generating alterative protein isoforms necessary for remodeling protein-protein interaction networks and signaling pathways that are required for neurogenesis and neuronal cell maturation and function (99). The essential developmental roles of SRRM4 in the differentiation of neural progenitor and neuronal cells lead us to hypothesize that SRRM4 can ultimately promote NEPC development in any AdPC cell-specific context (i.e. with different genetic and epigenetic backgrounds).

In this study, we report that SRRM4 induces a global NEPC-specific RNA splicing signature in a panel of prostate and prostate cancer cell models. However, SRRM4 induces heterogeneous transcriptomes and phenotypes among these cell models tested. The SRRM4-transduced DU145 cells are unique by which a pluripotency gene network including *SOX2* is activated. This discovery characterizes another SRRM4-mediated mechanism underlying lineage plasticity distinct from the LnNE model. This model, so called the DuNE model, recapitulates the molecular signatures of a subset of patient t-NEPC tumours expressing stem-like molecular features,

emphasizing its clinical relevance and application in investigating the complex molecular mechanisms of t-NEPC development.

3.2 RESULTS

3.2.1 SRRM4 induces heterogeneous t-NEPC transcriptomes in multiple cell models

Given the genetic and epigenetic heterogeneity innate to prostate tumour cells, we applied lentivirus encoding SRRM4 to transduce multiple cell lines with no endogenous SRRM4 protein expression previously reported by Li *et al.* (90) including prostate cancer lines (LNCaP, PC-3, DU145, 22Rv1), benign prostate epithelial lines (BPH-1 and RWPE-1), prostate stromal line (WPMY-1), and uterine smooth muscle line (hTERT-Myo) (Appendix Di). SRRM4 induced a previously reported NEPC-unique RNA splicing signature of 21 neural-specific transcripts in all of the eight cell models (Figure 3.1A), suggesting that SRRM4 is functionally active as an RNA splicing factor in these cells. Furthermore, SRRM4 induced an overall increase of multiple NE markers including *ASCL1*, *CHD2*, *SCG3*, *SYP*, and *SYT4* and decrease of LE markers including *CDH1* (encodes the E-cadherin protein), *KRT8*, and *Nkx3.1* (Figure 3.1B). However, the extent of the changes in NE and LE marker expression varied as shown by RT-qPCR and immunoblotting assays (Figure 3.1C). These results indicate that although SRRM4 can activate a global NEPC-specific RNA splicing program, the subsequent induction of a NEPC-unique transcriptome is heterogeneous, which may be explained by the different genetic and epigenetic backgrounds of these cell models as previously reported (160–162).

Figure 3.1

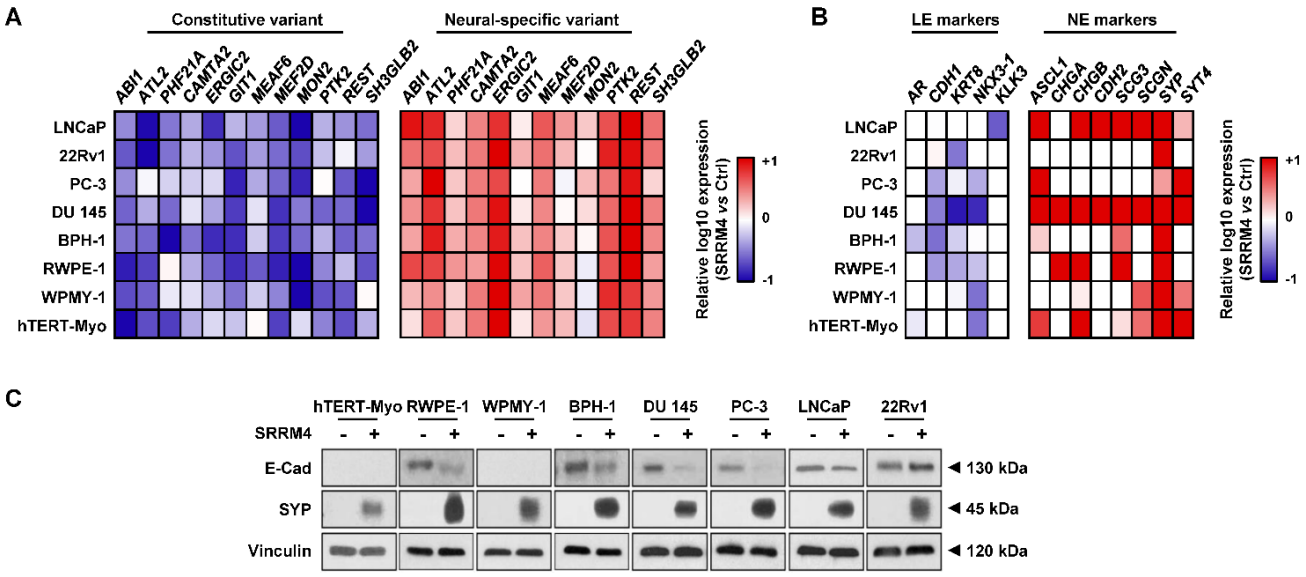

Figure 3.1 SRRM4 induces heterogeneous t-NEPC transcriptomes in multiple cell models. Total RNA was extracted from the AdPC (LNCaP, PC-3, DU145, 22Rv1), benign prostate epithelial (BPH-1 and RWPE-1), prostate stromal (WPMY-1) and uterine smooth muscle (hTERT-Myo) generated stable cell lines overexpressing SRRM4 or empty vector control. RT-qPCR was then performed to measure **(A)** the RNA splicing activity of SRRM4 in promoting the expression of neural-specific variants and decreasing expression levels of the respective constitutive variants and **(B)** the expression of LE and NE markers in SRRM4-overexpressing cells compared to that of the control cells. All heat maps represent the relative fold change in log10. **(C)** Protein lysates from all stable cell models were used to measure E-Cad, SYP, and vinculin protein levels by immunoblotting assays. Three independent biological replicates were performed for each experiment. AdPC, prostate adenocarcinoma; LE, luminal epithelial; NE, neuroendocrine; SYP, synaptophysin; E-Cad, E-cadherin.

3.2.2 Multifarious histological features of SRRM4-transduced prostate cancer xenografts

SRRM4 was incapable of inducing tumorigenesis of RWPE-1 cells that were inoculated into nude mice, indicating that SRRM4 is not essential for the oncogenesis of non-malignant prostate cells—at least not within the 14-wk duration of our experiment. All tumours were confirmed to express exogenous SRRM4 using RISH assays (Appendix Dii) as there are no commercially available antibodies that effectively recognize SRRM4 via IHC. However, SRRM4-transduced AdPC cell-derived xenografts

presented differential phenotypes (Figure 3.2). E-cadherin (or E-cad) was reduced in the SRRM4-transduced DU145 and PC-3 tumours, but not the 22Rv1 and LNCaP tumours (Figure 3.2A). Pan-cytokeratin levels were only robustly reduced in the SRRM4-transduced DU145, or DU145(SRRM4), tumours. In contrast, all xenografts strongly expressed the NE marker, SYP. The most striking difference that separated the DU145(SRRM4) tumours from the others was that the tumour cells grew in high density within the tumour mass with minimal stromal components (Figure 3.2B). All DU145(SRRM4) tumour cells were strongly Ki-67 positive. The Ki-67 index in DU145(SRRM4) tumours were 3-fold higher than that of all other xenografts (Figure 3.2C). This phenomenon is highly similar to NCI-H660 tumours, a bona fide NEPC cell model. These findings suggest that SRRM4 confers DU145 cells strong anti-apoptotic and proliferative properties even under a hypoxic microenvironment with minimal stroma support and limited nutritional supply.

Figure 3.2

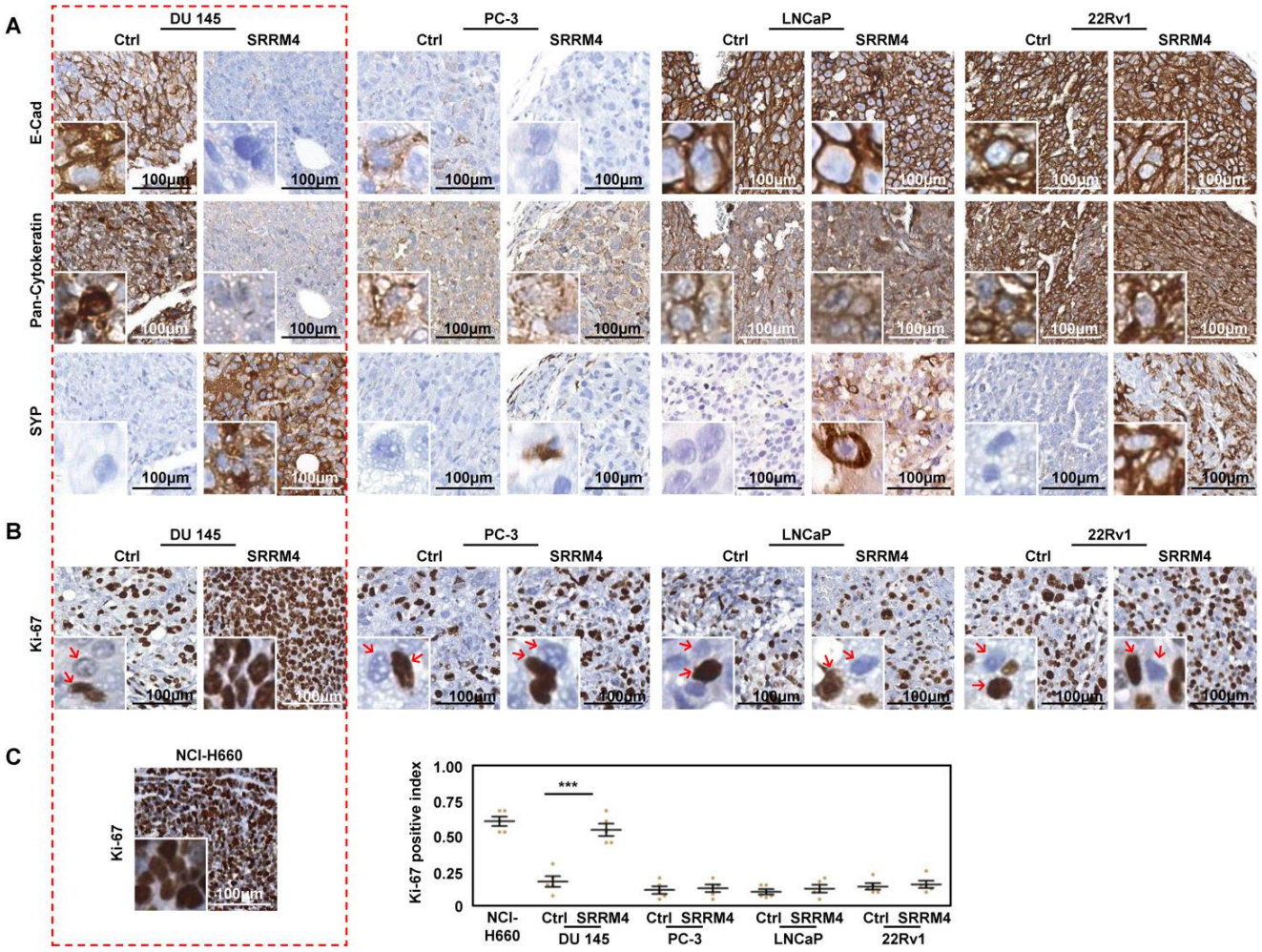

Figure 3.2 Multifarious histological features of SRRM4-transduced prostate cancer xenografts. DU145, PC-3, LNCaP, and 22Rv1 stable cell lines overexpressing SRRM4 or its respective control cells were inoculated in bilateral flanks subcutaneously in 6-8-week-old nude mice (n=3 mice per cell line). Mice were euthanized when tumour burdens reached experimental endpoint (volume of 1500 mm^3) and the tumours were harvested, fixed, paraffin embedded, and processed for IHC detection against **(A)** E-cad, pan-cytokeratin, SYP, and **(B-C)** Ki-67. **(C)** Previously processed NCI-H660 xenografts were also processed for IHC detection against Ki-67. Ki-67 was quantified by using the Aperio Image Analysis IHC menu (Leica Biosystems) and the results are represented on the dot plot. Results are presented as the mean ± SD (One-way ANOVA; n = 5; ***denotes p <0.001). Scale bars represent 100 μm. IHC, immunohistochemistry; E-Cad, E-cadherin; SYP, synaptophysin.

3.2.3 Differential cellular impacts of prostate cancer cell models by SRRM4

The cellular impacts of SRRM4 on multiple cell models were also studied. In contrast to PC-3, LNCaP, and 22Rv1 cells, only DU145(SRRM4) cells showed dramatic morphological changes (Figure 3.3A). When cultured under 2D-conditions, a reduction of the cytoplasmic to nuclear ratio and 5-fold reduction in size of the cell bodies were observed in the DU145(SRRM4) cells compared to that of its respective control, DU145(Ctrl), cells. Dendritic projections similar to that of neuronal cells were also observed, exemplified by F-actin staining. Consistent with the high Ki-67 index of DU145(SRRM4) xenografts, SRRM4 stimulated proliferation of DU145 cells, but not the other cell models under 2D-conditions (Figure 3.3B). For the reason that only the DU145(SRRM4) cell and xenograft models (designated as the DuNE models) have thus far shown unique characteristics of t-NEPC, we performed further functional assays on the DuNE cell model. DuNE cells formed spheroids on Matrigel and showed stronger cell proliferation measured by BrdU incorporation assays when compared to that of the DU145(Ctrl) cells (Figure 3.3C). Furthermore, they formed 3-times the number of colonies on soft agar compared to the DU145(Ctrl) cells (Figure 3.3D). When challenged with apoptosis inducers including UV irradiation or chemotherapy reagents docetaxel (Doce) and camptothecin (CPT), the DuNE cells showed stronger anti-apoptotic properties than that of its control cells, evidenced by the levels of cleaved PARP (c-PARP) (Figure 3.3E). These results indicate that the DuNE cell model presents cellular phenotypes similar to that of t-NEPC tumour cells.

Figure 3.3

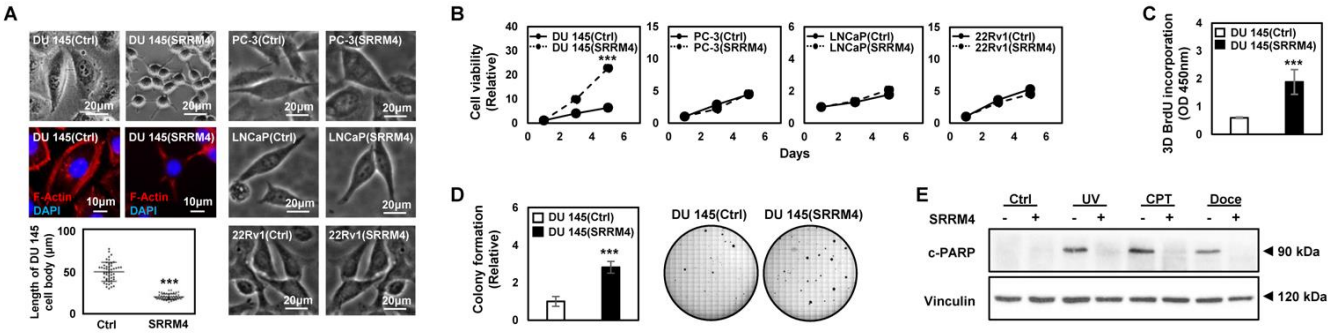

Figure 3.3 Differential cellular impacts of prostate cancer cell models by SRRM4. (A) The morphology of cells was imaged by Zeiss light microscope, where the scale bars represent 20 μm. Additionally, the DU145(SRRM4), or DuNE, cells and its control cells, DU145(Ctrl), were fixed for IF against F-actin using anti-F-actin antibody conjugated to Phalloidin-iFluor 488 and mounted with DAPI staining mount. Cells were then imaged by confocal microscopy, where the scale bar represents 10 μm. 50 cells were randomly selected to measure the average cell body length in μm in the Image J program and presented on the bar graph. **(B)** Cells were seeded in a 96-well plate for MTS assays to determine cell viability over a 5-day time course. The DuNE cells and its respective control cells, were seeded in **(C)** Matrigel for 3D BrdU proliferation assays, **(D)** soft agar for 10-day-long colony formation assays (where colonies >100 μm were counted), or (**E**) 10 cm^2 dish and treated the next day with Doce (20 nM), CPT (60 nM), vehicle (100% ethanol), or 10 mJ/cm^2 of UV irradiation. The protein lysates were then collected 48 hrs later and used to measure c-PARP and vinculin protein levels by immunoblotting assays. Three independent biological replicates were performed for each experiment. All results are presented as the mean ± SD (Student's 2-tailed *t*-test; *n* = 3; ***denotes *p*<0.001). IF, immunofluorescence; UV, ultra violet; CPT, camptothecin; Doce, docetaxel; c-PARP, cleaved PARP; OD, optical density; F-actin, filamentous actin; BrdU, bromodeoxyuridine.

3.2.4 DuNE cells possess a pluripotency gene network distinct from the LnNE model

To decipher signaling networks unique to DuNE, we performed Ion AmpliSeq Transcriptome analyses. There was a total of 3339 genes that were differentially upregulated and 2694 genes that were downregulated in the DuNE cells when compared to the DU145(Ctrl) cells. Gene set enrichment analyses (GSEA) revealed that the DuNE transcriptome was significantly enriched with gene sets related to lineage plasticity, cell survival, neuron differentiation, and neural-specific cell morphogenesis (Figure 3.4A). For example, SRRM4-target genes were enriched with gene ontology

(GO) terms of stem cell differentiation, neuron differentiation, and cell morphogenesis in neuron differentiation, but were negatively associated with the hallmark apoptosis gene set. These findings indicate that SRRM4 can re-program the AdPC phenotype of DU145 cells towards a neuronal phenotype by activating a pluripotency gene network.

Further analyses were performed to compare the transcriptomes of the DuNE and LnNE cell models (Figure 3.4B). GSEA revealed that the 3883 genes unique to the DuNE cell model were uniquely enriched with gene sets related to SC differentiation, neuronal SC population maintenance, anti-apoptosis, and neural precursor cell proliferation. Furthermore, we extracted the leading-edge subsets of genes associated with DuNE phenotype from the three GSEA gene sets under the “lineage plasticity” group from figure 4A (Appendix E). Of the 59-stem differentiation and SC-related genes, we validated the mRNA expressions of 13 genes including *SOX2* in the SRRM4-transduced DU145, PC-3, LNCaP, and 22Rv1 cell models by RT-qPCR (Figure 3.4C). These results demonstrate that SRRM4 regulates different transcriptomes to promote the transformation of DU145 and LNCaP AdPC cells into t-NEPC xenografts, and that SRRM4 regulates a pluripotency gene network in the DuNE model.

Figure 3.4

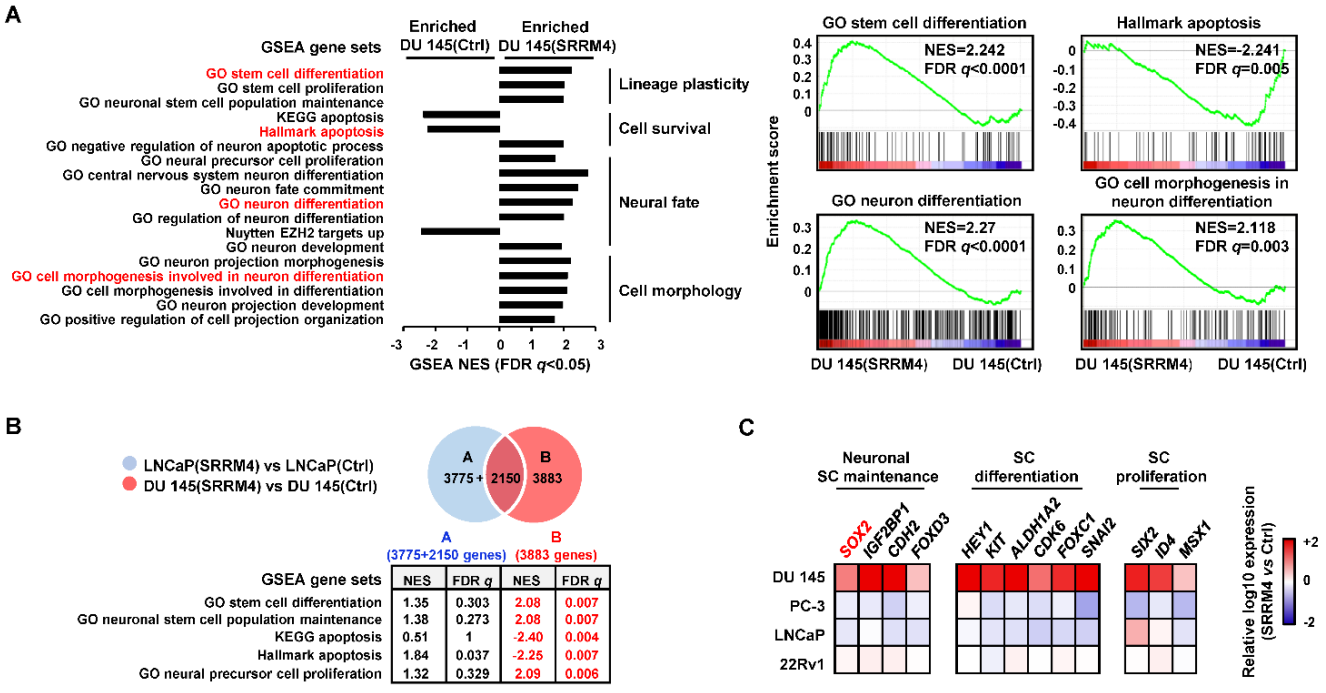

GSEA gene sets	NES	FDR q	NES	FDR q
GO stem cell differentiation	1.35	0.303	2.08	0.007
GO neuronal stem cell population maintenance	1.38	0.273	2.08	0.007
KEGG apoptosis	0.51	1	-2.40	0.004
Hallmark apoptosis	1.84	0.037	-2.25	0.007
GO neural precursor cell proliferation	1.32	0.329	2.09	0.006

Figure 3.4 DuNE cells possess a pluripotency gene network distinct from the LnNE model. (A) Transcriptome data of the DuNE, or DU145(SRRM4), cell model and its respective control, DU145(Ctrl) (*p*-value cut-off as 0.01) were analyzed by GSEA based on the latest MSigDB database for each collection. GSEA revealed the enrichment of genes associated with lineage plasticity, cell survival, neural fate, and cell morphology in the DuNE cells. **(B)** DEGs (*p*-value cut-off as 0.01) caused by SRRM4 transduction were compared between the DuNE (n=6063) and LnNE (n=5925) cell models. GSEA show more enrichment of the lineage plasticity and cell survival-associated genes in distinct DEGs (n=3883) mediated by SRRM4 in the DuNE model. **(C)** Thirteen SC- or pluripotency-related genes were selected from the leading-edge groups associated with the DuNE phenotype in the GSEA gene sets under the 'lineage plasticity' subgroup from subfigure 4A. The mRNA expression of these genes in the SRRM4-overexpressing DU145, PC-3, LNCaP, and 22Rv1 cell models were compared to that of its respective control cells via RT-qPCR. Heat maps represent the relative fold change in log10. GSEA, gene set enrichment analysis; DEGs, differential expression genes; GO, gene ontology; NES, normalized enrichment score; FDR, false discovery rate; CSS, charcoal-stripped serum; SC, stem cell.

3.2.5 SRRM4 enhances SOX2 expression in the DuNE cell model and in some GEMMs and PDX models

SOX2 was selected to further delineate the SRRM4-regulated pluripotency gene network as SOX2 was recently demonstrated to promote the lineage plasticity of AdPC cells during progression to t-NEPC (69,70). SOX2 protein expression was only detected

in the DuNE cells (Figure 3.5A). We showed that the upregulation of *SOX2* by SRRM4 was in both time- and dose-dependent manners when SRRM4-expressing plasmids were transiently transfected into DU145 cells (Figure 3.5B). Moreover, *SOX2* was downregulated when DuNE cells were challenged with SRRM4-targeted siRNA (Figure 3.5C), and *SOX2* depletion resulted in the reduction of several pluripotency gene expressions and NE markers and induction of LE markers (Figure 3.5D). The LTL 331-7/331-7-R PDXs that model the progression of AdPC to t-NEPC after castration surgery also showed positive correlations of *SRRM4* with *SOX2* and *SYP*, but negative correlations with *AR* expression (Figure 3.5E). Furthermore, analyses of the recently reported WT/SKO/DKO/TKO GEMMs by Ku *et al.* (70) revealed that *SOX2* was strongly and positively correlated with *SRRM4* (Figure 3.5F), and negatively associated with *AR* (Appendix Fi). This negative association of *SOX2* with *AR* was also observed in four clinical CRPC patient cohorts (Appendix Fii). However, *SRRM4* does not show a correlation with *SOX2* expression in the NPp53 GEMMs by Zou *et al.* (71) (Figure 3.5G), as well as the SRRM4-transduced PC-3, LNCaP, and 22Rv1 cell models, suggesting that the activation of the SRRM4-SOX2 axis does not apply to all prostate cancer models exhibiting t-NEPC features. Together our findings support that SOX2 is a major component of the pluripotency network regulated by SRRM4 in a subset of t-NEPC tumours.

Figure 3.5

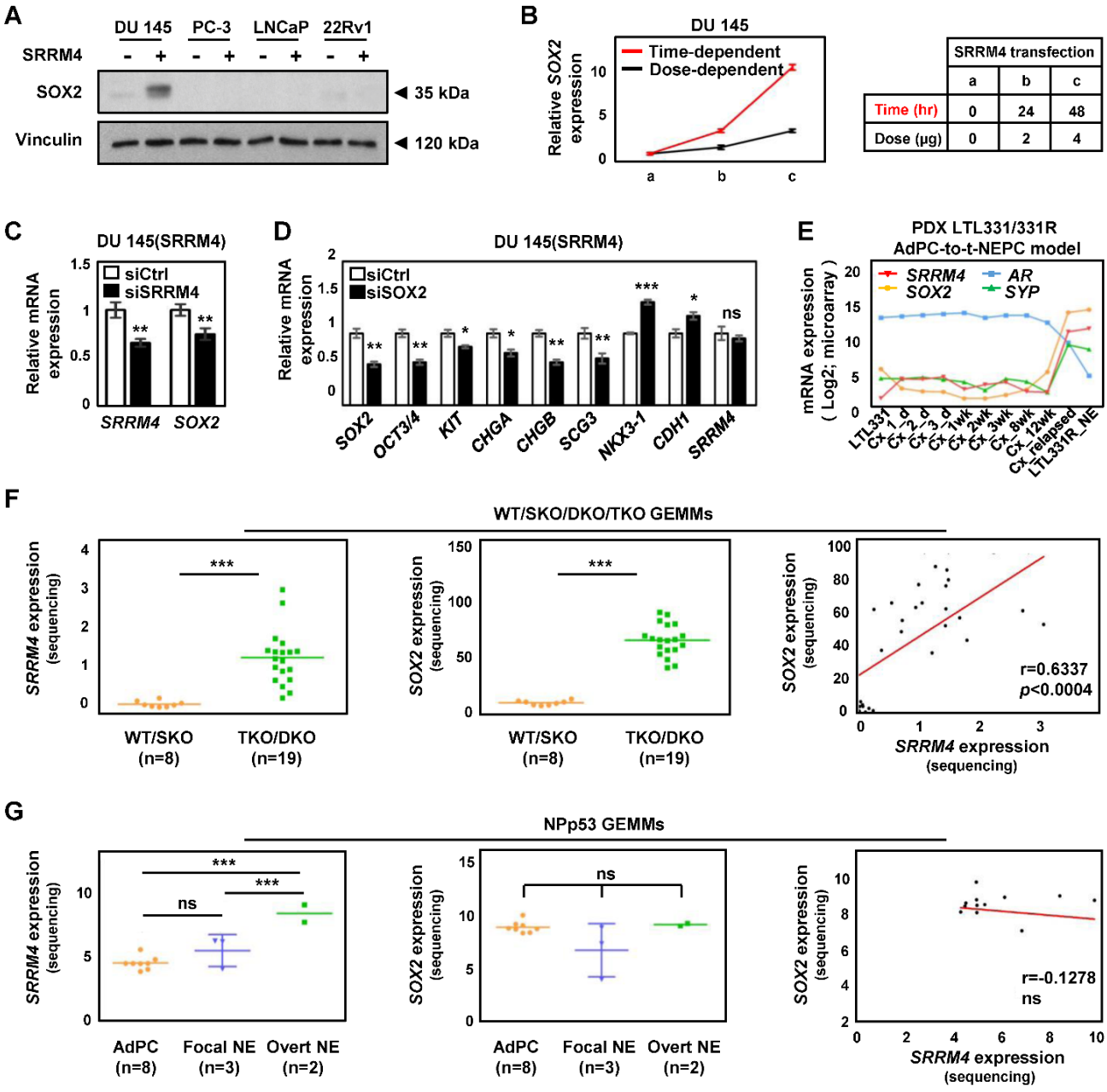

Figure 3.5 SRRM4 enhances SOX2 expression in the DuNE cell model and in some GEMMs and PDX models. (A) Protein lysates from the SRRM4-overexpressing DU145, PC-3, LNCaP, and 22Rv1 cell models and its respective controls were used to measure SOX2 and vinculin protein levels by immunoblotting assays. **(B)** For the time-dependent studies, DU145 cells were transiently transfected with 4 µg of SRRM4 or control plasmids, and total RNA was extracted at times 0, 24, and 48 hrs. For the dose-dependent studies, DU145 cells were transiently transfected with 0, 2, and 4 µg of SRRM4 or control plasmids, and total RNA was extracted after 24 hrs. *SOX2* expression was detected by RT-qPCR. **(C-D)** DuNE, or DU145(SRRM4), cells were transiently transfected with siRNA targeting *SRRM4* **(C)**, or *SOX2* **(D)** and extracted for RNA following transfection to detect expression levels of indicated genes. All results are presented as the mean ± SD (Student's 2-taile *t*-test; n = 3; * denotes $p<0.05$, ** $p<0.01$, and

***p<0.001). **(E)** The expressions of *SRRM4*, *SOX2*, *AR*, and *SYP* during the progression of AdPC (LTL331) to t-NEPC (LTL331R_NE) after castration in the PDX LTL331/331R model are shown. **(F)** *SRRM4* and *SOX2* expressions in WT/SKO/DKO/TKO GEMMs (Ku *et al.*, 2017) are shown as well as the Pearson's *r* correlation coefficient between *SRRM4* and *SOX2* expressions. All results are presented as the mean ± SD (Student's 2-tailed *t*-test; WT/SKO, n=8; TKO/DKO, n=19; *** denotes p<0.001). **(G)** *SRRM4* and *SOX2* expressions in different phenotypic subcategories of the NPp53 GEMMs (Zou *et al.*, 2017) are shown as well as the Pearson's *r* correlation coefficient between *SRRM4* and *SOX2* expressions. All results are presented as the mean ± SD (One-way ANOVA; AdPC, n=8; Focal NE, n=3; Overt NE, n=2; *** denotes p<0.001, and "ns" denotes not significant). GEMMs, genetically engineered mouse models; AdPC, prostate adenocarcinoma; WT, wild-type; SKO, single knock-out; DKO, double knock-out; TKO, triple knock-out; NE, neuroendocrine. PDX, patient-derived xenograft; AdPC-to-t-NEPC, prostate adenocarcinoma to treatment-induced neuroendocrine prostate cancer; d, day; wk, week; Cx, castration; NE, neuroendocrine.

3.2.6 The DuNE model represents a subset of clinical t-NEPC tumours with high SOX2 expression

To define the clinical relevance of SOX2, we found that high *SOX2* expression was correlated with poor prognosis in patients after receiving hormone therapies in the Grasso *et al.* (143) CRPC cohort (Figure 3.6A). When exploring the RNA-seq data of four patient cohorts reported by Beltran *et al.* (54), Robinson *et al.* (142), Kumar *et al.* (147), and Varambally *et al.* (146), we observed an overall positive association of *SOX2* with *SRRM4* expression (Appendix G). However, we found markedly distinct expressions of *SOX2* within the t-NEPC tumours from the Beltran *et al.* (54) cohort, the largest t-NEPC cohort containing pathological evaluation of each sample. There were five t-NEPC tumours with low *SOX2* expression, t-NEPC($SOX2^{low}$), similar to that of CRPC-Ad tumours, while the remaining ten t-NEPC tumours expressed a ~17.5-fold (log2) increase of *SOX2* levels, t-NEPC($SOX2^{high}$) (Figure 3.6B). These findings demonstrate that different subgroups of t-NEPC tumours exist, where a division of two subgroups is evident based on a robust difference in *SOX2* mRNA expression levels.

To determine the clinical relevance of the DuNE model to the t-NEPC(SOX2^{high}) subgroup, we applied GSEA to compare DuNE transcriptome to that of: 1) the top 500 differentially expressed genes between t-NEPC(SOX2^{high}) and CRPC-Ad, 2) the top 500 differentially expressed genes between t-NEPC(SOX2^{high}) and t-NEPC(SOX2^{low}), and 3) the top 500 genes differentially expressed between t-NEPC(SOX2^{low}) and CRPC-Ad (Figure 3.6C). We observed strong enrichment of the DuNE transcriptome with that of the t-NEPC(SOX2^{high}) subgroup. Moreover, GSEA revealed that the t-NEPC(SOX2^{high}) subgroup was enriched with gene sets associated with pluripotency and proliferation, where the leading-edge genes presented a consistent expression pattern in the DuNE cell model (Figure 3.6D). Furthermore, this SRRM4-SOX2 axis was also seen in t-NEPC patient tumour cores that have been previously characterized (91) (Figure 3.6E). In the six t-NEPC patient tumours, all were *SRRM4*-positive but only four were *SOX2*-positive. Collectively, these findings recognize two distinct subgroups of t-NEPC tumours classified by *SOX2* expression. Although both subgroups have relatively high levels of *SRRM4*, our results support that SRRM4 may promote t-NEPC development through different mechanisms (Figure 3.7). The DuNE model represents a clinically relevant model to study SRRM4-SOX2 axis during t-NEPC progression.

Figure 3.6

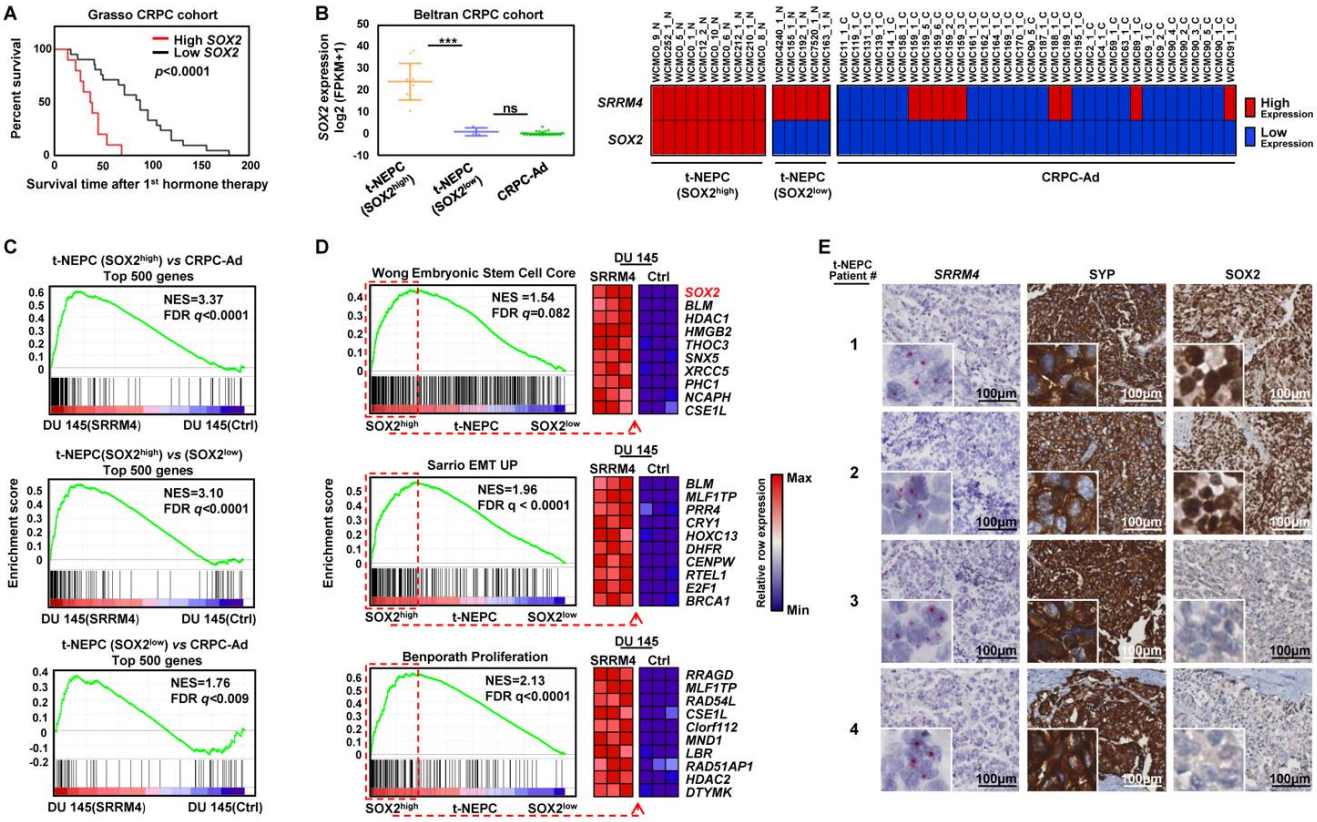

Figure 3.6 The DuNE model represents a subset of clinical t-NEPC tumours with high *SOX2* expression. (A) Overall survival Kaplan-Meier between low and high expression of *SOX2* in CRPC tumours from the Grasso *et al.* (2012) cohort. **(B)** *SOX2* expression was compared among CRPC tumour samples from the Beltran *et al.* (2016) cohort and separated into three groups, CRPC-Ad (n=34), t-NEPC expressing low level of *SOX2*, t-NEPC(SOX2^{low}) (n=5), and t-NEPC expressing high level of *SOX2*, t-NEPC(SOX2^{high}) (n=10). Results are presented as the mean ± SD (One-way ANOVA; *** denotes $p<0.001$, and "ns" denotes not significant). Expressions of *SOX2* and *SRRM4* in each patient sample (patient ID: "WCMC-") are indicated as high, red, or low, blue, where the median value of the SRRM4 datasets define the cut-off. **(C)** GSEA revealed enrichment of the DU145(SRRM4), or DuNE, model with that of the differentially expressed top 500 genes in the 1) t-NEPC(SOX2^{high}) tumours when compared with CRPC-Ad or 2) t-NEPC(SOX2^{low}) and in the 3) t-NEPC(SOX2^{low}) tumours compared with CRPC-Ad. **(D)** GSEA revealed the enrichment of the t-NEPC(SOX2^{high}) tumours with well-defined gene sets named "Wong Embryonic stem cell core," "Sarrio EMT up," and "Benporath Proliferation," where the leading-edge genes presented a consistent expression pattern in the DuNE cell model. **(E)** Six t-NEPC patient tumours were used to measure *SRRM4* and SOX2 expression by applying RISH and IHC assays, respectively. Due to limited space, two SOX2-positive and two SOX2-negative tumour cores are shown. Scale bars represent 100 μm. CRPC-Ad, castration-resistant prostate adenocarcinoma; t-NEPC, treatment-induced neuroendocrine prostate cancer; GSEA, gene set enrichment analysis; NES, normalized enrichment score; FDR, false discovery rate; EMT, epithelial-to-mesenchymal transition; RISH, RNA *in situ* hybridization; IHC, immunohistochemistry; SYP, synaptophysin.

Figure 3.7

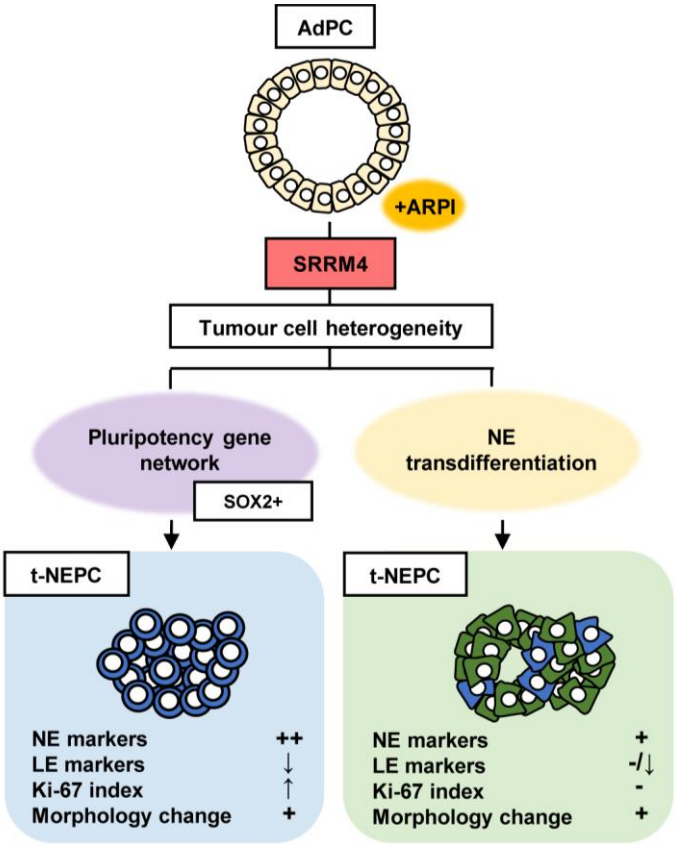

Figure 3.7 Proposed models for SRRM4 in promoting t-NEPC development through different mechanisms. A schematic diagram illustrates two mechanisms of SRRM4 in promoting the development of t-NEPC tumours. AdPC, prostate adenocarcinoma; t-NEPC, treatment-induced neuroendocrine prostate cancer; ARPI, androgen receptor pathway inhibitors; NE, neuroendocrine; LE, luminal epithelial.

3.3 DISCUSSION

This study identifies a novel mechanism by which SRRM4 transforms AdPC cells into t-NEPC xenografts through a pluripotency gene network containing *SOX2*. Importantly, this newly discovered SRRM4-SOX2 signaling axis can be stratified from a subgroup of t-NEPC in patients, emphasizing its clinical significance. Additionally, we have established a new NEPC cell and xenograft model (DuNE), which recapitulates

the phenotypes of clinical t-NEPC tumours expressing stem-like characteristics. Together with our previously reported LnNE model, we propose that SRRM4 can facilitate the transformation of AdPC into t-NEPC tumours through either a NE transdifferentiation pathway or a pluripotency gene network. Whether a pluripotency gene network is initiated by SRRM4 likely relies on the epigenetic and genomic heterogeneity of AdPC cells. These studies highlight the complexity of SRRM4 signaling in promoting tumour progression to t-NEPC to develop therapy resistance.

Heterogeneous genomic features of cancer cells within an AdPC tumour may contribute to the activation of the SRRM4-SOX2 signaling pathway in the progression of t-NEPC. Upregulation of *SRRM4* and *SOX2* expressions only occurs in the *Pten/Rb1* DKO and *Pten/Rb1/Trp53* TKO GEMMs, but not in the WT and *Pten* SKO GEMMs (Figure 3.5F), suggesting that *Rb1*-inactivation is necessary for the activation of the SRRM4-SOX2 signaling to confer the lineage plasticity of LE cells to a NE cell lineage. While the *Pten/Trp53* DKO NPp53 GEMMs show either focal or overt NE differentiation (71), the upregulation of SRRM4 does not concur with SOX2 stimulation (Figure 3.5G), indicating that the *Trp53*-inactivation is not sufficient in activating the SRRM4-SOX2 signaling axis. However, a recent study has shown that an increase in *SOX2* expression was observed in *PTEN*-deficient LNCaP cells with *TP53*- and *RB1*-inactivations, while SRRM4 remained negative in these cells (69). Although DU145 cells are also TP53- and RB1-deficient cells, RB1 silencing to SRRM4-transduced TP53-null PC-3 cells do not show similar phenotypes to the DuNE model (Appendix N). Collectively, these findings demonstrate that the activation of the SRRM4-SOX2 signaling axis cannot be solely explained by loss-of-function of PTEN, TP53 and RB1. This suggests that other

complex mechanisms in addition to the abovementioned genomic factors also contribute to the t-NEPC progression facilitated by a SRRM4-mediated pluripotency gene network.

Epigenetic mechanisms may be responsible for SRRM4 and SOX2 activation. CBX8 and EZH2 are the two most overexpressed epigenetic regulators in t-NEPC clinical samples and PDXs (54,63,74). It is known that EZH2 is implicated in t-NEPC development (63,75,163). Intensive H3K27Me3 covers the coding regions of the *SRRM4* and *SOX2* genes in LNCaP cells and prevents the transcription of these genes. Furthermore, it has been reported that LNCaP cells cultured in an androgen-free neural/neural crest stem medium can redirect the cells into a neural-fate possibly via EZH2-mediated epigenetic reprogramming (80), indicating the importance of the tumour microenvironment in regulating tumour cell plasticity (63,79). The DU145 cell line is originally derived from an AdPC metastasis lesion to the brain (78), suggesting that the neural microenvironment of the cell niche may have altered the epigenome of the DU145 cells to be predisposed to a NE lineage switch. In addition, although both DU145 and PC-3 cells exhibit stem-like phenotypes and properties such as expressions of SC markers and self-renewal capabilities (63,81,82), only the SRRM4-transduced DU145 cells undergo a robust NE differentiation via the activation of a pluripotency gene network containing *SOX2*. These findings indicate that the DU145 cells possess unique epigenetic features that may contribute to the SRRM4 and SOX2 signaling axis, although the connection between epigenetic factors and the SRRM4-SOX2 axis warrant further investigations.

Currently, there are limited t-NEPC cell and xenograft models that can be utilized to efficiently manipulate signaling pathways and study molecular mechanisms of t-NEPC development. The only NEPC cell line, NCI-H660, is very difficult to be transfected or transduced by lentivirus and has a doubling time of >100 hrs (164). More importantly, it is unclear whether this cell line was derived from AdPC cells or primary NEPC cells. The five newly developed LnNE xenografts, replicate the prolonged transition process of AdPC progression to t-NEPC in an *in vivo* environment (93). However, compared to the LnNE model, the DuNE model has several advantages. The DuNE cell model develops into xenografts faster than the LnNE model and exhibits more dramatic changes in LE and NE marker expressions. Additionally, the DuNE model is AR- and PSA-negative, TP53- and RB1-null, exhibits striking neuronal-like morphologies, and mimics the molecular signatures of a subset of clinical t-NEPC (i.e. SCNC) that present stem-like characteristics as previously demonstrated (63,165,166). Moreover, plasmid transfection efficiency can be achieved as high as 80%, and these cells have a doubling time of ~15-20 hrs in 2D-conditions. DuNE cells can be adapted into 3D-culture formats (such as petri dishes and hanging-drop systems) and studied as xenografts in immunocompromised mice, all systems of which are suitable for high-throughput drug screening.

In summary, our study reports a novel SRRM4-mediated mechanism underlying lineage plasticity where lineage switching is primarily mediated by a pluripotency network including SOX2, a key regulator of dedifferentiation and neural lineage-specific fate. Furthermore, the newly established DuNE model can also serve as a useful t-NEPC model to study the complexity of AdPC progression to t-NEPC.

Chapter 4 The role of alternative RNA splicing of the *MEAF6* gene during neuroendocrine prostate cancer progression

4.1 INTRODUCTION

Next-generation ARPI prolong survival of patients with metastatic CRPC (24,25). However, a consequence of the selection pressures exerted by these more potent ARPI is that they can promote the emergence of AR-independent CRPC, one variant of which is t-NEPC. T-NEPC is reported in up to 25% of post-ARPI CRPC patients and the rate of occurrence is predicted to rise with the widespread use of ARPI (41,63). Once diagnosed, t-NEPC patients succumb to death within <2 years (64). No targeted therapy is available for t-NEPC patients, only systemic chemotherapy regimens, reflecting our limited knowledge on the molecular underpinnings of t-NEPC progression.

There is accumulating evidence indicating that t-NEPC is clonally derived from AdPC cell precursors (46,54,63,66). Whole exome sequencing has shown similar mutational landscapes between t-NEPC and AdPC (54,66,67). Case studies reveal that cell populations of AdPC, AdPC with neuroendocrine differentiation, and t-NEPC co-exist in the same tumour (46,167). Intermediate morphological and phenotypical transitions exist in cancer cells between the boundaries of AdPC and t-NEPC cell populations, indicating dynamic NE differentiation processes. The transition of AdPC to t-NEPC has been reported in the LTL 331/331-R PDX models following castration, with no genotypic alterations pre- and post-castration (66). Moreover, in castrated mice, when neural RNA splicing factor SRRM4 is introduced exogenously, LNCaP AdPC cells can be transformed into t-NEPC xenografts (90). These findings collectively support that t-NEPC originates from AdPC.

The transition of AdPC to t-NEPC is a complicated process that may involve both cell differentiation and proliferation, two distinguishable and coordinated processes controlled by multiple genes. Luminal epithelial AR signaling is critical in the maintenance of epithelial cell differentiation in the adult prostate (2,5). As a result, AR inhibition can trigger prostate cancer cell de-differentiation to confer adaptive plasticity and promote phenotype reprogramming. While AR blockade is necessary for t-NEPC establishment, it is insufficient since <25% of ARPI-treated tumours are transformed into t-NEPC (41,63). Similarly, AdPC cells can acquire a NE phenotype when treated with microenvironment factors such as IL-6 or cAMP (155,168,169), but these cells have not been reported to be capable of forming a t-NEPC tumour. While AdPC with NE differentiation can be found in 10-100% of AdPC tumours (46,49–53), expression of NE markers is not sufficient for t-NEPC establishment. To establish a t-NEPC tumour, these NE-like differentiated cells must gain a proliferative state for clonal expansion. Targeting genes that facilitate NEPC cell proliferation would be more effective in delaying t-NEPC progression, particularly in patients under ARPI treatment.

Using whole-transcriptome sequencing of AdPC and NEPC patient biopsies from the Beltran 2011 (73) and VPC 2011 (92) cohorts, we report a t-NEPC-unique RNA splicing signature that is predominantly facilitated by SRRM4. SRRM4 can transform LNCaP AdPC cells into t-NEPC xenografts, suggesting that SRRM4 regulates RNA splicing of multiple transcripts that are responsible for NE differentiation and cell proliferation processes during t-NEPC progression. In fact, we have shown that SRRM4 regulates RNA splicing of the *REST* transcript and re-programs its functions to confer a NE phenotype in AdPC cells (90). However, REST knockdown in LNCaP cells does not

facilitate the development of t-NEPC xenografts, supporting the notion that SRRM4-mediated *REST* alternative RNA splicing leads to NE differentiation but does not induce proliferation sufficient for clonal expansion and t-NEPC tumour establishment. In searching for other t-NEPC-unique SRRM4-target transcripts that may contribute to NEPC progression, we have found a highly expressed splice variant of MYST/Esa1-associated factor 6 (*MEAF6*), *MEAF6-1*, in NEPC tumour samples. Although a protein component of the HAT complexes (130–134), there have been no studies on the cellular functions of MEAF6. *MEAF6-1* and *MEAF6-2* are two protein coding transcripts from the *MEAF6* gene, whereby exon 6 (30 bp) is included in *MEAF6-1* but skipped in *MEAF6-2* mRNA. Since increased *MEAF6-1* expression is closely associated with t-NEPC, we set out to determine whether MEAF6-1 contributes to t-NEPC progression.

4.2 RESULTS

4.2.1 Alternative RNA splicing of the MEAF6 transcript is associated with NEPC progression

Whole transcriptome sequencing data on AdPC and NEPC tumour samples from the VPC 2011 (8 AdPC and 5 NEPC samples) and Beltran 2011 (32 AdPC and 6 NEPC samples) cohorts were analyzed by a computational tool, COMPAS (90), which identified an increase in the ratio of *MEAF6-1:MEAF6-2* in NEPC patients (p=0.0034 in the VPC cohort and p=0.0002 in the Beltran cohort), while total *MEAF6* mRNA expression remained unchanged (Figure 4.1A-B). These results indicated that the inclusion of the neural-specific exon of the *MEAF6* transcript is a unique feature of NEPC. RT-qPCR assays on tumour samples from PDXs further confirmed that *MEAF6-*

1 mRNA levels in NEPC were about 150-fold higher than AdPC (p=0.001), while *MEAF6-2* mRNA levels in NEPC were not statistically different between NEPC and AdPC (p=0.338) (Figure 4.1B). Increased *MEAF6* RNA splicing was also positively correlated with elevated *SRRM4* mRNA expression in both xenograft (Figure 4.1C) and clinical CRPC samples (Appendix Hi). Additionally, RNA splicing activity of the *MEAF6* transcript was positively correlated with *REST* RNA splicing (Appendix Hii). These results collectively suggest that SRRM4 may be also be a regulator of alternative splicing of the *MEAF6* transcript. In prostate cancer cell lines, *MEAF6-1* was highly expressed in NEPC cell line NCI-H660 as well as SCLC cell lines NCI-H69 and NCI-H82, when compared to *MEAF6-1* expression levels in AdPC cell lines (p=0.00028). In contrast, *MEAF6-2* mRNA levels were not statistically different in AdPC lines from NCI-H660, NCI-H69, and NCI-H82 cell lines (Figure 4.1D). Further validation of MEAF6 protein expression could not be done because currently available antibodies cannot differentiate MEAF6 splicing variants from each other, and immunoblotting and immunohistochemistry assays were unable to recognize endogenous MEAF6 proteins. Together, these results indicate that up-regulation of the expression of *MEAF6-1* splice variant is closely associated with NEPC progression.

Figure 4.1

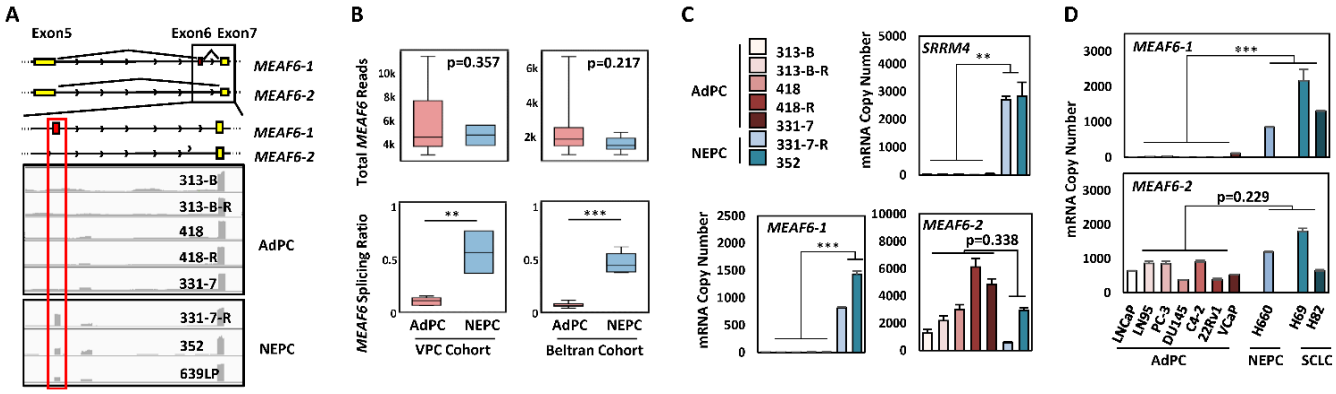

Figure 4.1 Alternative RNA splicing of the *MEAF6* transcript is associated with NEPC progression. **(A)** Illustration of *MEAF6-1* and *MEAF6-2* RNA. The alternatively spliced exon (exon 6) is illustrated in red, where constitutive exons are denoted in yellow. IGV was used to visualize the coverage of *MEAF6* by RNA-seq reads in AdPC and NEPC patient tumours and PDXs. Grey areas represent the sequencing depth of the respective exon, where the more prominent peaks reflect the significant presence of the positioned exon. **(B)** *MEAF6* splicing ratio (*MEAF6-1:MEAF6-2* RNA-seq reads per base-pair) and *MEAF6* total expression obtained from RNA-seq data of AdPC and NEPC patient tumour samples (NEPC n=5 and AdPC n=8 in VPC cohort; NEPC n=6 and AdPC n=32 in Beltran cohort) **(C)** Validation of RNA-seq data, Figure 1A, using RT-qPCR on RNA isolated from AdPC and NEPC PDX. **(D)** Profiling of mRNA copy numbers of *MEAF6* splice variants in a panel of AdPC cell lines (LNCaP, LN95, PC-3, DU145, C4-2, 22Rv1 and VCaP) and NEPC cell line (NCI-H660) as well as small cell lung cancer (SCLC; NCI-H69 and -H82), which is a neuroendocrine cancer of the lung. This was done via RT-qPCR for absolute quantification of total *MEAF6-1* and *MEAF6-2* using a standard curve. All results are presented as the mean ± SEM (Student's 2-tailed *t*-test *** denotes $p<0.001$ and ** denotes $p<0.01$). AdPC, adenocarcinoma prostate cancer; NEPC, neuroendocrine prostate cancer; VPC, Vancouver Prostate Centre; SCLC, small cell lung cancer; IGV, integrative genomics viewer; PDX, patient-derived xenograft.

4.2.2 SRRM4 regulates RNA splicing of the MEAF6 gene

To determine whether SRRM4 regulates alternative RNA splicing of the *MEAF6* transcript, we transiently transfected SRRM4 expression vector in LNCaP cells. SRRM4 did not alter the levels of total *MEAF6* transcripts (Figure 4.2A). Instead, it induced *MEAF6-1* but had no impact on *MEAF6-2* mRNA levels. SRRM4 regulation of *MEAF6* RNA splicing was further confirmed in *SRRM4* knockdown conditions via siRNA (Appendix I). To test whether other RNA splicing factors may also regulate the inclusion of the neural-specific exon of the *MEAF6* transcript, we repeated the experiments with

a panel of splicing factors and showed that RNA splicing of the *MEAF6* transcript is uniquely regulated by SRRM4 (Figure 4.2B). Furthermore, RNA-chromatin immunoprecipitation (RNA-ChIP) assays confirmed that SRRM4 is recruited to its putative 3' UGC splice site in the intron region upstream of the neural-specific exon in the *MEAF6* transcript, but not in the control intron region of the *GAPDH* transcript (Figure 4.2C). In addition, we found that RNA splicing or regulation of *MEAF6* mRNA expression was not altered by AR signaling (Appendix J). Collectively, these results demonstrate that SRRM4 is an important regulator of *MEAF6-1* splicing.

Figure 4.2

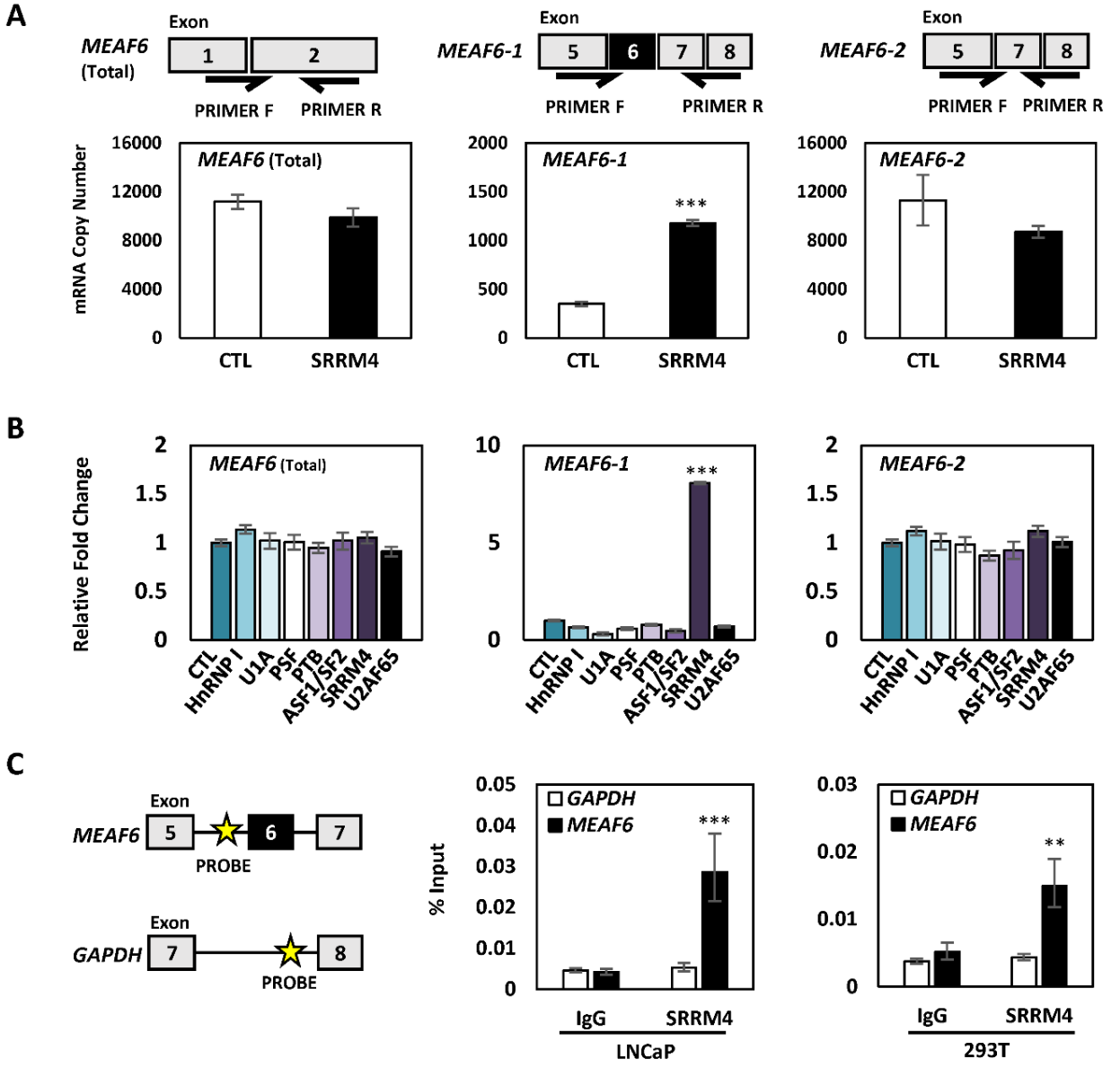

Figure 4.2 SRRM4 regulates RNA splicing of the *MEAF6* gene. (A) Illustration of splice variant-specific primers designed to detected total *MEAF6*, *MEAF6-1*, and *MEAF6-2* mRNA levels. LNCaP cells seeded in 6-well plates were transiently transfected with 4 µg of Flag-SRRM4 for 24-hrs and were isolated for RNA. RT-qPCR for absolute quantification of total *MEAF6*, *MEAF6-1*, and *MEAF6-2* using a standard curve was performed. **(B)** LNCaP cells were transiently transfected with a panel of RNA splicing factors (hnRnp I, U1A, PSF, PTB, ASF1/SF2, SRRM4, U2AF65). Cells were then extracted for RNA. Relative quantifications of total *MEAF6*, *MEAF6-1*, and *MEAF6-2* were compared to *18S* via RT-qPCR. Results are presented as the mean ± SEM (one-way ANOVA; n=3; *** denotes $p<0.001$). **(C)** RNA-ChIP was performed with 293T and LNCaP cells in 10 cm^2 dishes. Cells were transfected with 10 µg of Flag-SRRM4 and immunoprecipitated with anti-Flag antibody following fixation with paraformaldehyde. Eluted RNA fragments were used as templates for RT-qPCR primers antisense for intron sequence upstream of alternatively spliced exon of *MEAF6-1*. Position of probes for *MEAF6-1* and *GAPDH* is indicated by the yellow star. Otherwise indicated, results are presented as the mean ± SEM (Student's 2-tailed *t*-test, n=3 *** denotes $p<0.001$ and ** denotes $p<0.01$). F, forward; R, reverse; CTL, control (empty vector).

4.2.3 MEAF6-1 promotes prostate cancer cell growth and invasion

To study the biological functions of MEAF6-1 in prostate cancer cells, we constructed LNCaP and PC-3 cell lines that stably express exogenous MEAF6-1 or MEAF6-2 via lentiviral transduction (Appendix K). Neither MEAF6-1 nor MEAF6-2 changed the expression levels of NE markers *CHGA*, *ENO2*, *SYP*, *CHGB* or LE markers such as *CHD1* (Appendix L). These results indicate that neither of the MEAF6 splice variants are involved in NE trans-differentiation of prostate cancer cells.

Under 2D culture conditions, BrdU incorporation assays demonstrated that enhanced expression of MEAF6-1 but not MEAF6-2 in both LNCaP and PC-3 cells induced a 40–50% increase of cell proliferation rates (Figure 4.3A). Since NEPC cells lose its epithelial morphology and favor 3D growth conditions, we also seeded MEAF6-1 and MEAF6-2 stable lines into Matrigel to allow for the formation of multi-cellular spheroids and then performed BrdU incorporation assays. We repeatedly observed that MEAF6-1 stimulated cell proliferation (Figure 4.3B). MEAF6-1-overexpressed LNCaP cells also formed significantly larger sizes and numbers of anchorage-independent colonies than control and MEAF6-2-overexpressed cells (Figure 4.3C). Furthermore, MEAF6-1 enhanced the migration and invasion rates of PC-3 cells (Figure 4.3D). Collectively, these results demonstrate that MEAF6-1 and MEAF6-2 have different biological functions in promoting prostate cancer cell proliferation and invasion that can accelerate tumour progression.

Figure 4.3

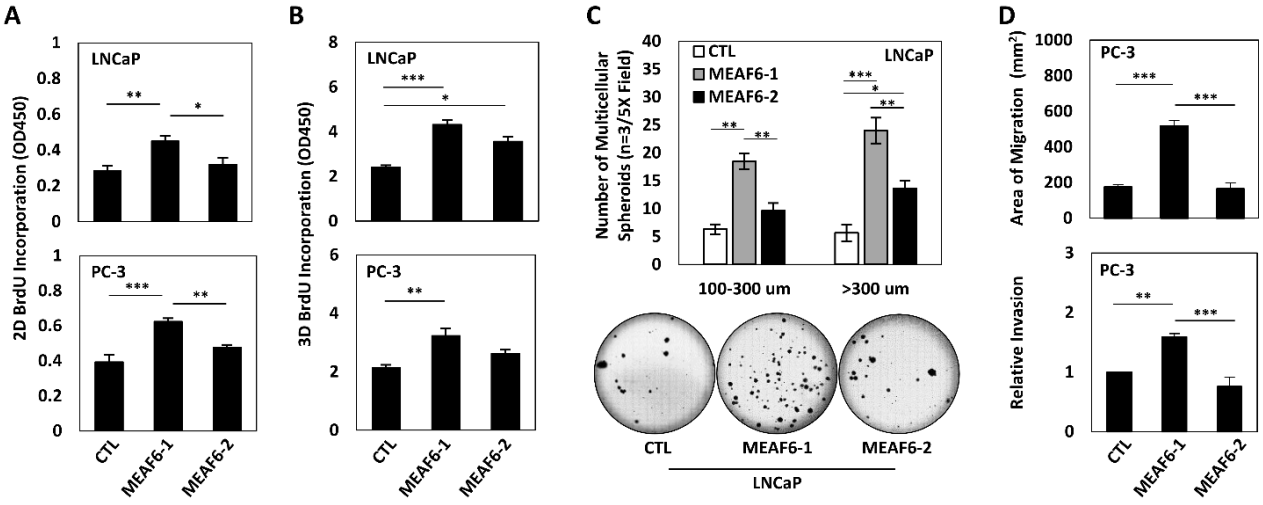

Figure 4.3 MEAF6-1 promotes prostate cancer cell growth and invasion. Using LNCaP or PC-3 cell lines stably expressing CTL, MEAF6-1, or MEAF6-2, **(A)** 2D BrdU cell proliferation assays were performed to measure proliferation of cells. BrdU results represent colorimetric quantitative measurements (OD at 450 nm wavelength) of cellular BrdU incorporation into DNA. **(B)** Cells were also seeded in Matrigel for BrdU proliferation assays to measure the proliferative ability under 3D conditions. **(C)** Soft agar assays were performed on LNCaP cells in a 6-well plate. Colonies were stained with crystal violet and counted by varied sizes (i.e. 100-300 µm or >300 µm). Images of wells were captured by Zeiss light microscope, representing one of the three independent biological replicates. **(D)** PC-3 stable cells were seeded in 6-well plates and incubated for 16-hrs for wound healing assays. Area of migration measured using Image J program. Cell invasion ability of PC-3 cell lines was measured using Matrigel Invasion chambers. All results are presented as the mean ± SEM (one-way ANOVA; n = 3; *** denotes $p<0.001$ and ** denotes $p<0.01$). CTL, control (empty vector); OD, optical density; BrdU, bromodeoxyuridine.

4.2.4 MEAF6-1 transcriptome in prostate cancers

To profile the MEAF6-1 transcriptome, we compared gene microarrays using LNCaP(CTL), LNCaP(MEAF6-1), and LNCaP(MEAF6-2) stable lines. There were 2044 genes differentially regulated by MEAF6-1 and 2702 genes by MEAF6-2. DAVID (Database for Annotation, Visualization, and Integrated Discovery) for GO analyses indicated that the functions of both gene groups regulated by MEAF6-1 or MEAF6-2 are very similar. GO terms indicated that MEAF6-1 and MEAF6-2-regulated genes are

associated with cell cycle, cellular response to stress, cell division, regulation of cell cycle, and DNA replication. Since MEAF6-1, but not MEAF6-2, promotes cell proliferation, anchorage-independent growth and invasion, we further stratified a group of 159 genes that were specifically regulated by MEAF6-1 (Figure 4.4A). Interestingly, *ID1* and *ID3* genes are the genes most upregulated by MEAF6-1. When the MEAF6-1-regulated gene list was analyzed by IPA (Ingenuity Pathway Analysis), it predicted that *ID1* and *ID3* gene networks were the most prominent downstream effectors for MEAF6-1 and are highly associated with cell proliferation, cell cycling, and cell migration and invasion functions (Figure 4.4B). These microarray results on MEAF6-1 transcriptome were further validated by our RT-qPCR assays showing that MEAF6-1 induced a 5-fold increase of *ID1* and a 4-fold of increase of *ID3* mRNA levels in LNCaP cells (Figure 4.4C). Moreover, MEAF6-1 increased protein expression levels of ID1. ID3 protein levels were not confirmed because of the poor quality of antibodies available against it. Additionally, MEAF6-1-induced *ID1* and *ID3* expression in LNCaP and PC-3 cells was dramatically compromised when cells were challenged by siRNA targeting *MEAF6* (Figure 4.4D-E). To further confirm that ID1 and ID3 mediates MEAF6-1 functions in cell proliferation and invasion, we silenced *ID1* or *ID3* with siRNA and observed that *ID1* and *ID3* depletion significantly attenuated MEAF6-1 actions on cell proliferation and invasion (Figure 4.4F). These results indicate that *ID1* and *ID3* genes play important roles in mediating MEAF6-1 actions for cancer cell proliferation and invasion.

Figure 4.4

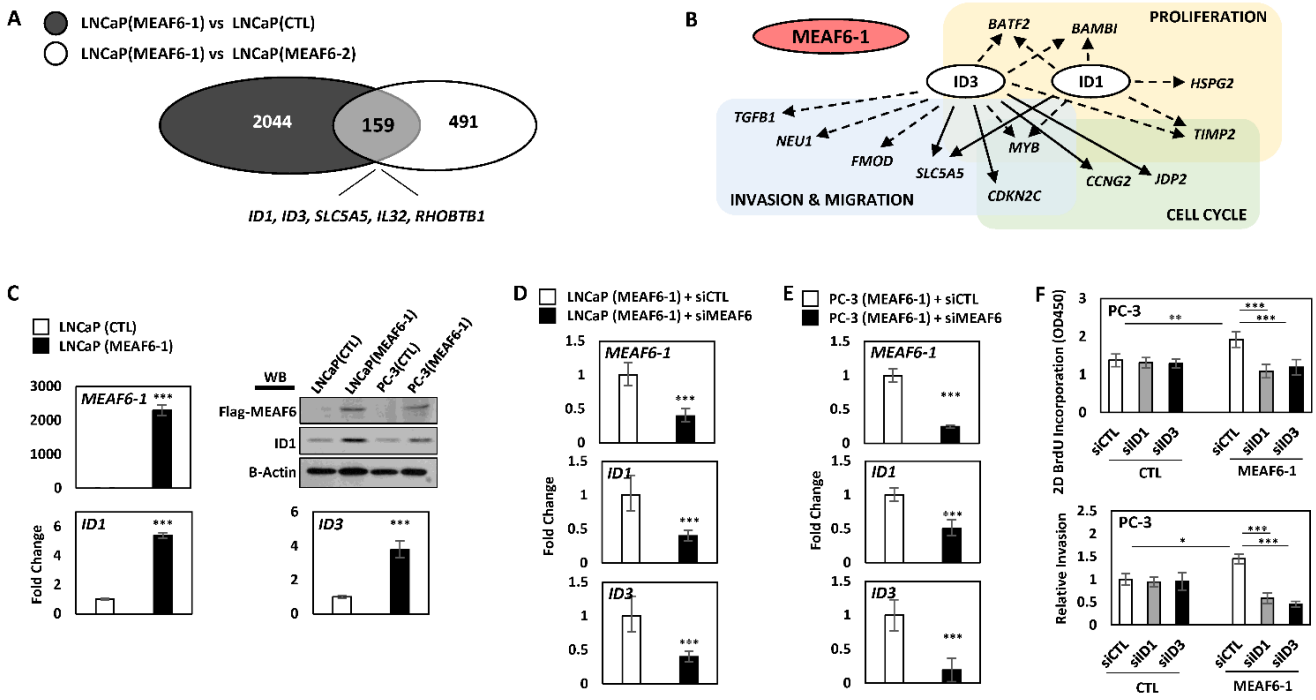

Figure 4.4 MEAF6-1 function is mediated through ID1 and ID3. Microarray was performed comparing LNCaP(CTL), LNCaP(MEAF6-1), and LNCaP(MEAF6-2). **(A)** Gene expressions with fold changes over 1.3 and an adjusted p-value of less than 0.05 from LNCaP(MEAF6-1) vs LNCaP(CTL) were overlapped with LNCaP(MEAF6-1) vs LNCaP(MEAF6-2) transcriptomes. **(B)** LNCaP(MEAF6-1) vs LNCaP(CTL) transcriptomes were uploaded and analyzed in IPA for pathway prediction algorithms of *ID1* and *ID3*. Dashed arrows represent indirect regulation, where solid arrows represent direct regulation. **(C)** MEAF6-1-regulation of *ID1* and *ID3* expression was then validated via RT-qPCR. ID1 protein expression was validated by Western blot. **(D)** LNCaP(CTL) and LNCaP(MEAF6-1) or **(E)** PC-3(CTL) and PC-3(MEAF6-1) stable lines were transfected with siRNA targeting *MEAF6* (siMEAF6) to study the effect of MEAF6-1 on *ID1* and *ID3* expression. Relative quantification of *MEAF6-1*, *ID1*, and *ID3* compared to *18S* via RT-qPCR. **(C-E)** All results are presented as the mean ± SEM (Student's 2-tailed *t*-test *** denotes $p<0.001$). **(F)** PC-3(CTL) and PC-3(MEAF6-1) stable cells were transfected with control (siCTL), *ID1* (siID1), or *ID3* (siID3) targeted siRNA. 2D BrdU cell proliferation assays were performed, where BrdU results represent colorimetric quantitative measurements (OD at 450 nm wavelength) of BrdU incorporation into DNA. Cell invasion ability of the PC-3 stable cells with siRNA transfections were measured using Matrigel Invasion chambers. All results are presented as the mean ± SEM (one-way ANOVA; n=3; *** denotes $p<0.001$; ** denotes $p<0.01$; * denotes $p<0.05$). CTL, control (empty vector); OD, optical density; BrdU, bromodeoxyuridine; IPA, ingenuity pathway analysis.

4.2.5 MEAF6-1 accelerates xenograft tumour growth

To study the impact of MEAF6-1 on xenograft growth, we transplanted PC-3(CTL) or PC-3(MEAF6-1) cells subcutaneously into nude mice. Tumour uptake at ~3

weeks was similar in both groups. However, tumour volume of PC-3(MEAF6-1) xenografts increased significantly faster than control tumours (Figure 4.5A). Mice were sacrificed once tumour burden reached experimental points and xenograft tissues were collected. RT-qPCR and immunoblotting assays validated exogenous MEAF6-1 expression in PC-3(MEAF6-1) xenografts as well as MEAF6-1 upregulation of *ID1* mRNA and protein and *ID3* mRNA levels (Figure 4.5B). Together with the results from Figure 4.3 and Figure 4.4, these results confirm that MEAF6-1 promotes prostate xenograft growth in part through *ID1* and *ID3* genes.

Figure 4.5

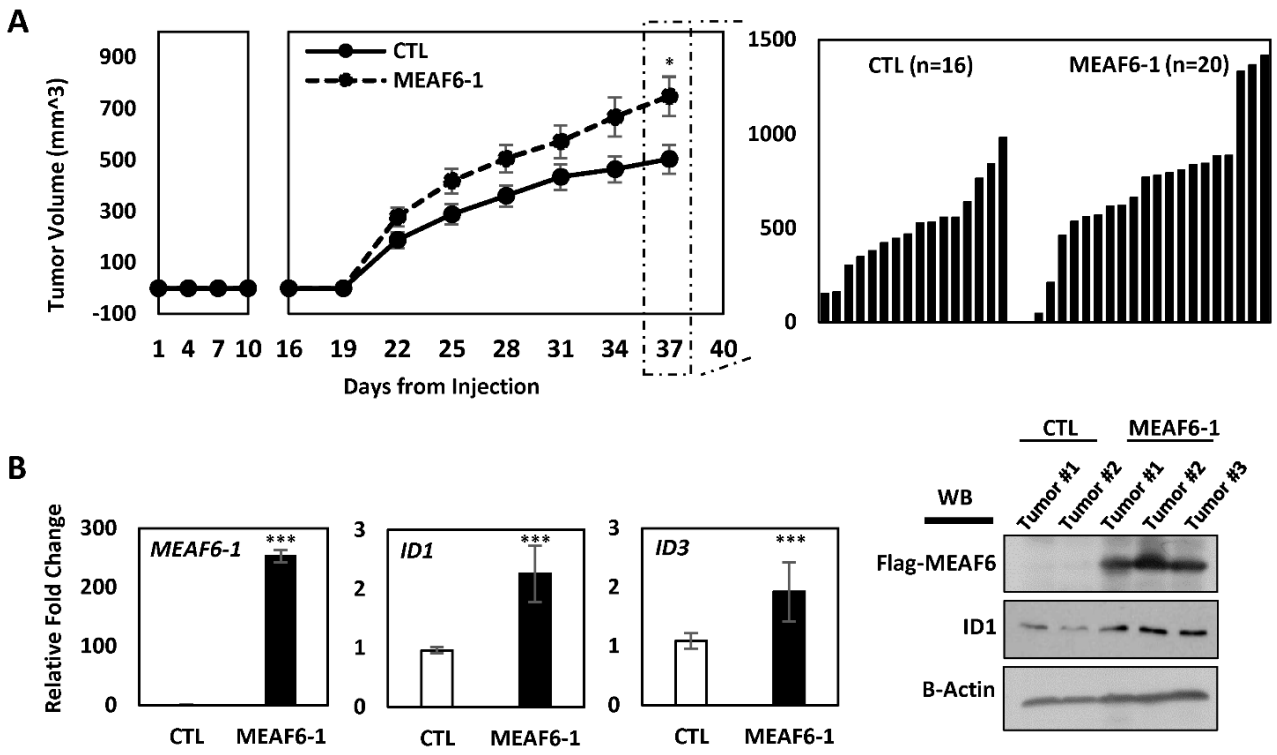

Figure 4.5 MEAF6-1 accelerates xenograft tumour growth. (A) 1x10^6 PC-3(CTL) or PC-3(MEAF6-1) were subcutaneously injected into nude mice (CTL n=16; MEAF6-1 n=20). Tumour volume was measured using a caliper. **(B)** Tumours were extracted and processed for RNA and protein analysis. Relative quantification of *MEAF6-1*, *ID1*, and *ID3* compared to *18S* via RT-qPCR. Protein expressions was detected via Western blot using antibodies against exogenous Flag-MEAF6, ID1, and loading control beta-actin. CTL, control (empty vector).

4.3 DISCUSSION

This study reports that a functionally reprogrammed *MEAF6* transcript via alternative splicing by neuronal splicing factor SRRM4 facilitates prostate cancer cell proliferation, invasion, and migration, which may contribute to NEPC progression. Spliced by SRRM4, the MEAF6-1 variant does not mediate neuroendocrine differentiation of prostate cancer cells, but rather promotes cell proliferation and invasion to accelerate tumour growth. MEAF6-1 exerts these actions mainly via the *ID1* and *ID3* genes, which are well characterized inhibitors of cell differentiation as well as enhancers of cell proliferation and multipotency preservation (170). These findings highlight the critical role of alternative RNA splicing in NEPC progression and support SRRM4 as a key facilitator of t-NEPC. Through RNA splicing, SRRM4 simultaneously reprograms REST functions to confer a neuroendocrine phenotype in AdPC cells and re-directs MEAF6 functions to stimulate tumour cell proliferation and invasion (Figure 4.6).

Figure 4.6

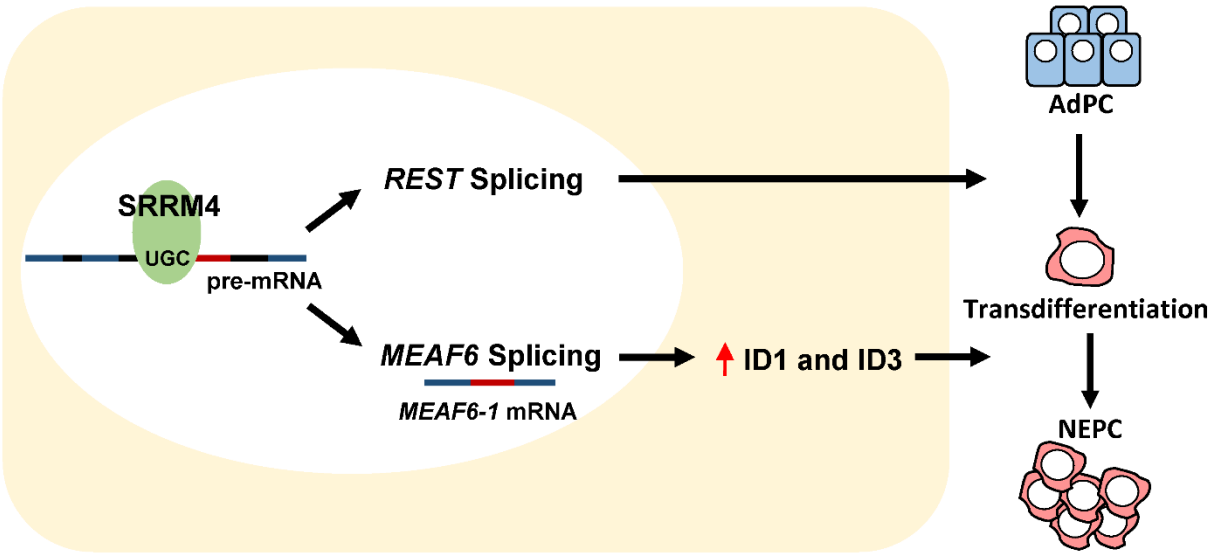

Figure 4.6 Differentiation and proliferation: two distinguishable and coordinated processes for AdPC to NEPC tumour establishment. SRRM4 re-directs MEAF6 functions via alternative RNA splicing to stimulate tumour cell proliferation and invasion through ID1 and ID3. AdPC, prostate adenocarcinoma; NEPC, neuroendocrine prostate cancer.

To our knowledge, this is the first report that characterizes the biological functions of the *MEAF6* gene with a particular focus on the actions of *MEAF6* alternative RNA splicing and its role in NEPC progression. It is known that MEAF6 is a component of 4 different MYST family of HAT complexes in cells that modulate gene transcription through posttranslational modifications of histones (130–134). However, no studies have confirmed whether MEAF6 can exert enzymatic activities directly to acetylate histones or whether it serves as an adapter to recruit differential protein factors to the HAT complexes. Until this study, it was not clear whether or not MEAF6 can regulate transcription of endogenous genes. The existence of this protein in the HAT complex has only been confirmed by mass spectrometry (171); however, this method cannot differentiate between the different splice variants of MEAF6. Our studies show that the

constitutive *MEAF6-2* splice variant is ubiquitously expressed in AdPC, while *MEAF6-1* is specifically expressed in NEPC patient, PDX, and cell models. While MEAF6-2 regulates a similar transcriptome as MEAF6-1, it does not affect prostate cancer cell differentiation, proliferation, or invasion, suggesting that the unique MEAF6-1-regulated transcriptome (i.e. 159 genes) is more important for prostate cancer proliferation, invasion, and tumour growth. These results are consistent with previous studies reporting that SRRM4 commonly targets “microexons” to modulate protein-interaction networks during neurogenesis, where misregulation of microexon-mediated networks is associated with neural-related disorders such as autism (95). Since *SRRM4* and *MEAF6-1* expression is NEPC tumour specific, we propose that SRRM4-mediated inclusion of the neural-specific exon results in the functional reprogramming of the MEAF6-1 protein, which may contribute to NEPC progression by accelerating proliferation of prostate cancer cells that have acquired neuroendocrine phenotypes.

We report that MEAF6-1 facilitates NEPC progression mainly by activating the *ID1* and *ID3* gene networks. The ID family of proteins are inhibitors of bHLH, ETS, and PAX transcription factors and RB family members which regulate cell differentiation (172). ID protein expression is high in stem and progenitor cells and, while often downregulated during normal cell differentiation, are reactivated in cancer (170). While tumour suppressor proteins such as Rb1 and p53 inhibit ID proteins from activation (173,174), excessive ID proteins override the tumour suppressor functions of RB1 (175). Therefore, MEAF6-1-induced ID1 and ID3 may create a condition mimicking genetic inactivation of *RB1* and *TP53*. In this context, MEAF6-1 may play a similar role as SV40 in the TRAMP mouse model, where prostate-specific expression of SV40

sequesters Rb1 and p53 functions and leads TRAMP tumour progression into NEPC (176,177). As a result, our findings suggest a SRRM4-MEAF6-1-Rb1/p53 axis that may contribute to NEPC progression.

In summary, our studies demonstrate that SRRM4-mediated RNA splicing of the *MEAF6* transcript may contribute to NEPC progression via the neural-specific MEAF6-1 splice variant, where MEAF6-1 may facilitate prostate cancer cell proliferation and tumorigenesis required for the development of and progression to NEPC.

Chapter 5 The role of alternative RNA splicing of the *GIT1* gene during neuroendocrine prostate cancer progression

5.1 INTRODUCTION

While *de novo* NEPC represent <2% of all prostate cancer incidences, the increasing prevalence of t-NEPC as an outcome of selection pressures exerted by ARPI treatments is becoming a paramount clinical issue (46,62,63). Currently, t-NEPC accounts for >16% of all cases of CRPC patients (41,63). Patients with t-NEPC have a mean survival rate of ~7 months post-diagnosis, as the disease is already very aggressive and more resistant to contemporary chemo- and radiation therapies (46,64). Presently, there are no targeted therapies available to treat t-NEPC effectively due to the limited understanding of the mechanisms initiating its origin and development. Furthermore, t-NEPC is predicted to become even more prevalent considering the extensive clinical applications of ARPI therapies (63). This highlights the importance of delineating the molecular underpinnings of t-NEPC to inform future therapies that can prevent or mitigate its development.

Emerging evidence suggests that t-NEPC is derived from AdPC, and this transition can occur as a result of NE differentiation. While AdPC and NEPC tumours have similar genotypes (i.e. somatic copy number, point mutations, and polyploidy), its transcriptome, epigenome, and cellular morphologies differ (46,54,59,66,67). In recent studies, we have demonstrated that a pre-mRNA splicing factor, SRRM4, can facilitate NE differentiation that transforms LNCaP AdPC cells into t-NEPC tumours by reprogramming the transcriptome via alternative RNA splicing under ARPI (90). Following this study, we have established a new t-NEPC cell model, called LnNE, which

utilizes the SRRM4-overexpressing LNCaP cells to create 5 generations of xenografts and cell models (93). Interestingly, this SRRM4-directed RNA splicing profile shares a similar pattern to the diverse alternative splicing patterns seen in the neural system during development, where SRRM4-spliced target genes have recognized functions that are crucial for neural programs early in development (95,96,98). Furthermore, our studies have reported that this reprogrammed RNA splicing signature is unique to NEPC patient tumours, PDX models, and cell models, demonstrating a clear variance in the phenotype of NEPC and AdPC tumours (90,94,138). The SRRM4-mediated t-NEPC-specific reprograming of the transcriptome modifies anti-apoptotic factors (e.g. Bif-1), epigenetic modifiers (e.g. PHF21A, MEAF6-1), and transcriptional regulators (e.g. REST) that are important for regulating cell survival (94), proliferation and tumorigenesis (178), and neural differentiation (90), respectively. Together, these studies propose a model in which SRRM4 facilitates t-NEPC development via alternative RNA splicing of downstream transcripts.

Among the transcripts alternatively spliced by SRRM4, the G-protein-coupled receptor kinase-interacting protein 1 (*GIT1*) transcript is differentially spliced into *GIT1-A* and *GIT1-C*, where the *GIT1-A* splice variant is uniquely found in t-NEPC (90). GIT1 is a multifaceted signaling scaffold protein within the ArfGAP family of proteins that contains a conserved architecture, including an N-terminal ArfGAP domain, three ankryin repeats, a Spa2-homology domain, a coiled-coil domain, and a focal adhesion (FA) targeting domain (179). GIT1 has a variety of canonical biological functions, such as endocytosis regulation of receptors, FA regulation, cell motility, morphogenesis, angiogenesis, and neural functions (such as synapse and dendritic spine

morphogenesis) (179). One of the key functions of GIT1 in epithelial cells is its recruitment of FA proteins, which is important for the formation of stable invadopodia structures. Invadopodia structures utilize stable FAs to degrade the ECM and enable efficient invasion of cancer cells (180,181). In neural systems, GIT1-mediated recruitment of FA proteins activates signaling pathways important for regulating directed spine morphogenesis, cell-to-cell communication, and stability of synapses (136,137). FA-mediated signaling can involve other fundamental aspects of cell biology including survival, proliferation, and environmental sensing of the ECM, mechanical stress, growth hormones, and hypoxic conditions (i.e. oxygen and pH alteration) (182,183). Additionally, dysregulation or malfunction of GIT1 has been associated with various neural-associated diseases, such as Huntington's disease and glioblastoma (179). Increased GIT1 expression has also been reported to promote the migration, invasion, and metastasis of liver, colon, melanoma, lung, renal, and non-small cell lung cancer cells (179,184–187). However, the function of GIT1 in the progression of prostate cancer as well as the role of *GIT1* RNA splicing in any cancers is unknown and has not been previously studied. Here, we investigate the role of *GIT1* alternative RNA splicing during t-NEPC progression and the function of its alternative splicing isoforms, GIT1-A and GIT1-C.

5.2 RESULTS

5.2.1 Expression profiling of GIT1 splice variants in NEPC patients, PDXs, and cell models

Whole-transcriptome datasets of Beltran 2011 (73), Beltran 2016 (54), and VPC 2018 (149) patient cohorts, LTL PDX models (66,148), and LnNE (90) RNA-sequenced

datasets were analyzed to determine the expression of *GIT1* splice variants in the various prostate cancer models. The software Integrative Genomics Viewer was used to visualize the coverage of RNA-seq reads corresponding to the *GIT1* transcript. We confirmed the presence of *GIT1-A*, which differ from *GIT1-C* by an alternatively spliced 27 bp microexon (exon 8), in the NEPC models, but not the AdPC models (Figure 5.1A). All three patient cohorts confirmed a robust increase in *GIT1-A* expression in NEPC tumours ($p<0.0001$) when the expression was compared to that of AdPC or CRPC-Ad (Figure 5.1B). Interestingly, *GIT1-C* expression was decreased by 6- ($p<0.05$), 11- ($p<0.01$), and 13-fold ($p<0.0001$) in NEPC tumours when the expression was compared to AdPC subtypes in the VPC 2018, Beltran 2011, and Beltran 2016 cohorts, respectively. Although total *GIT1* levels were increased in the Beltran 2011 NEPC tumours, neither the VPC 2018 or Beltran 2016 cohorts showed significant changes in its total *GIT1* expression ($p=0.91$ and $p=0.077$, respectively). This inverse relationship between the expression of the two splice variants was validated by RT-qPCR in the LTL PDX models (Figure 5.1C), as well as in the NEPC cell models LnNE and DuNE (Figure 5.1D). Here, NEPC PDX and cell models expressed increased levels of *GIT1-A* mRNA, but decreased levels of *GIT1-C*, when compared to the levels in AdPC models. Noteworthy, the 331-7-R PDX and LnNE cells are t-NEPC models that differentiated from its AdPC phenotypes (331-7 and LNCaP, respectively) after castration (66,90). Furthermore, profiling *GIT1-A* and *GIT1-C* expression in a panel of different prostate cell lines (i.e. benign, AdPC, NEPC, SCLC) revealed that, overall, NEPC and SCLC cell lines expressed higher mRNA copy numbers of *GIT1-A* and lower mRNA copy numbers of *GIT1-C*, when compared to its expressions in benign and AdPC cell lines (Figure

5.1E). Together, these data suggest that the alternative RNA splicing of the *GIT1* transcript may be associated with the progression to t-NEPC.

Figure 5.1

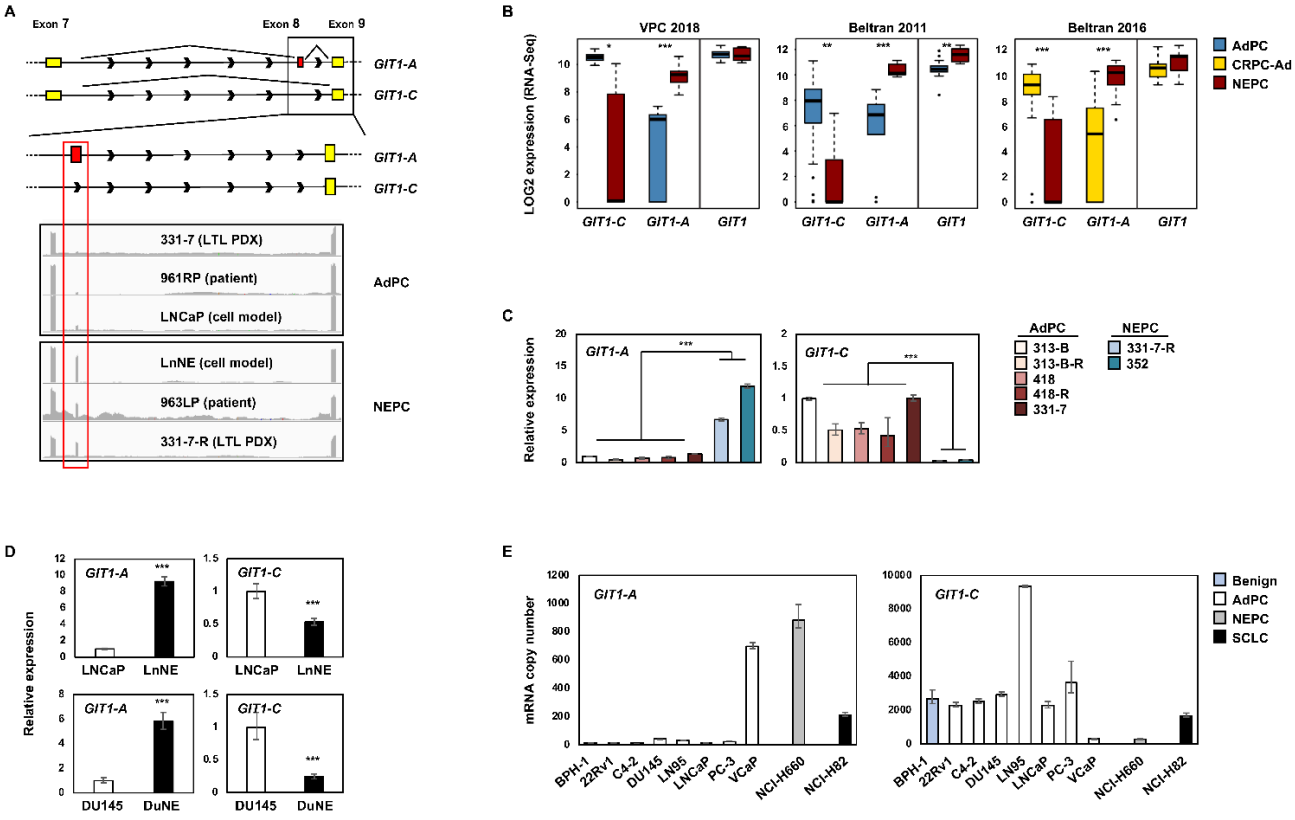

Figure 5.1 Expression profiling of *GIT1* splice variants in NEPC patient, PDX, and cell models. (A) Illustration of the *GIT1-C* and *GIT1-A* exonic regions, where yellow represents the constitutive exons and red represents the 9-amino acid alternatively spliced microexon (exon 8). Integrative Genomics Viewer was used to visualize the coverage of *GIT1* by RNA-seq reads. Grey peaks represent the sequencing depth of each respective exon. **(B)** Analyzed RNA-seq data of total *GIT1* and splice variant expressions from VPC 2018 (AdPC n=24 and NEPC n=5), Beltran 2011 (AdPC n=30 and NEPC n=7), and Beltran 2016 (CRPC-Ad n=34 and NEPC n=15) cohorts is shown. **(C-D)** Relative RNA levels of *GIT1* splice variants in **(C)** the LTL PDX models and **(D)** in the AdPC subtype (LNCaP) and NEPC cell models (LnNE and DuNE) was validated. **(E)** *GIT1* splice variant expressions were profiled from a benign prostate cell line (BPH-1), a panel of AdPC cell lines (22Rv1, C4-2, DU145, LN95, LNCaP PC-3, and VCaP), a NEPC cell line (NCI-H660) and a SCLC cell line (NCI-H82) via RT-qPCR for absolute quantification of *GIT1-A* and *GIT1-C* using a standard curve. All results are presented as the mean ±SD (Student's 2-tailed *t*-test; *, **, and *** represent $p<0.05$, $p<0.01$, and $p<0.0001$, respectively). AdPC, prostate adenocarcinoma; NEPC, neuroendocrine prostate cancer; CRPC-Ad, castration-resistant adenocarcinoma; LTL, living tumour laboratory; PDX, patient-derived xenograft; VPC, Vancouver Prostate Centre; SCLC, small-cell lung cancer.

5.2.2 RNA splicing of GIT1 is associated with clinical NEPC tumours

Currently, there are no commercially available GIT1 antibodies to specifically detect each splice variant. As a result, we utilized RISH, a well-established alternative technique (91,94,138), on a TMA to study and confirm the expression of *GIT1-A* and *GIT1-C*. We created probes to target the unique exon 7/8 junction of *GIT1-A*, as well as the exon 7/9 junction of *GIT1-C*, to detect RNA expression levels on the TMA. The human CRPC TMA contains 64 cores: 52 AdPC, 6 AdNC, and 6 SCNC. Details of these prostate cancer subtype classifications have been previously published by our group (91,94,138). Briefly, AdPC is classified by the presence of glandular structures, large cells with a prominent nucleolus, and no NE cells. Next, SCNC tumours contain only NE cell populations, grow as solid sheets, and exhibit typical NE cell features, such as scant cytoplasm, salt-and-pepper nuclei, and a high nucleus-to-cytoplasm ratio. Finally, AdNC subtypes are histologically similar to AdPC, however, they are atypical tumours comprised of a mixed-cell population containing ≥10% NE cells and are positive for at least two NE markers.

We found that *GIT1-A* is expressed in 20 out of 64 tissue cores (Appendix C). The 20 cores positive for *GIT1-A* included all 6 SCNC cores (5 of 6 had a RISH score of 2) and 5 AdNC cores (Figure 5.2A). Conversely, 51 of 52 AdPC cores were positive for *GIT1-C*, whereas only 2 AdNC and 1 SCNC cores were positive (RISH score of 1). Correlation studies indicate that *GIT1-A* expression levels increase in AdNC, and even further in SCNC, when compared to the expression in AdPC. Moreover, *GIT1-C* expression levels decrease in AdNC and SCNC when compared to the expression levels in AdPC (Figure 5.2B-C). *GIT1-A* expression showed significant positive

correlation (p<0.0001) with all three NE markers (CHGA, r=0.7209; SYP, r=0.7152; and CD56, r=0.7148) and negative correlation with markers of AdPC (AR, r=-0.3937, p=0.0013; and PSA, r=-0.3259, p=0.0086). Inversely, *GIT1-C* expression was negatively correlated with CHGA (r=-0.6193, p<0.0001), SYP (r=-0.6353, p<0.0001), and CD56 (r=-0.4158, p<0.01) expression, but positively correlated with AR expression (r=0.4105, p<0.001; Table 5.1). Furthermore, *GIT1-A* expression was positively correlated with the number of positive NE markers in a tissue core (r=0.7172, p<0.001), while *GIT1-C* expression was negatively correlated (r=-0.6473, p<0.001; Figure 5.2D).

Table 5.1 Correlation of *GIT1* splice variants with clinical diagnostic markers of AdPC and NEPC. Pearson's r correlation was performed between the expression of *GIT1-A* or *GIT1-C* and expressions of NEPC (i.e. CHGA, SYP, and CD56) or AdPC (i.e. AR and PSA) diagnostic markers used in the clinic. NEPC, neuroendocrine prostate cancer; AdPC, prostate adenocarcinoma.

Correlation with *GIT1-A*	Pearson *r* value	*p* value
CHGA	**0.7209**	**<0.0001**
SYP	**0.7152**	**<0.0001**
CD56	**0.7148**	**<0.0001**
AR	**-0.3937**	**0.0013**
PSA	**-0.3259**	**0.0086**

Correlation with *GIT1-C*	Pearson *r* value	*p* value
CHGA	**-0.6193**	**<0.0001**
SYP	**-0.6353**	**<0.0001**
CD56	**-0.4158**	**<0.001**
AR	**0.4105**	**<0.001**
PSA	**0.04045**	**ns**

Figure 5.2

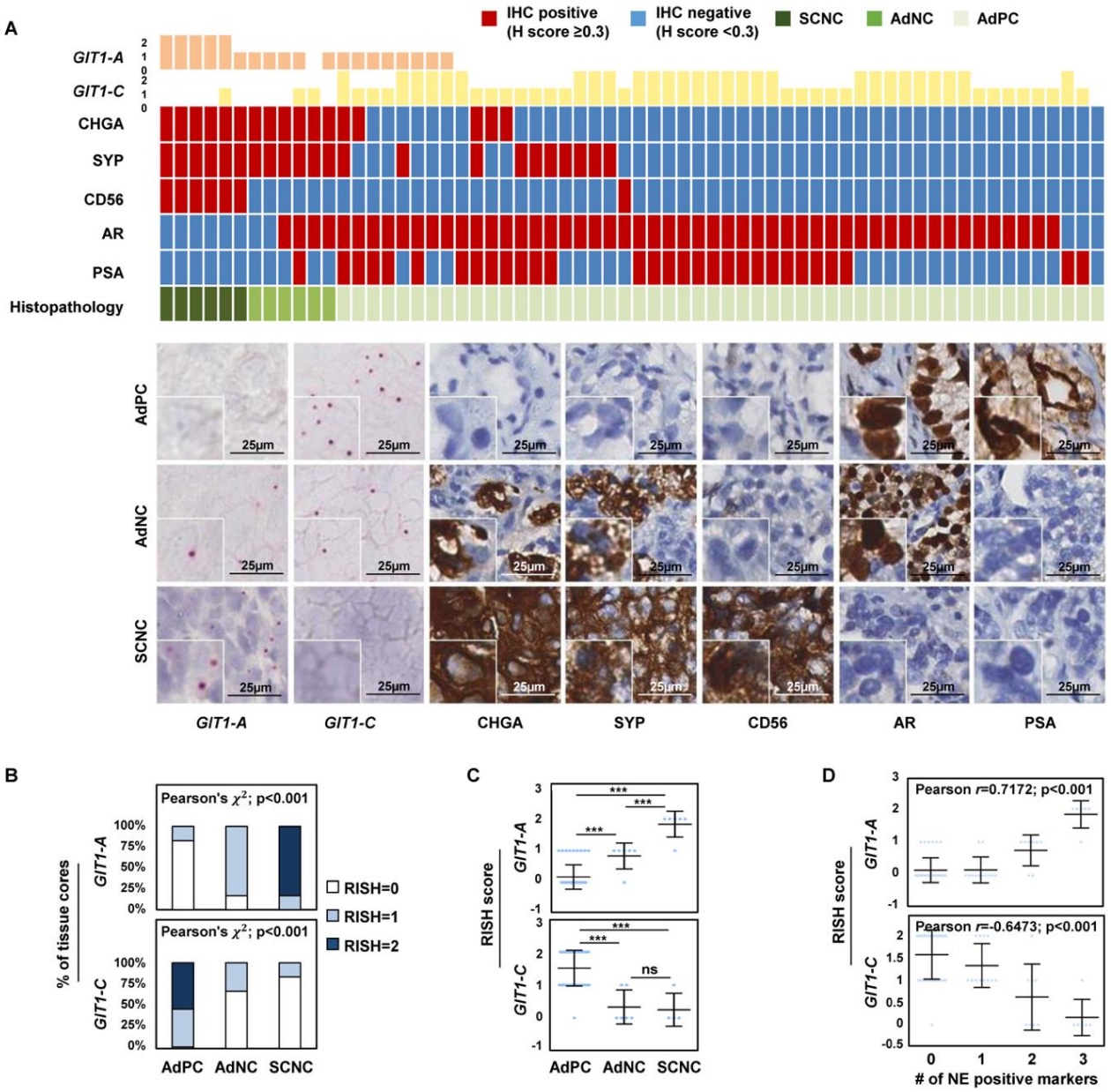

Figure 5.2 RNA splicing of *GIT1* is associated with clinical NEPC tumours. (A) RISH probes targeting the exons 7/8 or exons 7/9 junction were created to detect *GIT1-A* or *GIT1-C*, respectively, in a human CRPC TMA (n=64 cores). The TMA was stained against CHGA, SYP, CD56, AR and PSA via IHC. The columns in the heatmap represents one of sixty-four cores. One representative core from each of the histologically diagnosed AdPC (n=52), AdNC (n=6), and SCNC (n=6) core is shown. Scale bars represent 25 μm. **(B-C)** The cores were grouped accordingly to its histopathology report, and its respective RISH scores were plotted to present the **(B)** percentage of cores containing the same RISH score (Pearson's χ^2 test) or **(C)** average RISH score within each tumour subtype (one-way ANOVA; ***, p<0.001; "ns", non-significant). **(D)** RISH scores from each core were plotted with respect to the number of positive NE markers within the same core (Pearson's r correlation). RISH, RNA *in situ* hybridization; TMA, tissue microarray; CRPC, castration-resistant prostate cancer; IHC, immunohisochemistry; AdPC, prostate adenocarcinoma; AdNC, adenocarcinoma prostate cancer with neuroendocrine cells; SCNC, small-cell neuroendocrine prostate cancer; NE, neuroendocrine.

To determine the diagnostic reliability of *GIT1-A* to detect a NEPC phenotype, we defined AdNC and SCNC as a NEPC phenotype. Fisher's exact test revealed that the *GIT1-A* sensitivity of correctly identifying the NEPC phenotype was 0.917 and the specificity was 0.827 (Table 5.2). These results indicate that while *GIT1-A* is detectable in NEPC cores, the low specificity suggests that AdPC tumours may also express *GIT1-A*. However, it is unknown whether these AdPC *GIT1-A*-positive cores progressed to NEPC. Overall, these collective findings indicate a strong positive association between *GIT1* splice variant expression and t-NEPC development, namely that *GIT1-A* expression manifests largely in NEPC tumours.

Table 5.2 Sensitivity and specificity of *GIT1-A* as a biomarker for NEPC. Fisher's exact test was performed to determine the sensitivity and specificity of *GIT1-A* as a diagnostic biomarker for NEPC prediction. SCNC and AdNC is defined as NEPC in this case. NEPC, neuroendocrine prostate cancer; AdPC, prostate adenocarcinoma; SCNC, small-cell neuroendocrine prostate cancer; AdNC, adenocarcinoma prostate cancer with neuroendocrine cells.

	GIT1-A +	**GIT1-A -**	***Marginal Row Totals***	**Sensitivity**	**Specificity**
AdPC	9	43	*52*	**0.917**	**0.827**
NEPC	11	1	*12*		
Marginal Column Totals	*20*	*44*	*64 (Grand Total)*		

***p* value <0.00001**

5.2.3 SRRM4 regulates RNA splicing of GIT1

Based on our previous report, SRRM4 predominately facilitates the t-NEPC-unique RNA splicing signature, promoting the transformation of AdPC to a NEPC phenotype (90,138). RISH probes targeting *SRRM4* were hybridized on identical CRPC TMA cores (Appendix C). *SRRM4* expression was strongly correlated with *GIT1-A*

(*r*=0.7994, *p*<0.0001) and negatively correlated with *GIT1-C* expression (*r*=-0.6067, *p*<0.0001; Figure 5.3A & Table 5.3). To investigate how SRRM4 mediates *GIT1* splicing, we overexpressed SRRM4 in LNCaP cells and detected a 5-fold increase in *GIT1-A* expression and a ~40% reduction in *GIT1-C* expression (Figure 5.3B). Transfection with siRNA in the LnNE model was used to knock-down SRRM4, which reduced *GIT1-A* expression by ~20% and increased *GIT1-C* expression by 6-fold (Figure 5.3C). Within the panel of splicing factors tested, SRRM4 was unique for its *GIT1*-splicing activity (Figure 5.3D). We designed a ChIP probe specific to the 3' intron splicing site upstream of the alternatively spliced microexon 8 of *GIT1*. Using an RNA-ChIP binding assay, we determined that SRRM4 directly binds to *GIT1* and facilitates its splicing at exon 8 but does not bind to the negative control region on *GAPDH* (Figure 5.3E). Collectively, these results demonstrate that SRRM4 directly splices the *GIT1* transcript to promote the neural-specific *GIT1-A* splice product.

Table 5.3 *SRRM4* expression is associated with *GIT1* splice variant expressions in CRPC.
Pearson's *r* correlation was applied between the expressions of *GIT1-A* or *GIT1-C* and *SRRM4* expression. CRPC, castration-resistant prostate cancer; RISH, RNA in situ hybridization.

***GIT1-A* RISH score**

***SRRM4* RISH score**	**0**	**1**	**2**
0	42	5	0
1	2	7	1
2	0	3	4

***r*= 0.7994; *p*<0.0001**

***GIT1-C* RISH score**

***SRRM4* RISH score**	**0**	**1**	**2**
0	0	21	26
1	3	4	3
2	6	1	0

***r*= -0.6067; *p*<0.0001**

Figure 5.3

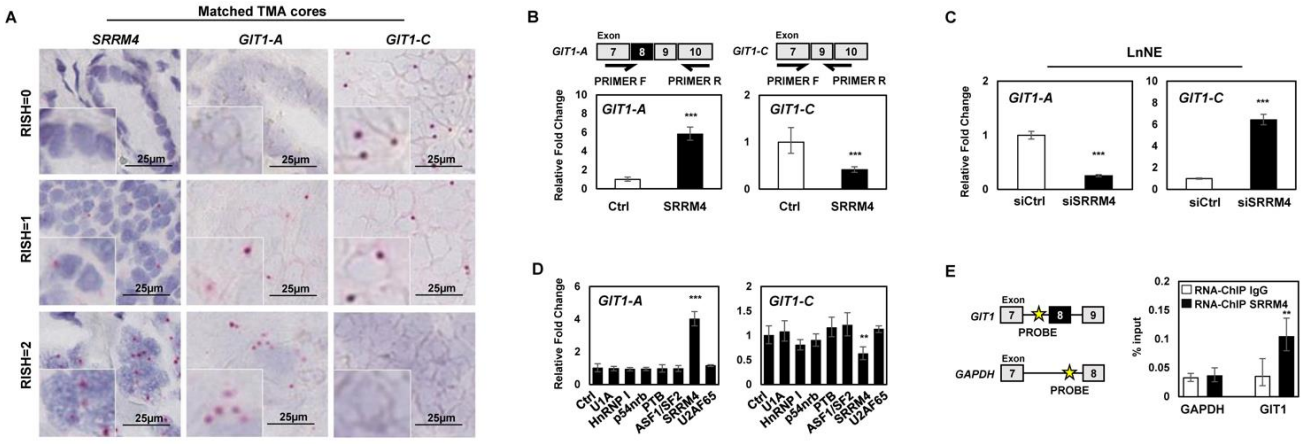

Figure 5.3 SRRM4 regulates RNA splicing of *GIT1*. (A) Matched TMA cores are shown to represent the associations of the expressions of *SRRM4* with *GIT1-A* and *GIT1-C*. Scale bars represent 25 μm. **(B)** LNCaP cells were transfected with 4 μg of flag-SRRM4 and subsequently extracted for RNA. Relative expressions of *GIT1-A* or *GIT1-C* were compared to *18S* via RT-qPCR. Primer pairs designed for unique exon junctions in *GIT1-A* and *GIT1-C* variants are illustrated. **(C)** NEPC cell model, LnNE, was transfected with 20 μM of siRNA targeting SRRM4 or negative control siRNA to determine the splicing activity of *GIT1*. **(D)** 4 μg of various RNA splicing factors or control (empty vector) were transfected into LNCaP cells and subsequently extracted for RNA. RT-qPCR was performed to compare *GIT1* splice variant expression compared to *18S* (one-way ANOVA; n=3; ** and *** denotes $p<0.01$ and $p<0.001$, respectively). **(E)** RNA-ChIP probes for the intron sequence upstream of the alternatively spliced microexon (exon 8) of *GIT1* and probes for negative-control gene *GADPH* were created, as indicated by the yellow star. RNA-ChIP was performed with LNCaP cells transfected with 10 μg of Flag-SRRM4 and immunoprecipitated with anti-Flag antibody. RNA fragments were eluted and used as templates for the antisense primers/probes via RT-qPCR. All experiments were repeated three times. Unless otherwise indicated, results are presented as the mean ±SD (Student's 2-tailed *t*-test, n=3; **, $p<0.01$; ***, $p<0.001$). Ctrl, control; TMA, tissue microarray; RNA-ChIP, RNA-chromatin immunoprecipitation.

5.2.4 Transcriptome and cellular functions of GIT1 splice variants

To determine the functional significance of GIT1-A and GIT1-C, we transduced DU145 cells to overexpress GIT1-A (DU145(GIT1-A)) or GIT1-C (DU145(GIT1-C)) and confirmed its expression by immunoblotting and RT-qPCR (Figure 5.4A). Using Ion AmpliSeq Transcriptome analyses, we profiled and compared the DU145(GIT1-A) or DU145(GIT1-C) transcriptome to DU145(Ctrl) (n=524 and n=755 genes, respectively) (Figure 5.4B). The transcriptomes were mostly distinct, with the exception of 177 genes

in common. To investigate further into the biological differences between the GIT1-A and GIT1-C transcriptomes, we performed GSEA and compared the two phenotypes, revealing that the GIT1-A transcriptome was enriched with gene sets related to neural function, morphogenesis, environmental sensing, and epigenetic regulation (Figure 5.4C). The GIT1-C transcriptome was enriched with gene sets associated with general immune function and metabolism (Appendix M). Within the four subgroups enriched in the GIT1-A transcriptome, we extracted the leading-edge genes from the “GO regulation of cell adhesion mediated by integrin,” “GO cardiac epithelial to mesenchymal transition,” and “GO neuron recognition” MSigDB gene sets and generated a heatmap using GSEA software (Figure 5.4D). Among these genes identified, we validated the expression of 9 using RT-qPCR (Figure 5.4E). These results suggest that GIT1-A and GIT1-C exhibit differential functions, whereby GIT1-A facilitates progression to a neuronal transcriptome indicative of NEPC. Consistent to the GESA predictions, we confirmed that the GIT1 splice variants differentially regulate FAs (Figure 5.5). We observed that GIT1-A promoted, while GIT1-C compromised the stability of FAs, indicated by vinculin (a universal FA marker), when DU145 cells were treated with nocodazole. Collectively, our transcriptomic and FA assays indicate distinctive functional roles of GIT1 splice variants in regulating FA stability, which may contribute to NEPC development.

Figure 5.4

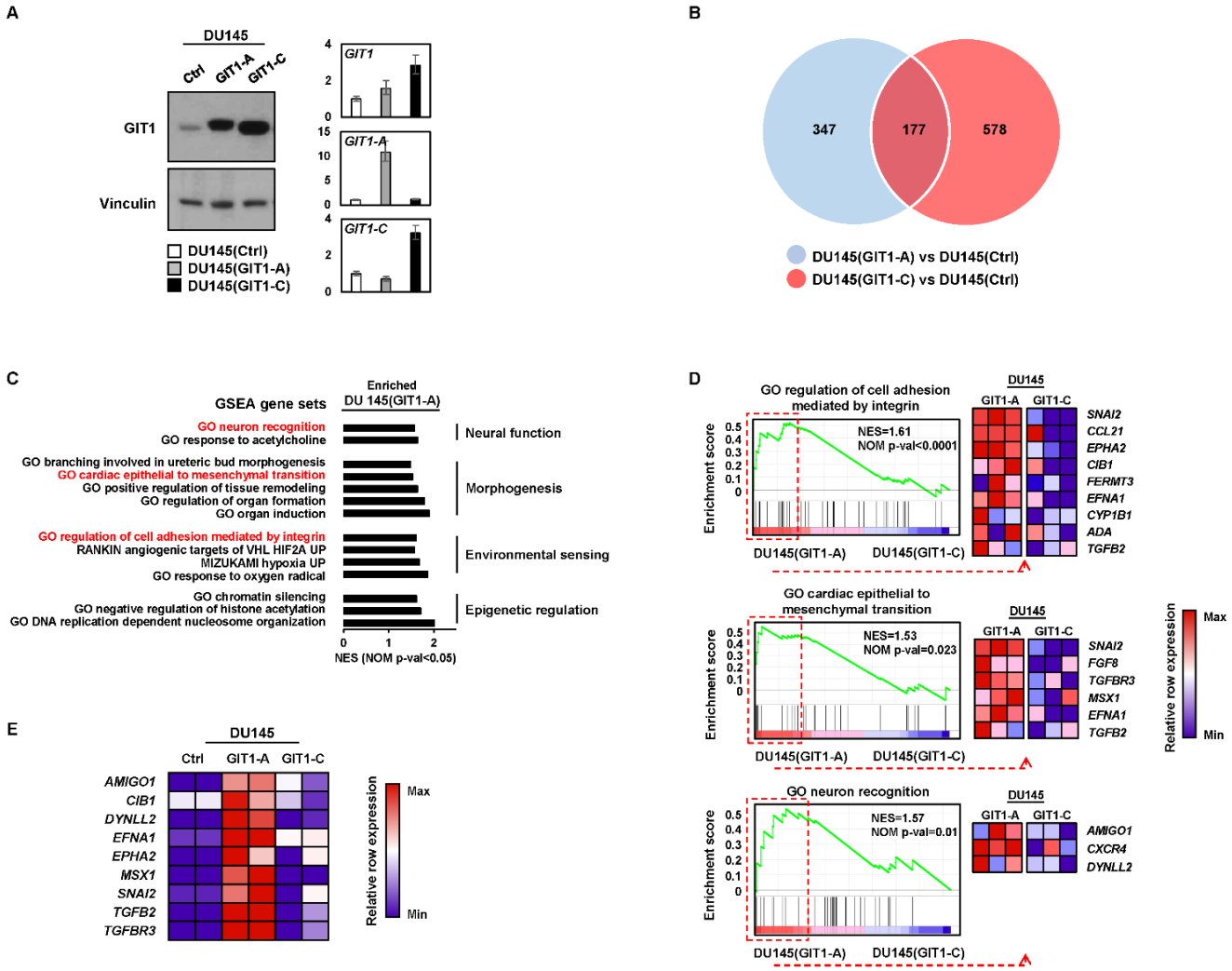

Figure 5.4 Transcriptome profiling of GIT1 splice variants. (A) DU145 stable cell lines overexpressing GIT1-A, GIT1-C, or empty vector (Ctrl) were created via lentiviral transduction and expressions were validated by immunoblot and RT-qPCR. **(B-C)** Transcriptomes of these cell lines (Ctrl, n=2; GIT1-A, n=3; GIT1-C, n=3) were profiled by Ion AmpliSeq Transcriptome. **(B)** Compared to control, genes unique to the transcriptomes of GIT1-A (n=4326) or GIT1-C (n=5003) were overlapped (n=200). **(C)** The transcriptomes of GIT1-A and GIT1-C were analyzed by GSEA based on the latest MSigDB database for each collection. GSEA revealed the enrichment of genes associated neural function, morphogenesis, and environmental sensing in the DU145(GIT1-A) cells. GSEA enrichment plots from these categories are presented where differential expressions of the leading-edge genes are shown in the heatmaps created by the GSEA software. **(D)** Expression of nine of these genes were validated and confirmed by RT-qPCR relative to the DU145(Ctrl) cell line (n=2 per cell line). Heatmap was created using the normalized z-scores of each row. All experiments were repeated three times. GSEA, gene set enrichment analysis; GO, gene ontology; NES, normalized enrichment score; NOM p-val, nominal p-value.

Figure 5.5

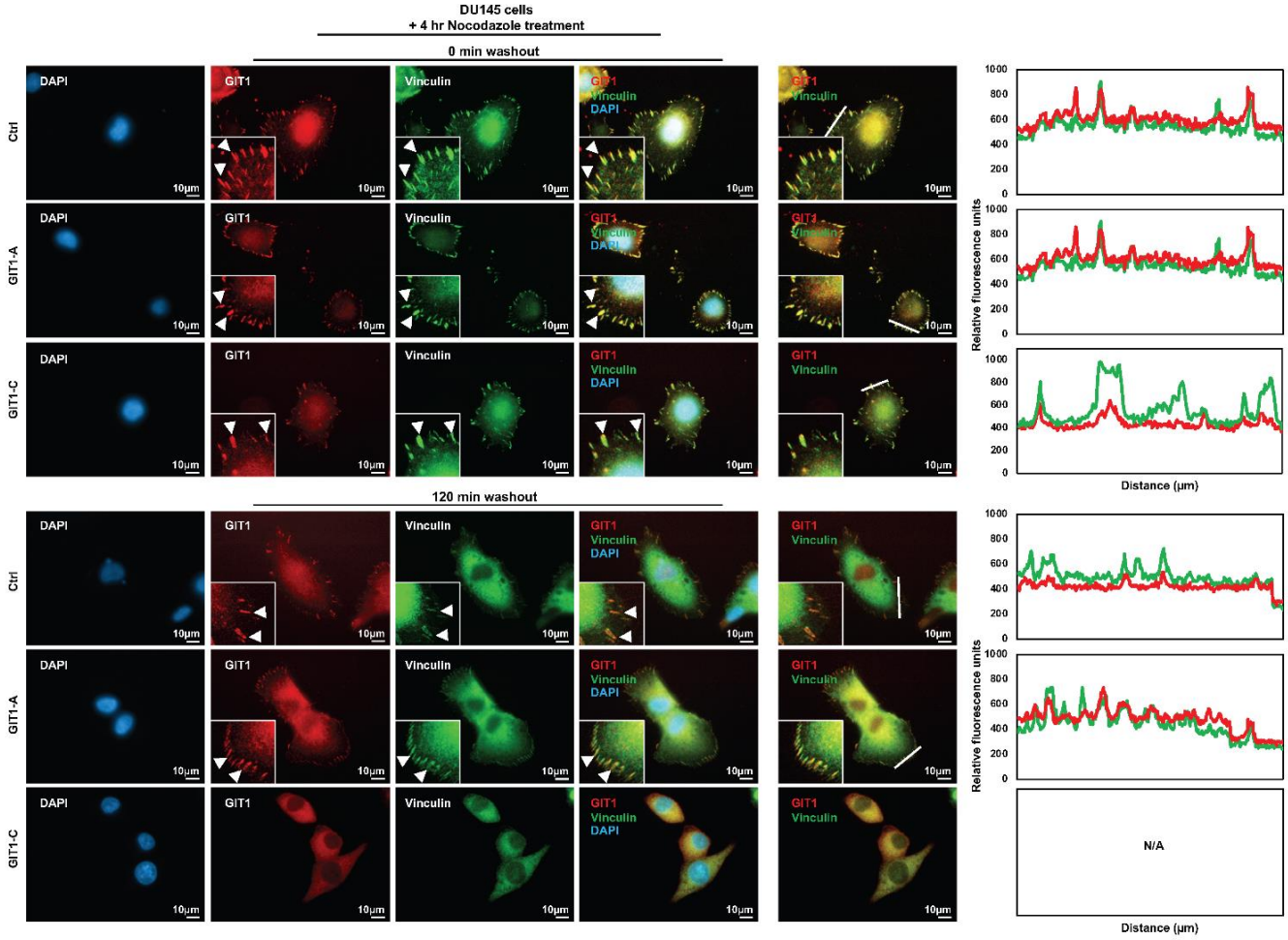

Figure 5.5 Differential functions of the GIT1 splice variants in FA stability. DU145 stable cell lines overexpressing GIT1-A, GIT1-C, or empty vector were seeded on coverslips and serum-starved the next day. They were treated with 10 μM Nocodazole for 4 hrs, subsequently washed away, and replaced with serum-containing medium. Cells were fixed at 0 or 120 min after the washout, co-stained against GIT1 and vinculin, and then mounted with DAPI staining mount. Cells were imaged using the ZEISS AxioObserver Z1 microscope, where the scale bar represents 10 μm. Arrowheads indicate FA complexes. Overlapping signals between GIT1 and vinculin appear yellow. The overlapping of the two signals in a cross section (indicated by the white line) of FA complexes were profiled by the ZEN program. All experiments were repeated three times. IF, immunofluorescence; FA, focal adhesion; ZEN, ZEISS efficient navigation.

5.3 DISCUSSION

Using patient tumour samples, PDX models, and cell models, we are the first to characterize the alternative RNA splicing of the *GIT1* transcript in its association with

NEPC progression. We found that an inverse correlation of high *GIT1-A* and low *GIT1-C* expressions are associated with the NEPC phenotype, when compared to *GIT1* splice variant expressions in AdPC subtypes (Figure 5.1 and 5.2 & Table 5.1 and 5.2). We demonstrate that SRRM4 is an important regulator of *GIT1* post-transcriptional modifications, whereby SRRM4 expression in NEPC tumours is associated with the splicing of the *GIT1* transcript (Figure 5.3 & Table 5.3). From whole-transcriptome analyses, we report differential transcriptomes of GIT1-A and GIT1-C, where GIT1-A regulates gene sets that are associated with morphogenesis, neural function, environmental sensing, and epigenetic regulation (Figure 5.4). Consistent with our transcriptomic analyses, we report opposing functions of GIT1-A and GIT1-C in the stability of FAs, whereby GIT1-A-overexpressing cells promote FA stability (Figure 5.5). Altogether, our study demonstrates that SRRM4-mediated RNA splicing of the *GIT1* transcript reprograms its function involving FA-mediated signaling and cell processes, which may contribute to t-NEPC development.

Our current understanding of SRRM4-facilitated NEPC progression involves multiple processes, including NE differentiation, apoptosis evasion, cell proliferation, and tumorigenesis. Subsequent studies have found that these processes involved in NEPC progression are facilitated by REST, Bif-1, and MEAF6 which are functionally reprogrammed via SRRM4-mediated alternative splicing to facilitate NE differentiation (90), apoptosis evasion (94), and cell proliferation and tumorigenesis (178), respectively. However, there are many other cellular functions of SRRM4 waiting to be defined. In fact, this study is the first to report that SRRM4 regulates RNA splicing of *GIT1* to reprogram its function, whereby the neural-specific GIT1-A splice variant

regulates genes associated with cell-adhesion processes (Figure 5.4C) and enhances FA stability (Figure 5.5). In support of this, DuNE is an SRRM4-mediated NEPC model that also expresses genes related to FA processes, suggesting that SRRM4 may modulate FA-mediated signaling and cell processes through the GIT1 splice variants. This understanding demonstrates that multiple gene networks and cellular processes are altered during NEPC progression, by which cell-adhesion gene networks are only a part of this multifaceted process. Moreover, SRRM4 splices genes that are canonical components of many epigenetic complexes, such as *MEAF6* and *PHF21A* (90,138,178). GIT1 has also been suggested to regulate epigenetic modifications via its interaction with MAT2B, which synthesizes methyl donors for DNA and histone methylation during cancer progression (179). Additionally, our transcriptomic analyses reveal that the GIT1-A transcriptome is enriched with gene sets related to epigenetic regulation (Figure 5.4C). Though specific epigenetic regulation of GIT1 has yet to be reported, we hypothesize that SRRM4-mediated RNA splicing mechanisms may interplay with epigenetic mechanisms to reprogram AdPC cells and facilitate t-NEPC development.

In conclusion, our research suggests that RNA splicing of the *GIT1* transcript is associated with the progression of NEPC, evident by our comprehensive transcriptomic data, which reveals distinct molecular changes regulated by GIT1-A and GIT1-C. In addition, we confirm that GIT1 splice variants differentially regulate the stability of FAs. Since SRRM4 is a demonstrated facilitator of NEPC progression, our studies may reveal a novel function of SRRM4 in regulating FA-mediated processes through *GIT1* alternative RNA splicing.

Chapter 6 Conclusions

6.1 SUMMARY OF FINDINGS

This dissertation work uncovers a novel mechanism by which SRRM4 mediates lineage plasticity required for t-NEPC development. We have demonstrated that SRRM4 mediates NE differentiation of AdPC cells via a pluripotency gene network including the *SOX2* gene in the DuNE cell model. Given the cellular heterogeneity innate to prostate tumours seen in the clinic, these results suggest that SRRM4-mediated mechanisms of t-NEPC likely relies on the cell context (i.e. specific genetic or epigenetic backgrounds). Furthermore, we have investigated a novel SRRM4-SOX2 axis which is also present in clinical NEPC patients, PDXs, and GEMMs.

Moreover, our studies characterize the downstream mechanisms and functional consequences of SRRM4-mediated alternative RNA splicing of the *MEAF6* and *GIT1* transcripts. We have found that alternative RNA splicing of the *MEAF6* and *GIT1* transcripts are directly mediated by SRRM4 and are unique to NEPC patient tumours, PDX, and cell models. Though SRRM4-mediated RNA splicing of the *MEAF6* and *GIT1* transcripts does not promote NE differentiation in AdPC cells, other functions of these t-NEPC-unique splice variants have been demonstrated to contribute to the various facets promoting t-NEPC development. SRRM4-mediated splicing of the *MEAF6* transcript reprograms the function of the neural-specific MEAF6-1 isoform to facilitate cell proliferation, migration, invasion, and tumorigenesis via the *ID1* and *ID3* genes. In fact, this study uncovers a potential novel facet involved in t-NEPC progression—invasion and migration. This cellular process is of interest as t-NEPC tumours are very aggressive and exhibit sites of metastasis in the liver and brain (26,46,188).

Consequently, SRRM4-mediated alterative splicing of the *GIT1* transcript reprograms its function involving FA-mediated signaling and cell processes through GIT1-A, which may also contribute to the migration and invasion facets involved in t-NEPC development. Importantly, this suggests a novel function of SRRM4 in regulating FA-mediated signalling pathways or processes via *GIT1* splicing.

It is not entirely possible to elucidate the origin and progression of t-NEPC solely through studying the overall genomic landscape as there are very little overlap between NEPC and AdPC phenotypes. Only recently have differences in the molecular signatures beyond the overall genomic mutational profiles been discovered, such as RNA splicing signatures. However, characterizing RNA splicing signatures of diseases are not common in our field of study, as microexons are commonly ignored during whole transcriptome analyses. Therefore, these findings contribute to an understudied field of alternative splicing-mediated reprogramming of protein function—specifically the SRRM4-mediated neural-specific exon network required for the t-NEPC disease progression. This thesis work suggests a role of SRRM4 and RNA splicing signatures (i.e. *MEAF6/GIT1*) as potential biomarkers of t-NEPC detection and diagnosis. Moreover, these studies support the notion that SRRM4 is an important facilitator of t-NEPC development. By regulating alternative RNA splicing, SRRM4 not only stimulates AdPC lineage plasticity to the NE cell lineage, but also promotes cancer cell survival, proliferation, migration, invasion, FA-processes, and tumorigenesis via alternative RNA splicing of a neural-specific exon network (Figure 6.1).

Figure 6.1

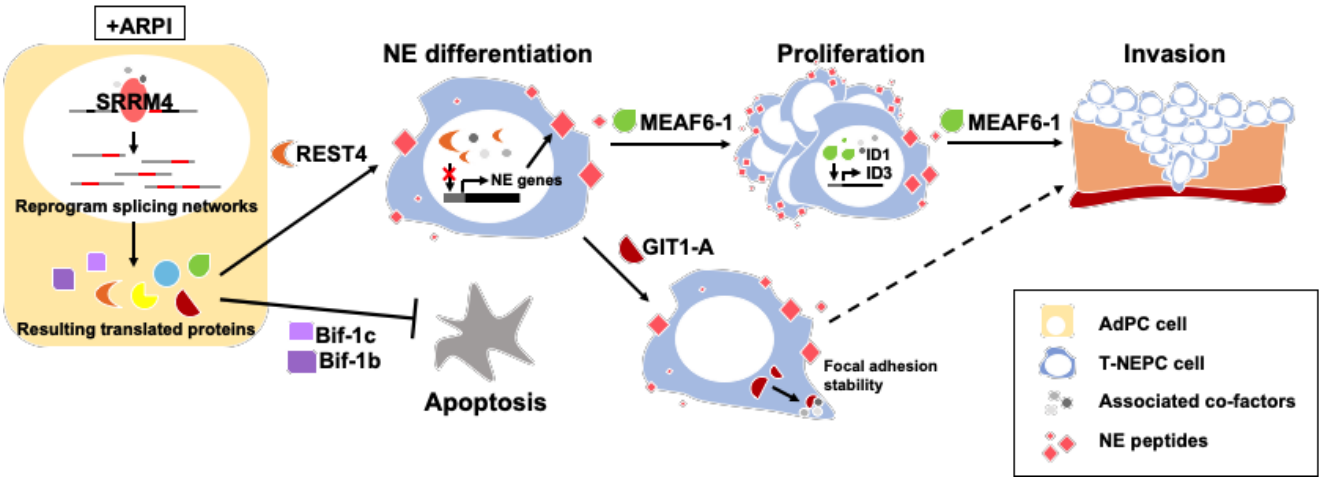

Figure 6.1 The full picture: multifaceted roles of SRRM4 in t-NEPC development is mediated by downstream neural-specific exon networks. SRRM4 promotes several facets of t-NEPC development through the alternative RNA splicing of a t-NEPC-unique splicing program. SRRM4 promotes NE differentiation via the REST4 isoform of REST (90), evasion of apoptosis via the Bif-1b and Bif-1c isoforms of Bif-1 (94), proliferation and invasion via the MEAF6-1 isoform of MEAF6, and focal adhesion-mediated cell processes and signaling which may also contribute to migration and invasion of prostate cancer cells. ARPI, androgen receptor pathway inhibitors; NE, neuroendocrine; AdPC, prostate adenocarcinoma; t-NEPC, treatment-induced neuroendocrine prostate cancer.

6.2 LIMITATIONS

6.2.1 Cell-context dependency

The heterogeneity of NEPC subtypes suggests that there are many complex mechanisms involved in the development of t-NEPC. Therefore, to understand the role of SRRM4 under the context of a heterogeneous cell population, we created several SRRM4-overexpressing cell models of different cell types. The results of this study (Chapter 3) demonstrate that SRRM4 function is cell-context dependent. Though striking NE phenotypic and morphologic alterations were seen in our DuNE model, SRRM4 function in PC-3 cells did not show such robust NE phenotypes. PC-3 cells are similar to DU145 cells as they are AR- and p53-null and exhibit stem-like characteristics. Even when depleting *RB1* expression in the SRRM4-overexpressing

PC-3 cell model, there were no changes in SRRM4 function, and these cells did not present any NE morphological or phenotypical changes (Appendix N). This reveals that exclusivity of the cell lines used and cell-context dependence on the functions of our gene-of-interests may be a large limitation in the subsequent chapters. However, to by-pass this limitation, multiple prostate cancer cell lines were used to create GIT1 and MEAF6 cell lines. Though cell context-dependent phenomena are inherent, significant discordant functions of the MEAF6 and GIT1 splice variants were not seen throughout the various AdPC cell models created. However, it would be essential to investigate the functions of SRRM4, GIT1, and MEAF6 in NEPC cell models. Unfortunately, there are limited NEPC models (including one bona fide NEPC cell model) to utilize. This challenge will be discussed in the below sections.

6.2.2 Previous knowledge of MEAF6 and GIT1 splice variants

Though these findings on the function of *MEAF6* and *GIT1* neural-specific splice variants have provided a novel contribution to the field of alternative splicing, t-NEPC, and potentially other neural-related diseases, the limited knowledge on the functional significance of these splice variants have proved to be challenging during the studies. One of the main limitations of this work is the lack of analyses on the splice variant expressions at the protein level as there are no commercially available antibodies for these specific splice variants. Characterizing and detecting the splicing activity of the transcripts in human tumour samples would provide a stronger rationale in the use of RNA splicing as a biomarker of NEPC progression and phenotype. However, to circumvent this challenge, our lab has established RISH techniques and generated specific probes to detect *SRRM4* and *GIT1* splice variants in clinical tumour samples.

As discussed in our Chapter 5 results, the expressions of *SRRM4* and *GIT1* splice variants are associated with the different phenotypes of prostate cancer (i.e. AdPC, AdNC, and SCNC). High, low, and no expression levels of *SRRM4* and *GIT1-A* (i.e. a RISH score of 2, 1, and 0, respectively) are detected in SCNC, AdNC, and AdPC, respectively, whereas *GIT1-C* expressions reveal an opposite trend. This suggests that splicing activity of *GIT1* and *SRRM4* increases as the disease progresses from AdPC to SCNC, where AdNC phenotypes are suggested to be an intermediate phase of AdPC and SCNC. However, further investigation is required for the *MEAF6* splice variant expressions in these CRPC tumour cohorts.

Moreover, one of the criticisms of our MEAF6 and GIT1 splice variant-overexpressing cell models is that endogenous levels of constitutive MEAF6 and GIT1 variants are naturally expressed in the prostate cancer cell lines used. Thus, this basal expression combined with the exogenous expressions may interfere with the phenotypes and functions seen in our cell models. To counteract this, it is required to deplete the endogenous mRNA expression levels in the overexpressing cell lines. One method of knockdown is through a shRNA targeting the untranslated regions (UTR) of the transcript. In fact, we have found a shRNA targeting the 3' UTR region of the *GIT1* transcript (189) and have created stable cell lines with both the depletion of endogenous GIT1 and overexpression of GIT1 splice variants (Appendix Oi). Though these cell models have produced similar results as the single overexpression cell models, revealing no changes in migration, proliferation, invasion, and differentiation, GIT1 functions in FA stability have demonstrated to be more robust in the double expression cell models when compared to sole overexpression (Appendix Oii). Unfortunately, due

to the difficulty in constructing shRNA targeting the UTR regions of the *MEAF6* transcript, we could not perform the same experiments. However, given that the GIT1 splice variant functions did not exhibit significant differences when co-expressed with total GIT1 depletion, we suspect that MEAF6 splice variant functions under the depletion of endogenous MEAF6 will remain similar to the single overexpression cell models, if not increased. Additionally, due to the novelty of studying the splice variants of *MEAF6* and *GIT1*, there are no commercially available siRNA or shRNA targeting the specific splice variants of *MEAF6* and *GIT1*. This creates a challenge in investigating the functional significance of the neural-specific variants in NEPC models, which highly express the neural-specific splice variants of *MEAF6* and *GIT1*. Though efforts have been made with the only bona fide NEPC cell model, NCI-H660, these cell lines have proved to be difficult in culturing, transfecting, and transducing.

6.2.3 Challenges of NEPC in the lab

6.2.3.1 NEPC models

As previously mentioned in the discussions of my main chapters, there are limited NEPC cell and xenograft models that can be utilized to efficiently manipulate signaling pathways in order to study the molecular mechanisms of NEPC development. The only bona fide NEPC cell line, NCI-H660, is a slow growing cell line with a doubling time of >100 hrs (164), rendering cell transfections and transductions very difficult. The newly developed LnNE NEPC models have global transcription signatures and phenotypical characteristics similar to that of NEPC patient tumours (90,93). Because the tumours are generated by serially passaging for 5 generations in castrated mice, the LnNE P1 to P5 (P, passage) models replicate prolonged transition processes of AdPC

progression to NEPC, whereby the P5 cells and tumours, although AR positive, become PSA negative even in the presence of androgens (93). Excitingly, this thesis work has created another NEPC cell and xenograft model called the DuNE model. In comparison to the LnNE model, the DuNE cells develop into xenografts faster, and its derived xenografts present more robust LE and NE marker profiles. The DuNE model closely recapitulates the molecular and cellular phenotypes resembling SCNC subtypes of NEPC, whereby both the DuNE model and SCNC tumours express pluripotency gene networks including high *SOX2* expressions. Moreover, the DuNE model may be a suitable model for high-throughput drug screening. Altogether, this newly established DuNE NEPC model adds to the small handful of available NEPC cell and tumour models and may be a clinically relevant model to study the molecular complexity of AdPC progression to NEPC.

6.2.3.2 NEPC as a chronic disease

Despite great advances and efforts in t-NEPC, the diverse and dynamic changes in which tumour cells undergo to become malignant and tumorigenic remains an enigma due to its perplexity. One of the utmost challenges in delineating the molecular mechanisms of t-NEPC development is that the transition from AdPC to t-NEPC is a chronic process involving multiple intermediate phenotypes and molecular events such as genetic aberrations or epigenetic alterations (46,48,58). Furthermore, this disease progression is difficult to monitor as its aggressiveness results in a short viability from the time of diagnosis to patient death. As mentioned in the section above, to study this chronic and progressive disease, we have utilized a CRPC tumour cohort that contains AdPC, AdNC, and SCNC. Though it is unknown whether the tumours presenting AdNC

phenotypes progressed to SCNC, these tumours exhibit an intermediate phenotype. Yet, whether SRRM4 promotes t-NEPC in the clinic is unknown since the progression is hard to follow. Furthermore, the ARPI-induced AdPC to t-NEPC progressive LTL 331/331-R PDX model was studied to characterize the role of SRRM4 and SRRM4-mediated alternative splicing during this progression. However, as seen in Figure 3.6, we could not interpret any significant associations of the expressions of *AR*, *SRRM4*, *SYP*, and *SOX2* with the disease progression of AdPC to t-NEPC. In fact, we only observe an increase in the expression of *SOX2* and decrease in the *AR* expression prior to relapse (i.e. week 12 of castration), whereas *SYP* and *SRRM4* expression spikes in the relapsed tumours. Though *SRRM4* expression seems to be a result of ARPI, our lab has recently observed existing *SRRM4*-positive populations in ~16% of the treatment-naïve AdPC tumour cores studied, where the prevalence and expression of *SRRM4* increases after therapeutic interventions such as ARPI in CRPC-Ad tumours (91). In that study, we propose that one of the earliest initial molecular events in the emergence of SRRM4-mediated t-NEPC occurs in two possible ways. One way is that the existing *SRRM4*-positive population of prostate cancer cells is selected for survival under the selection pressures of ARPI. Alternatively, prolonged ARPI can increase *SRRM4* expression via epigenetic alterations regulated, in part, by AR. Although the specific molecular cross-talk mechanisms between AR and SRRM4 remain to be discovered, this suggests that the conjunction of ARPI and *SRRM4* expression may promote CRPC-Ad progression to t-NEPC rather than the expression of *SRRM4* as a passenger in the event of t-NEPC emergence.

6.3 FUTURE DIRECTIONS

Future directions of my project certainly involve further investigation on the functions of SRRM4 as well as MEAF6 and GIT1 splice isoforms in our newly established LnNE and DuNE NEPC tumour models as well as up-and-coming 3D NEPC organoid models. Furthermore, it is also important to note that SRRM4 may facilitate t-NEPC progression in conjunction with other recognized pathways and factors important for t-NEPC development, such as epigenetic and environmental factors (Figure 6.2). In this section, further directions of this thesis work will be discussed as well as how SRRM4 may be connected to these different factors to promote t-NEPC progression.

Figure 6.2

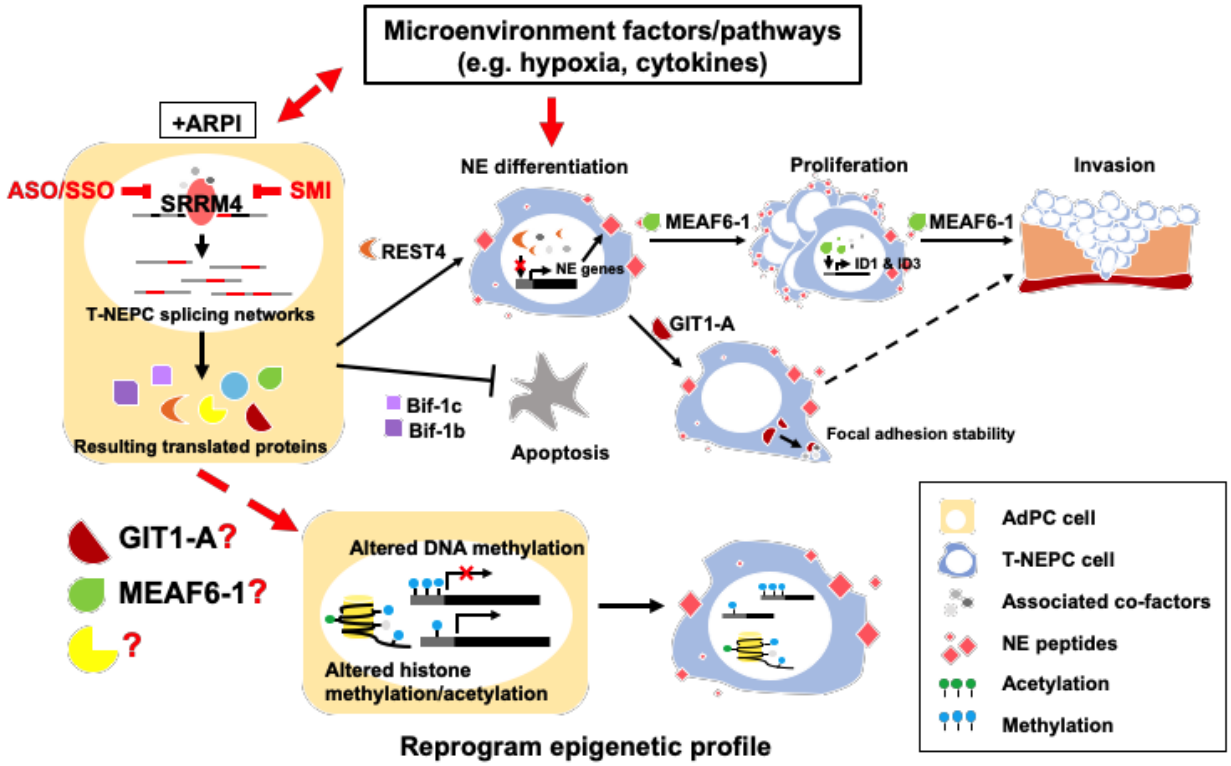

Figure 6.2 Future directions. Given that SRRM4 splices genes (i.e. MEAF6, PHF21A, and potentially GIT1) related to epigenetic functions, we hypothesize that SRRM4 may function at the epigenetic level as well or work in conjunction or cross-regulation with epigenetic mechanisms or microenvironmental factors (such as hypoxia and cytokines). ARPI, androgen receptor pathway inhibitors; NE, neuroendocrine; AdPC, prostate adenocarcinoma; t-NEPC, treatment-induced neuroendocrine prostate cancer; SMI, small molecule inhibitors; ASO, antisense oligonucleotides; SSO, splice-switching oligonucleotides.

6.3.1 SRRM4 and the epigenome

Given that SRRM4 splices transcripts (i.e. *MEAF6*, *PHF21A*, and potentially *GIT1*) related to epigenetic functions, we hypothesize that SRRM4 may function at the epigenetic level as well or work in conjunction or cross-regulation with epigenetic mechanisms. For example, the constitutive PHF21A variant may facilitate altered histone deacetylation or demethylase activity as the SRRM4-mediated inclusion of the alternatively spliced exon disrupts an AT hook responsible for DNA binding, as well as one of the two predicted nuclear localization signals of PHF21A (190). Similarly, in the neural-specific *MEAF6*-1 mRNA, the inclusion of the neural-specific exon affects the nuclear localization signal at the C-terminus of the resulting protein. Our pilot studies on the sub-localization of the MEAF6 splice variants reveal differential localization of the splice variants (Appendix P). The ubiquitously expressed MEAF6-2 splice isoform localizes strictly within the nucleoli, whereas the t-NEPC-specific MEAF6-1 variant localizes within both the nucleus and in the nucleoli, suggesting its role in both the nucleoli and nucleus. Though the canonical function of the nucleoli is to house ribosomal biogenesis, it has recently been suggested to be a hub in the regulation of several other fundamental cellular processes such as epigenetic regulation and maintenance of genomic stability (191). Therefore, it would be interesting to profile any epigenetic changes induced by SRRM4 and/or investigate the contributions of the downstream splice variants to t-NEPC-specific epigenetic signatures.

6.3.2 SRRM4 and the microenvironment

It is important to note that SRRM4 may facilitate t-NEPC progression in conjunction with other known pathways and factors important for t-NEPC development, such as the tumour microenvironment. For example, stress factors from therapeutics such as ARPI have been demonstrated to induce t-NEPC (46,54,83) and potentially *SRRM4* expression (91) as previously mentioned (section 6.2.3.2). Although further studies are required to elucidate the complexity of the mechanisms associated with environmental factor-mediated emergence of t-NEPC, studies to date have suggested that the microenvironment is an important inducer of lineage plasticity and differentiation to the NE cell lineage. Other studies have revealed other various environmental factors important in NEPC development such as cAMP (155,157), cytokines (i.e. IL6 and IL8) (156,168), and hypoxia (154,159). However, the induction of the NE phenotype by environmental factors is ultimately reversible, suggesting that other factors or molecular mechanisms—perhaps SRRM4—are essential to the development of t-NEPC.

Mitogenic cytokines, such as IL8 and IL6 (156,168,192,193), in the tumour stromal microenvironment have been proposed to promote the emergence of t-NEPC. It has recently been demonstrated that IL6 can induce NE differentiation in LNCaP cells by suppressing REST function, whereas exogenous REST can abolish the IL6-induced NE program (168). Another study reports that depletion of REST expression is essential for IL6-induced NE differentiation (194). Interestingly, both IL6 and REST have both been implicated in hypoxia-induced NE differentiation (154). Hypoxia is another important regulator of NE differentiation in prostate cancer cells. In fact, hypoxia-

induced NE differentiation of prostate cancer cells relies on the inhibition of REST, which is also a regulator of hypoxia-induced genes (154,195). These studies suggest a possible mechanism of tumour microenvironment factors, such as hypoxia and cytokines, and REST in promoting NE differentiation. Connecting these pathways together, it is possible that SRRM4 may interplay with the environment, where inhibition of REST function can be augmented by SRRM4 to promote the NE lineage cell fate in AdPC cells under hypoxic conditions. Consequently, it is possible that SRRM4 may act in conjunction or synergy with tumour microenvironment factors (such as IL6), regulators (i.e. regulator of hypoxia, REST), and stressors (i.e. ARPI and hypoxia) to push t-NEPC development and progression. Tumour microenvironment-induced pathways and factors have gained a lot of attention in the progression of AdPC tumours to t-NEPC as hypoxia-induced characteristics such as necrosis and high mitotic index are very common in t-NEPC tumours (46,196). Defining any mechanistic connections between the roles and mechanisms of SRRM4 and the tumour microenvironment would, not only be a novel discovery, but also provide a more intimate understanding of the t-NEPC tumour biology.

6.3.3 Targeting SRRM4

The fact that a plethora of factors have recognized involvements in facilitating or contributing to t-NEPC development, emphasizes the heterogeneity of t-NEPC at several levels. Therefore, further investigation is needed to understand how these different molecular mechanisms and players, environmental factors, and signaling pathways interplay to promote the emergence and development of t-NEPC. Ultimately this knowledge will provide insight for personalized medicine-based strategies for

prostate cancer patients. These efforts will rationalize SRRM4 and its t-NEPC-unique splice variants as potential diagnostic or prognostic biomarkers and SRRM4 as a therapeutic target in t-NEPC patients.

In fact, SRRM4 fulfills several criteria to be a possible therapeutic target. Although SRRM4 has been shown to be critical during neural development (95,96,98,116), a partial deletion of 2710 bp of the 3' end of the *srrm4* gene (resulting in the removal of the last exon encoding the RS domain, which is important for its RNA-splicing and splice-site function) does not result in embryonic lethality in Bronx Waltzer mice (121). These mice present abnormal splicing patterns in their hearing and balance organ (i.e. hair cells) and exhibit abnormal neural behaviors such as deafness and impaired balance. However, this study reports no splicing defects in the cerebellum and neocortex (centres of the brain involved in balance, coordinated motor movements, higher brain function such as perception, cognition, and reasoning) of the mice and demonstrates that SRRM4 function is not critical in all neural tissues (121). This suggests that specific inactivation of the SRRM4 splicing activity, while maintaining the majority of the protein, may have limited side effects. Furthermore, SRRM4 expression, though high in the brain during embryonic development of the neural system, decreases in adult tissues and is rarely detected in non-neuronal cells (95,98,100). Nevertheless, it would be important to carefully design SRRM4-specific inhibitors that cannot cross the blood-brain barrier in order to limit potential off-target effects of SRRM4-targeted drugs to the nervous system.

There are several ways to block SRRM4 function. Small molecule inhibitors (SMI) can either target the RNA-binding domain of SRRM4 to prevent it from

recognizing its RNA substrates or can directly inhibit the C-terminus domains important for the splicing activity of SRRM4. In fact, although the exact mechanism of splicing inhibition is currently unknown, a SMI compound called LMI070 is currently under clinical trials to treat spinal muscular atrophy, by binding to the RNA itself or RNA-binding domains of splicing factors (197). Before designing SRRM4-targeting SMI, the SRRM4 protein must be crystalized via microfluidics reaction technology or cryo-electron microscopy methods. However, these techniques face many challenges, such as the requirement of a large amount of protein purification and low resolution, respectively. Furthermore, the RS domain of SRRM4 is highly charged, rendering crystallization of the protein very difficult. If SRRM4 crystallization is a success, SMI that bind to either the RS domain or the C-terminus domain may be designed. Alternatively, antisense oligonucleotides (ASO) or splice-switching oligonucleotides (SSO), which can inhibit or redirect SRRM4-mediated alternative splicing events, may be effective in inhibiting SRRM4 splicing events of t-NEPC-unique transcripts (i.e. *MEAF6*/*GIT1*). In fact, the first Food and Drug Administration-approved ASO/SSO called SPINRAZA™ has shown to be effective in patients with spinal muscular atrophy, a genetic disorder whereby altered RNA splicing patterns of the survival motor neuron (SMN) transcript result in an unstable and dysfunctional SMN protein (197,198). SPINRAZA™ targets the splicing events of the SMN transcript by silencing the splicing silencer element in the intron region upstream of the alternatively spliced exon. Although further mechanistic studies are warranted, a similar method may be applied in mitigating t-NEPC progression, whereby cautiously engineered ASO/SSO could inhibit the SRRM4-recognized consensus RNA-binding UGC motifs on target transcripts (98). These

methods highlight the potential of targeting SRRM4 for future t-NEPC therapeutic programs.

Bibliography

1. Bray F, Ferlay J, Soerjomataram I, Siegel RL, Torre LA, Jemal A. Global cancer statistics 2018: GLOBOCAN estimates of incidence and mortality worldwide for 36 cancers in 185 countries. CA Cancer J Clin. 2018;

2. Wein AJ, Kavoussi LR, Campbell MF (Meredith F. Campbell-Walsh urology. Vol. 4. Urology. Vol. 4. 2012.

3. Hayward SW, Cunha GR. The prostate: Development and physiology. Radiologic Clinics of North America. 2000.

4. Hayward SW, Haughney PC, Rosen MA, Greulich KM, Weier HUG, Dahiya R, et al. Interactions between adult human prostatic epithelium and rat urogenital sinus mesenchyme in a tissue recombination model. Differentiation. 1998;

5. Zhou Y, Bolton EC, Jones JO. Androgens and androgen receptor signaling in prostate tumorigenesis. J Mol Endocrinol [Internet]. 2015;54(1):R15-29. Available from: http://www.ncbi.nlm.nih.gov/pubmed/25351819

6. Pointis G, Latreille MT, Mignot TM, Janssens Y, Cedard L. Regulation of testosterone synthesis in the fetal mouse testis. J Steroid Biochem. 1979;

7. Pointis G, Latreille MT, Cedard L. Gonado-pituitary relationships in the fetal mouse at various times during sexual differentiation. J Endocrinol. 1980;

8. Yan G, Fukabori Y, Nikolaropoulos S, Wang F, McKeehan WL. Heparin-binding keratinocyte growth factor is a candidate stromal-to-epithelial-cell andromedin. Mol Endocrinol. 1992;

9. Lu W, Luo Y, Kan M, McKeehan WL. Fibroblast growth factor-10: A second candidate stromal to epithelial cell andromedin in prostate. J Biol Chem. 1999;

10. Wang Y, Hayward SW, Cao M, Thayer KA, Cunha GR. Cell differentiation lineage in the prostate. Differentiation. 2001;

11. McNeal JE. The zonal anatomy of the prostate. Prostate. 1981;

12. De Marzo AM, Meeker AK, Epstein JI, Coffey DS. Prostate stem cell compartments: Expression of the cell cycle inhibitor p27(Kip1) in normal, hyperplastic, and neoplastic cells. Am J Pathol. 1998;

13. Aumüller G, Leonhardt M, Renneberg H, von Rahden B, Bjartell A, Abrahamsson PA. Semiquantitative morphology of human prostatic development and regional distribution of prostatic neuroendocrine cells. Prostate. 2001;

14. Lee SWH, Chan EMC, Lai YK. The global burden of lower urinary tract symptoms suggestive of benign prostatic hyperplasia: A systematic review and meta-analysis. Sci Rep. 2017;

15. Tosoian JJ, Alam R, Ball MW, Carter HB, Epstein JI. Managing high-grade prostatic intraepithelial neoplasia (HGPIN) and atypical glands on prostate biopsy. Nature Reviews Urology. 2018.

16. Mottet N, Bellmunt J, Briers E, Bolla M, Cornford P, De Santis M, et al. EAU - ESTRO - SIOG Guidelines on Prostate Cancer. Eur Assoc Urol. 2016;

17. Patel AR, Klein EA. Risk factors for prostate cancer. Nature Clinical Practice Urology. 2009.

18. Huggins C, Hodges C V. Studies on prostatic cancer i. the effect of castration, of estrogen and of androgen injection on serum phosphatases in metastatic carcinoma of the prostate. Cancer Res. 1941;

19. Prensner JR, Rubin MA, Wei JT, Chinnaiyan AM. Beyond PSA: The next generation of prostate cancer biomarkers. Science Translational Medicine. 2012.

20. Sridhar SS, Freedland SJ, Gleave ME, Higano C, Mulders P, Parker C, et al. Castration-resistant prostate cancer: From new pathophysiology to new treatment. European Urology. 2014.

21. Mohler JL. Castration-recurrent prostate cancer is not androgen-independent. In: Advances in Experimental Medicine and Biology. 2008.

22. Paller CJ, Antonarakis ES. Management of biochemically recurrent prostate cancer after local therapy: Evolving standards of care and new directions. Clin Adv Hematol Oncol. 2013;

23. Karantanos T, Corn PG, Thompson TC. Prostate cancer progression after androgen deprivation therapy: Mechanisms of castrate resistance and novel therapeutic approaches. Oncogene. 2013.

24. de Bono JS, Logothetis CJ, Molina A, Fizazi K, North S, Chu L, et al. Abiraterone and increased survival in metastatic prostate cancer. N Engl J Med [Internet]. 2011/05/27. 2011;364(21):1995–2005. Available from: https://www.ncbi.nlm.nih.gov/pubmed/21612468

25. Scher HI, Fizazi K, Saad F, Taplin ME, Sternberg CN, Miller K, et al. Increased survival with enzalutamide in prostate cancer after chemotherapy. N Engl J Med [Internet]. 2012/08/17. 2012;367(13):1187–97. Available from: https://www.ncbi.nlm.nih.gov/pubmed/22894553

26. Pezaro CJ, Omlin A, Lorente D, Nava Rodrigues D, Ferraldeschi R, Bianchini D, et al. Visceral disease in castration-resistant prostate cancer. Eur Urol. 2014;

27. Locke JA, Guns ES, Lubik AA, Adomat HH, Hendy SC, Wood CA, et al. Androgen Levels increase by intratumoral de novo steroidogenesis during progression of castration-resistant prostate cancer. Cancer Res. 2008;

28. Labrie F, Bélanger A, Luu-The V, Labrie C, Simard J, Cusan L, et al. Gonadotropin-releasing hormone agonists in the treatment of prostate cancer. Endocrine Reviews. 2005.

29. Montgomery RB, Mostaghel EA, Vessella R, Hess DL, Kalhorn TF, Higano CS, et al. Maintenance of intratumoral androgens in metastatic prostate cancer: A mechanism for castration-resistant tumor growth. Cancer Res. 2008;

30. Visakorpi T, Hyytinen E, Koivisto P, Tanner M, Keinanen R, Palmberg C, et al. In vivo amplification of the androgen receptor gene and progression of human prostate cancer. Nat Genet [Internet]. 1995;9(4):401–6. Available from: http://www.ncbi.nlm.nih.gov/pubmed/7795646

31. Marcelli M, Ittmann M, Mariani S, Sutherland R, Nigam R, Murthy L, et al. Androgen receptor mutations in prostate cancer. Cancer Res [Internet]. 2000;60(4):944–9. Available from: http://www.ncbi.nlm.nih.gov/pubmed/10706109

32. Linja MJ, Savinainen KJ, Saramaki OR, Tammela TL, Vessella RL, Visakorpi T. Amplification and overexpression of androgen receptor gene in hormone-refractory prostate cancer. Cancer Res [Internet]. 2001;61(9):3550–5. Available from: http://www.ncbi.nlm.nih.gov/pubmed/11325816

33. Joseph JD, Lu N, Qian J, Sensintaffar J, Shao G, Brigham D, et al. A clinically relevant androgen receptor mutation confers resistance to second-generation antiandrogens enzalutamide and ARN-509. Cancer Discov [Internet]. 2013;3(9):1020–9. Available from: http://www.ncbi.nlm.nih.gov/pubmed/23779130

34. Korpal M, Korn JM, Gao X, Rakiec DP, Ruddy DA, Doshi S, et al. An F876L mutation in androgen receptor confers genetic and phenotypic resistance to MDV3100 (enzalutamide). Cancer Discov [Internet]. 2013;3(9):1030–43. Available from: http://www.ncbi.nlm.nih.gov/pubmed/23842682

35. Guo Z, Yang X, Sun F, Jiang R, Linn DE, Chen H, et al. A novel androgen receptor splice variant is up-regulated during prostate cancer progression and promotes androgen depletion-resistant growth. Cancer Res [Internet]. 2009/02/27. 2009;69(6):2305–13. Available from: https://www.ncbi.nlm.nih.gov/pubmed/19244107

36. Hu R, Dunn TA, Wei S, Isharwal S, Veltri RW, Humphreys E, et al. Ligand-independent androgen

receptor variants derived from splicing of cryptic exons signify hormone-refractory prostate cancer. Cancer Res [Internet]. 2009/01/02. 2009;69(1):16–22. Available from: https://www.ncbi.nlm.nih.gov/pubmed/19117982

37. Sun S, Sprenger CC, Vessella RL, Haugk K, Soriano K, Mostaghel EA, et al. Castration resistance in human prostate cancer is conferred by a frequently occurring androgen receptor splice variant. J Clin Invest [Internet]. 2010/07/21. 2010;120(8):2715–30. Available from: https://www.ncbi.nlm.nih.gov/pubmed/20644256

38. Li H, Xie N, Chen R, Verreault MM, Fazli L, Gleave ME, et al. UGT2B17 expedites progression of castration-resistant prostate cancers by promoting ligand-independent AR signaling. Cancer Res. 2016;76(22):6701–11.

39. Arora VK, Schenkein E, Murali R, Subudhi SK, Wongvipat J, Balbas MD, et al. Glucocorticoid receptor confers resistance to antiandrogens by bypassing androgen receptor blockade. Cell [Internet]. 2013/12/10. 2013;155(6):1309–22. Available from: https://www.ncbi.nlm.nih.gov/pubmed/24315100

40. Watson PA, Arora VK, Sawyers CL. Emerging mechanisms of resistance to androgen receptor inhibitors in prostate cancer. Nat Rev Cancer [Internet]. 2015/11/14. 2015;15(12):701–11. Available from: https://www.ncbi.nlm.nih.gov/pubmed/26563462

41. Bluemn EG, Coleman IM, Lucas JM, Coleman RT, Hernandez-Lopez S, Tharakan R, et al. Androgen Receptor Pathway-Independent Prostate Cancer Is Sustained through FGF Signaling. Cancer Cell [Internet]. 2017;32(4):474–489 e6. Available from: http://www.ncbi.nlm.nih.gov/pubmed/29017058

42. Hirano D, Okada Y, Minei S, Takimoto Y, Nemoto N. Neuroendocrine differentiation in hormone refractory prostate cancer following androgen deprivation therapy. Eur Urol [Internet]. 2004/04/15. 2004;45(5):586–92; discussion 592. Available from: https://www.ncbi.nlm.nih.gov/pubmed/15082200

43. Sasaki T, Komiya A, Suzuki H, Shimbo M, Ueda T, Akakura K, et al. Changes in chromogranin a serum levels during endocrine therapy in metastatic prostate cancer patients. Eur Urol [Internet]. 2005/07/12. 2005;48(2):224–30. Available from: https://www.ncbi.nlm.nih.gov/pubmed/16005374

44. Aparicio A, Logothetis CJ, Maity SN. Understanding the lethal variant of prostate cancer: power of examining extremes. Cancer Discov [Internet]. 2012/05/16. 2011;1(6):466–8. Available from: https://www.ncbi.nlm.nih.gov/pubmed/22586648

45. Vlachostergios PJ, Puca L, Beltran H. Emerging Variants of Castration-Resistant Prostate Cancer. Curr Oncol Rep [Internet]. 2017/04/01. 2017;19(5):32. Available from: https://www.ncbi.nlm.nih.gov/pubmed/28361223

46. Akamatsu S, Inoue T, Ogawa O, Gleave ME. Clinical and molecular features of treatment-related neuroendocrine prostate cancer. Int J Urol [Internet]. 2018;25(4):345–51. Available from: http://www.ncbi.nlm.nih.gov/pubmed/29396873

47. Deng Q, Tang DG. Androgen receptor and prostate cancer stem cells: biological mechanisms and clinical implications. Endocr Relat Cancer [Internet]. 2015/08/20. 2015;22(6):T209-20. Available from: https://www.ncbi.nlm.nih.gov/pubmed/26285606

48. Beltran H, Tomlins S, Aparicio A, Arora V, Rickman D, Ayala G, et al. Aggressive variants of castration-resistant prostate cancer. Clin Cancer Res. 2014;20(11):2846–50.

49. Azzopardi JG, Evans DJ. Argentaffin cells in prostatic carcinoma: differentiation from lipofuscin and melanin in prostatic epithelium. J Pathol [Internet]. 1971/08/01. 1971;104(4):247–51. Available from: https://www.ncbi.nlm.nih.gov/pubmed/4109300

50. Kazzaz BA. Effect of 5-hydroxytryptophan on the differentiation of argyrophil to argentaffin cells in

the intestine of the guinea-pig after pre-treatment with iproniazid and reserpine. J Pathol [Internet]. 1973/05/01. 1973;110(1):75–82. Available from: https://www.ncbi.nlm.nih.gov/pubmed/4541868

51. Capella C, Usellini L, Buffa R, Frigerio B, Solcia E. The endocrine component of prostatic carcinomas, mixed adenocarcinoma-carcinoid tumours and non-tumour prostate. Histochemical and ultrastructural identification of the endocrine cells. Histopathology [Internet]. 1981/03/01. 1981;5(2):175–92. Available from: https://www.ncbi.nlm.nih.gov/pubmed/6163691

52. Abrahamsson PA, Alumets J, Wadstrom LB, Falkmer S, Grimelius L. Peptide hormones, serotonin, and other cell differentiation markers in benign hyperplasia and in carcinoma of the prostate. Prog Clin Biol Res [Internet]. 1987/01/01. 1987;243A:489–502. Available from: https://www.ncbi.nlm.nih.gov/pubmed/2443920

53. Vashchenko N, Abrahamsson PA. Neuroendocrine differentiation in prostate cancer: implications for new treatment modalities. Eur Urol [Internet]. 2005/01/22. 2005;47(2):147–55. Available from: http://www.ncbi.nlm.nih.gov/pubmed/15661408

54. Beltran H, Prandi D, Mosquera JM, Benelli M, Puca L, Cyrta J, et al. Divergent clonal evolution of castration-resistant neuroendocrine prostate cancer. Nat Med [Internet]. 2016/02/09. 2016;22(3):298–305. Available from: http://www.ncbi.nlm.nih.gov/pubmed/26855148

55. Nadal R, Schweizer M, Kryvenko ON, Epstein JI, Eisenberger MA. Small cell carcinoma of the prostate. Nature Reviews Urology. 2014.

56. Rickman DS, Beltran H, Demichelis F, Rubin MA. Biology and evolution of poorly differentiated neuroendocrine tumors. Nature Medicine. 2017.

57. Epstein JI, Amin MB, Beltran H, Lotan TL, Mosquera JM, Reuter VE, et al. Proposed morphologic classification of prostate cancer with neuroendocrine differentiation. Am J Surg Pathol [Internet]. 2014/04/08. 2014;38(6):756–67. Available from: https://www.ncbi.nlm.nih.gov/pubmed/24705311

58. Terry S, Beltran H. The many faces of neuroendocrine differentiation in prostate cancer progression. Front Oncol [Internet]. 2014;4(March):60. Available from: http://journal.frontiersin.org/article/10.3389/fonc.2014.00060/abstract

59. Park JW, Lee JK, Sheu KM, Wang L, Balanis NG, Nguyen K, et al. Reprogramming normal human epithelial tissues to a common, lethal neuroendocrine cancer lineage. Science (80-) [Internet]. 2018;362(6410):91–5. Available from: http://www.ncbi.nlm.nih.gov/pubmed/30287662

60. Santoni M, Conti A, Burattini L, Berardi R, Scarpelli M, Cheng L, et al. Neuroendocrine differentiation in prostate cancer: Novel morphological insights and future therapeutic perspectives. Biochimica et Biophysica Acta - Reviews on Cancer. 2014.

61. Parimi V, Goyal R, Poropatich K, Yang XJ. Neuroendocrine differentiation of prostate cancer: a review. Am J Clin Exp Urol. 2014;

62. Helpap B, Köllermann J, Oehler U. Neuroendocrine differentiation in prostatic carcinomas: Histogenesis, biology, clinical relevance, and future therapeutical perspectives. Urologia Internationalis. 1999.

63. Davies AH, Beltran H, Zoubeidi A. Cellular plasticity and the neuroendocrine phenotype in prostate cancer. Nat Rev Urol [Internet]. 2018;15(5):271–86. Available from: http://www.ncbi.nlm.nih.gov/pubmed/29460922

64. Aparicio AM, Harzstark AL, Corn PG, Wen S, Araujo JC, Tu SM, et al. Platinum-based chemotherapy for variant castrate-resistant prostate cancer. Clin Cancer Res. 2013;

65. Ather MH, Abbas F, Faruqui N, Israr M, Pervez S. Correlation of three immunohistochemically detected markers of neuroendocrine differentiation with clinical predictors of disease progression in prostate cancer. BMC Urol [Internet]. 2008;8:21. Available from:

http://www.ncbi.nlm.nih.gov/pubmed/19115997

66. Lin D, Wyatt AW, Xue H, Wang YY, Dong X, Haegert A, et al. High fidelity patient-derived xenografts for accelerating prostate cancer discovery and drug development. Cancer Res [Internet]. 2013/12/21. 2014;74(4):1272–83. Available from: https://www.ncbi.nlm.nih.gov/pubmed/24356420

67. Aparicio AM, Shen L, Tapia EL, Lu JF, Chen HC, Zhang J, et al. Combined Tumor Suppressor Defects Characterize Clinically Defined Aggressive Variant Prostate Cancers. Clin Cancer Res [Internet]. 2015/11/08. 2016;22(6):1520–30. Available from: https://www.ncbi.nlm.nih.gov/pubmed/26546618

68. Greenberg NM, DeMayo F, Finegold MJ, Medina D, Tilley WD, Aspinall JO, et al. Prostate cancer in a transgenic mouse. Proc Natl Acad Sci U S A [Internet]. 1995;92(8):3439–43. Available from: http://www.ncbi.nlm.nih.gov/pubmed/7724580

69. Mu P, Zhang Z, Benelli M, Karthaus WR, Hoover E, Chen CC, et al. SOX2 promotes lineage plasticity and antiandrogen resistance in TP53- and RB1-deficient prostate cancer. Science (80-) [Internet]. 2017;355(6320):84–8. Available from: http://www.ncbi.nlm.nih.gov/pubmed/28059768

70. Ku SY, Rosario S, Wang Y, Mu P, Seshadri M, Goodrich ZW, et al. Rb1 and Trp53 cooperate to suppress prostate cancer lineage plasticity, metastasis, and antiandrogen resistance. Science (80-) [Internet]. 2017/01/07. 2017;355(6320):78–83. Available from: https://www.ncbi.nlm.nih.gov/pubmed/28059767

71. Zou M, Toivanen R, Mitrofanova A, Floch N, Hayati S, Sun Y, et al. Transdifferentiation as a Mechanism of Treatment Resistance in a Mouse Model of Castration-Resistant Prostate Cancer. Cancer Discov [Internet]. 2017;7(7):736–49. Available from: http://www.ncbi.nlm.nih.gov/pubmed/28411207

72. Chen H, Sun Y, Wu C, Magyar CE, Li X, Cheng L, et al. Pathogenesis of prostatic small cell carcinoma involves the inactivation of the P53 pathway. Endocr Relat Cancer [Internet]. 2012;19(3):321–31. Available from: http://www.ncbi.nlm.nih.gov/pubmed/22389383

73. Beltran H, Rickman DS, Park K, Chae SS, Sboner A, MacDonald TY, et al. Molecular characterization of neuroendocrine prostate cancer and identification of new drug targets. Cancer Discov [Internet]. 2012/03/06. 2011;1(6):487–95. Available from: https://www.ncbi.nlm.nih.gov/pubmed/22389870

74. Clermont PL, Lin D, Crea F, Wu R, Xue H, Wang Y, et al. Polycomb-mediated silencing in neuroendocrine prostate cancer. Clin Epigenetics [Internet]. 2015/04/11. 2015;7:40. Available from: https://www.ncbi.nlm.nih.gov/pubmed/25859291

75. Dardenne E, Beltran H, Benelli M, Gayvert K, Berger A, Puca L, et al. N-Myc Induces an EZH2-Mediated Transcriptional Program Driving Neuroendocrine Prostate Cancer. Cancer Cell [Internet]. 2016/10/12. 2016;30(4):563–77. Available from: https://www.ncbi.nlm.nih.gov/pubmed/27728805

76. Mickey GH, Vollmer RT, David D. Heterotransplantation of a Human Prostatic Adenocarcinoma Cell Line in Nude Mice. Cancer Res. 1977;

77. Nupponen NN, Hyytinen ER, Kallioniemi AH, Visakorpi T. Genetic alterations in prostate cancer cell lines detected by comparative genomic hybridization. Cancer Genet Cytogenet. 1998;

78. Stone KR, Mickey DD, Wunderli H, Mickey GH, Paulson DF. Isolation of a human prostate carcinoma cell line (DU 145). Int J Cancer. 1978;

79. Imamura T, Uesaka M, Nakashima K. Epigenetic setting and reprogramming for neural cell fate determination and differentiation. Philos Trans R Soc L B Biol Sci [Internet]. 2014;369(1652). Available from: http://www.ncbi.nlm.nih.gov/pubmed/25135972

80. Nouri M, Caradec J, Lubik AA, Li N, Hollier BG, Takhar M, et al. Therapy-induced developmental reprogramming of prostate cancer cells and acquired therapy resistance. Oncotarget [Internet]. 2017;8(12):18949–67. Available from: http://www.ncbi.nlm.nih.gov/pubmed/28145883

81. Rybak AP, He L, Kapoor A, Cutz JC, Tang D. Characterization of sphere-propagating cells with stem-like properties from DU145 prostate cancer cells. Biochim Biophys Acta [Internet]. 2011;1813(5):683–94. Available from: http://www.ncbi.nlm.nih.gov/pubmed/21277911

82. Pfeiffer MJ, Schalken JA. Stem cell characteristics in prostate cancer cell lines. Eur Urol [Internet]. 2010;57(2):246–54. Available from: http://www.ncbi.nlm.nih.gov/pubmed/19200636

83. Munkley J, Livermore K, Rajan P, Elliott DJ. RNA splicing and splicing regulator changes in prostate cancer pathology. Hum Genet [Internet]. 2017/04/07. 2017;136(9):1143–54. Available from: https://www.ncbi.nlm.nih.gov/pubmed/28382513

84. Antonarakis ES, Lu C, Wang H, Luber B, Nakazawa M, Roeser JC, et al. AR-V7 and resistance to enzalutamide and abiraterone in prostate cancer. N Engl J Med [Internet]. 2014;371(11):1028–38. Available from: http://www.ncbi.nlm.nih.gov/pubmed/25184630

85. Liu LL, Xie N, Sun S, Plymate S, Mostaghel E, Dong X. Mechanisms of the androgen receptor splicing in prostate cancer cells. Oncogene [Internet]. 2013/07/16. 2014;33(24):3140–50. Available from: https://www.ncbi.nlm.nih.gov/pubmed/23851510

86. Qu Y, Dai B, Ye D, Kong Y, Chang K, Jia Z, et al. Constitutively active AR-V7 plays an essential role in the development and progression of castration-resistant prostate cancer. Sci Rep [Internet]. 2015;5:7654. Available from: http://www.ncbi.nlm.nih.gov/pubmed/25563505

87. Henzler C, Li Y, Yang R, McBride T, Ho Y, Sprenger C, et al. Truncation and constitutive activation of the androgen receptor by diverse genomic rearrangements in prostate cancer. Nat Commun [Internet]. 2016;7:13668. Available from: http://www.ncbi.nlm.nih.gov/pubmed/27897170

88. Kohli M, Ho Y, Hillman DW, Van Etten JL, Henzler C, Yang R, et al. Androgen Receptor Variant AR-V9 Is Coexpressed with AR-V7 in Prostate Cancer Metastases and Predicts Abiraterone Resistance. Clin Cancer Res [Internet]. 2017;23(16):4704–15. Available from: http://www.ncbi.nlm.nih.gov/pubmed/28473535

89. Zhang X, Coleman IM, Brown LG, True LD, Kollath L, Lucas JM, et al. SRRM4 Expression and the Loss of REST Activity May Promote the Emergence of the Neuroendocrine Phenotype in Castration-Resistant Prostate Cancer. Clin Cancer Res [Internet]. 2015/06/14. 2015;21(20):4698–708. Available from: https://www.ncbi.nlm.nih.gov/pubmed/26071481

90. Li Y, Donmez N, Sahinalp C, Xie N, Wang YY, Xue H, et al. SRRM4 Drives Neuroendocrine Transdifferentiation of Prostate Adenocarcinoma Under Androgen Receptor Pathway Inhibition. Eur Urol [Internet]. 2016/05/18. 2016;71(1):68–78. Available from: https://www.ncbi.nlm.nih.gov/pubmed/27180064

91. Li Y, Zhang Q, Lovnicki J, Chen R, Fazli L, Wang Y, et al. SRRM4 gene expression correlates with neuroendocrine prostate cancer. Prostate [Internet]. 2018; Available from: http://www.ncbi.nlm.nih.gov/pubmed/30155992

92. Lapuk A V., Wu C, Wyatt AW, McPherson A, McConeghy BJ, Brahmbhatt S, et al. From sequence to molecular pathology, and a mechanism driving the neuroendocrine phenotype in prostate cancer. J Pathol [Internet]. 2012/05/04. 2012;227(3):286–97. Available from: https://www.ncbi.nlm.nih.gov/pubmed/22553170

93. Li Y, Chen R, Bowden M, Mo F, Lin YY, Gleave M, et al. Establishment of a neuroendocrine prostate cancer model driven by the RNA splicing factor SRRM4. Oncotarget [Internet]. 2017/10/06. 2017;8(40):66878–88. Available from: https://www.ncbi.nlm.nih.gov/pubmed/28978002

94. Gan Y, Li Y, Long Z, Lee AR, Xie N, Lovnicki JM, et al. Roles of Alternative RNA Splicing of the Bif-1 Gene by SRRM4 During the Development of Treatment-induced Neuroendocrine Prostate Cancer. EBioMedicine. 2018;31.

95. Irimia M, Weatheritt RJ, Ellis JD, Parikshak NN, Gonatopoulos-Pournatzis T, Babor M, et al. A highly conserved program of neuronal microexons is misregulated in autistic brains. Cell [Internet]. 2014/12/20. 2014;159(7):1511–23. Available from: https://www.ncbi.nlm.nih.gov/pubmed/25525873

96. Raj B, O'Hanlon D, Vessey JP, Pan Q, Ray D, Buckley NJ, et al. Cross-regulation between an alternative splicing activator and a transcription repressor controls neurogenesis. Mol Cell [Internet]. 2011/09/03. 2011;43(5):843–50. Available from: http://dx.doi.org/10.1016/j.molcel.2011.08.014

97. Xiong HY, Alipanahi B, Lee LJ, Bretschneider H, Merico D, Yuen RK, et al. RNA splicing. The human splicing code reveals new insights into the genetic determinants of disease. Science (80-) [Internet]. 2015;347(6218):1254806. Available from: http://www.ncbi.nlm.nih.gov/pubmed/25525159

98. Raj B, Irimia M, Braunschweig U, Sterne-Weiler T, O'Hanlon D, Lin ZY, et al. A global regulatory mechanism for activating an exon network required for neurogenesis. Mol Cell [Internet]. 2014;56(1):90–103. Available from: http://www.ncbi.nlm.nih.gov/pubmed/25219497

99. Raj B, Blencowe BJ. Alternative Splicing in the Mammalian Nervous System: Recent Insights into Mechanisms and Functional Roles. Neuron. 2015.

100. Quesnel-Vallieres M, Irimia M, Cordes SP, Blencowe BJ. Essential roles for the splicing regulator nSR100/SRRM4 during nervous system development. Genes Dev [Internet]. 2015/04/04. 2015;29(7):746–59. Available from: https://www.ncbi.nlm.nih.gov/pubmed/25838543

101. Pan Q, Shai O, Lee LJ, Frey BJ, Blencowe BJ. Deep surveying of alternative splicing complexity in the human transcriptome by high-throughput sequencing. Nat Genet [Internet]. 2008/11/04. 2008;40(12):1413–5. Available from: https://www.ncbi.nlm.nih.gov/pubmed/18978789

102. Wang ET, Sandberg R, Luo S, Khrebtukova I, Zhang L, Mayr C, et al. Alternative isoform regulation in human tissue transcriptomes. Nature [Internet]. 2008/11/04. 2008;456(7221):470–6. Available from: https://www.ncbi.nlm.nih.gov/pubmed/18978772

103. Long JC, Caceres JF. The SR protein family of splicing factors: master regulators of gene expression. Biochem J [Internet]. 2009;417(1):15–27. Available from: http://www.ncbi.nlm.nih.gov/pubmed/19061484

104. Huang Y, Steitz JA. SRprises along a messenger's journey. Mol Cell [Internet]. 2005;17(5):613–5. Available from: http://www.ncbi.nlm.nih.gov/pubmed/15749011

105. Kohtz JD, Jamison SF, Will CL, Zuo P, Luhrmann R, Garcia-Blanco MA, et al. Protein-protein interactions and 5'-splice-site recognition in mammalian mRNA precursors. Nature [Internet]. 1994;368(6467):119–24. Available from: http://www.ncbi.nlm.nih.gov/pubmed/8139654

106. Wu JY, Maniatis T. Specific interactions between proteins implicated in splice site selection and regulated alternative splicing. Cell [Internet]. 1993;75(6):1061–70. Available from: http://www.ncbi.nlm.nih.gov/pubmed/8261509

107. Lin S, Fu XD. SR proteins and related factors in alternative splicing. Adv Exp Med Biol [Internet]. 2007;623:107–22. Available from: http://www.ncbi.nlm.nih.gov/pubmed/18380343

108. Boucher L, Ouzounis CA, Enright AJ, Blencowe BJ. A genome-wide survey of RS domain proteins. RNA [Internet]. 2001;7(12):1693–701. Available from: http://www.ncbi.nlm.nih.gov/pubmed/11780626

109. Irimia M, Blencowe BJ. Alternative splicing: decoding an expansive regulatory layer. Curr Opin Cell Biol [Internet]. 2012/04/03. 2012;24(3):323–32. Available from: https://www.ncbi.nlm.nih.gov/pubmed/22465326

110. Kramer A. The structure and function of proteins involved in mammalian pre-mRNA splicing. Annu Rev Biochem [Internet]. 1996;65:367–409. Available from: http://www.ncbi.nlm.nih.gov/pubmed/8811184

111. Will CL, Luhrmann R. Spliceosomal UsnRNP biogenesis, structure and function. Curr Opin Cell Biol [Internet]. 2001;13(3):290–301. Available from: http://www.ncbi.nlm.nih.gov/pubmed/11343899

112. Mermoud JE, Cohen PT, Lamond AI. Regulation of mammalian spliceosome assembly by a protein phosphorylation mechanism. EMBO J [Internet]. 1994;13(23):5679–88. Available from: http://www.ncbi.nlm.nih.gov/pubmed/7988565

113. Tazi J, Kornstadt U, Rossi F, Jeanteur P, Cathala G, Brunel C, et al. Thiophosphorylation of U1-70K protein inhibits pre-mRNA splicing. Nature [Internet]. 1993;363(6426):283–6. Available from: http://www.ncbi.nlm.nih.gov/pubmed/8387646

114. Cao W, Jamison SF, Garcia-Blanco MA. Both phosphorylation and dephosphorylation of ASF/SF2 are required for pre-mRNA splicing in vitro. RNA [Internet]. 1997;3(12):1456–67. Available from: http://www.ncbi.nlm.nih.gov/pubmed/9404896

115. Xiao SH, Manley JL. Phosphorylation of the ASF/SF2 RS domain affects both protein-protein and protein-RNA interactions and is necessary for splicing. Genes Dev [Internet]. 1997;11(3):334–44. Available from: http://www.ncbi.nlm.nih.gov/pubmed/9030686

116. Calarco JA, Superina S, O'Hanlon D, Gabut M, Raj B, Pan Q, et al. Regulation of vertebrate nervous system alternative splicing and development by an SR-related protein. Cell [Internet]. 2009/09/10. 2009;138(5):898–910. Available from: http://dx.doi.org/10.1016/j.cell.2009.06.012

117. Shen H, Green MR. A pathway of sequential arginine-serine-rich domain-splicing signal interactions during mammalian spliceosome assembly. Mol Cell [Internet]. 2004;16(3):363–73. Available from: http://www.ncbi.nlm.nih.gov/pubmed/15525510

118. Barbosa-Morais NL, Irimia M, Pan Q, Xiong HY, Gueroussov S, Lee LJ, et al. The evolutionary landscape of alternative splicing in vertebrate species. Science (80-) [Internet]. 2012;338(6114):1587–93. Available from: http://www.ncbi.nlm.nih.gov/pubmed/23258890

119. Merkin J, Russell C, Chen P, Burge CB. Evolutionary dynamics of gene and isoform regulation in Mammalian tissues. Science (80-) [Internet]. 2012;338(6114):1593–9. Available from: http://www.ncbi.nlm.nih.gov/pubmed/23258891

120. Shimojo M, Paquette AJ, Anderson DJ, Hersh LB. Protein kinase A regulates cholinergic gene expression in PC12 cells: REST4 silences the silencing activity of neuron-restrictive silencer factor/REST. Mol Cell Biol [Internet]. 1999/09/22. 1999;19(10):6788–95. Available from: https://www.ncbi.nlm.nih.gov/pubmed/10490617

121. Nakano Y, Jahan I, Bonde G, Sun X, Hildebrand MS, Engelhardt JF, et al. A mutation in the Srrm4 gene causes alternative splicing defects and deafness in the Bronx waltzer mouse. PLoS Genet [Internet]. 2012/10/12. 2012;8(10):e1002966. Available from: https://www.ncbi.nlm.nih.gov/pubmed/23055939

122. Song Z, Zhao D, Zhao H, Yang L. NRSF: an angel or a devil in neurogenesis and neurological diseases. J Mol Neurosci [Internet]. 2015;56(1):131–44. Available from: http://www.ncbi.nlm.nih.gov/pubmed/25479824

123. Shimojo M, Shudo Y, Ikeda M, Kobashi T, Ito S. The small cell lung cancer-specific isoform of RE1-silencing transcription factor (REST) is regulated by neural-specific Ser/Arg repeat-related

protein of 100 kDa (nSR100). Mol Cancer Res [Internet]. 2013/08/10. 2013;11(10):1258–68. Available from: https://www.ncbi.nlm.nih.gov/pubmed/23928058

124. Wang DB, Uo T, Kinoshita C, Sopher BL, Lee RJ, Murphy SP, et al. Bax interacting factor-1 promotes survival and mitochondrial elongation in neurons. J Neurosci [Internet]. 2014/02/14. 2014;34(7):2674–83. Available from: https://www.ncbi.nlm.nih.gov/pubmed/24523556

125. Lan F, Collins RE, De Cegli R, Alpatov R, Horton JR, Shi X, et al. Recognition of unmethylated histone H3 lysine 4 links BHC80 to LSD1-mediated gene repression. Nature [Internet]. 2007/08/10. 2007;448(7154):718–22. Available from: https://www.ncbi.nlm.nih.gov/pubmed/17687328

126. Shi YJ, Matson C, Lan F, Iwase S, Baba T, Shi Y. Regulation of LSD1 histone demethylase activity by its associated factors. Mol Cell [Internet]. 2005/09/06. 2005;19(6):857–64. Available from: https://www.ncbi.nlm.nih.gov/pubmed/16140033

127. Klajn A, Ferrai C, Stucchi L, Prada I, Podini P, Baba T, et al. The rest repression of the neurosecretory phenotype is negatively modulated by BHC80, a protein of the BRAF/HDAC complex. J Neurosci [Internet]. 2009/05/15. 2009;29(19):6296–307. Available from: https://www.ncbi.nlm.nih.gov/pubmed/19439607

128. Iwase S, Januma A, Miyamoto K, Shono N, Honda A, Yanagisawa J, et al. Characterization of BHC80 in BRAF-HDAC complex, involved in neuron-specific gene repression. Biochem Biophys Res Commun [Internet]. 2004;322(2):601–8. Available from: http://www.ncbi.nlm.nih.gov/pubmed/15325272

129. Wang Y, Wu Q, Yang P, Wang C, Liu J, Ding W, et al. LSD1 co-repressor Rcor2 orchestrates neurogenesis in the developing mouse brain. Nat Commun. 2016;

130. Carrozza MJ, Utley RT, Workman JL, Cote J. The diverse functions of histone acetyltransferase complexes. Trends Genet [Internet]. 2003/06/13. 2003;19(6):321–9. Available from: https://www.ncbi.nlm.nih.gov/pubmed/12801725

131. Avvakumov N, Cote J. The MYST family of histone acetyltransferases and their intimate links to cancer. Oncogene [Internet]. 2007/08/19. 2007;26(37):5395–407. Available from: https://www.ncbi.nlm.nih.gov/pubmed/17694081

132. Sapountzi V, Cote J. MYST-family histone acetyltransferases: beyond chromatin. Cell Mol Life Sci [Internet]. 2010/12/07. 2011;68(7):1147–56. Available from: https://www.ncbi.nlm.nih.gov/pubmed/21132344

133. Doyon Y, Cayrou C, Ullah M, Landry AJ, Cote V, Selleck W, et al. ING tumor suppressor proteins are critical regulators of chromatin acetylation required for genome expression and perpetuation. Mol Cell [Internet]. 2006;21(1):51–64. Available from: https://www.ncbi.nlm.nih.gov/pubmed/16387653

134. Ullah M, Pelletier N, Xiao L, Zhao SP, Wang K, Degerny C, et al. Molecular architecture of quartet MOZ/MORF histone acetyltransferase complexes. Mol Cell Biol [Internet]. 2008;28(22):6828–43. Available from: http://www.pubmedcentral.nih.gov/articlerender.fcgi?artid=2573306&tool=pmcentrez&rendertype=abstract

135. Merson TD, Dixon MP, Collin C, Rietze RL, Bartlett PF, Thomas T, et al. The Transcriptional Coactivator Querkopf Controls Adult Neurogenesis. J Neurosci. 2006;

136. Parnas D, Haghighi AP, Fetter RD, Kim SW, Goodman CS. Regulation of postsynaptic structure and protein localization by the Rho-type guanine nucleotide exchange factor dPix. Neuron [Internet]. 2001;32(3):415–24. Available from: http://www.ncbi.nlm.nih.gov/pubmed/11709153

137. Zhang H, Webb DJ, Asmussen H, Niu S, Horwitz AF. A GIT1/PIX/Rac/PAK signaling module

regulates spine morphogenesis and synapse formation through MLC. J Neurosci [Internet]. 2005;25(13):3379–88. Available from: http://www.ncbi.nlm.nih.gov/pubmed/15800193

138. Lee AR, Gan Y, Tang Y, Dong X. A novel mechanism of SRRM4 in promoting neuroendocrine prostate cancer development via a pluripotency gene network. EBioMedicine [Internet]. 2018;35:167–77. Available from: http://www.ncbi.nlm.nih.gov/pubmed/30100395

139. Schneider CA, Rasband WS, Eliceiri KW. NIH Image to ImageJ: 25 years of image analysis. Nature Methods. 2012.

140. Li W, Turner A, Aggarwal P, Matter A, Storvick E, Arnett DK, et al. Comprehensive evaluation of AmpliSeq transcriptome, a novel targeted whole transcriptome RNA sequencing methodology for global gene expression analysis. BMC Genomics. 2015;16:1069.

141. Yu Y, Liu L, Xie N, Xue H, Fazli L, Buttyan R, et al. Expression and Function of the Progesterone Receptor in Human Prostate Stroma Provide Novel Insights to Cell Proliferation Control. 2013;98(7):2887–96.

142. Robinson D, Van Allen EM, Wu YM, Schultz N, Lonigro RJ, Mosquera JM, et al. Integrative clinical genomics of advanced prostate cancer. Cell [Internet]. 2015;161(5):1215–28. Available from: http://www.ncbi.nlm.nih.gov/pubmed/26000489

143. Grasso CS, Wu YM, Robinson DR, Cao X, Dhanasekaran SM, Khan AP, et al. The mutational landscape of lethal castration-resistant prostate cancer. Nature [Internet]. 2012;487(7406):239–43. Available from: http://www.ncbi.nlm.nih.gov/pubmed/22722839

144. Gao J, Aksoy BA, Dogrusoz U, Dresdner G, Gross B, Sumer SO, et al. Integrative analysis of complex cancer genomics and clinical profiles using the cBioPortal. Sci Signal [Internet]. 2013;6(269):pl1. Available from: http://www.ncbi.nlm.nih.gov/pubmed/23550210

145. Cerami E, Gao J, Dogrusoz U, Gross BE, Sumer SO, Aksoy BA, et al. The cBio cancer genomics portal: an open platform for exploring multidimensional cancer genomics data. Cancer Discov [Internet]. 2012;2(5):401–4. Available from: http://www.ncbi.nlm.nih.gov/pubmed/22588877

146. Varambally S, Yu J, Laxman B, Rhodes DR, Mehra R, Tomlins SA, et al. Integrative genomic and proteomic analysis of prostate cancer reveals signatures of metastatic progression. Cancer Cell [Internet]. 2005;8(5):393–406. Available from: http://www.ncbi.nlm.nih.gov/pubmed/16286247

147. Kumar A, Coleman I, Morrissey C, Zhang X, True LD, Gulati R, et al. Substantial interindividual and limited intraindividual genomic diversity among tumors from men with metastatic prostate cancer. Nat Med [Internet]. 2016;22(4):369–78. Available from: http://www.ncbi.nlm.nih.gov/pubmed/26928463

148. Akamatsu S, Wyatt AW, Lin D, Lysakowski S, Zhang F, Kim S, et al. The Placental Gene PEG10 Promotes Progression of Neuroendocrine Prostate Cancer. Cell Rep [Internet]. 2015;12(6):922–36. Available from: http://www.ncbi.nlm.nih.gov/pubmed/26235627

149. Ramnarine VR, Alshalalfa M, Mo F, Nabavi N, Erho N, Takhar M, et al. The long noncoding RNA landscape of neuroendocrine prostate cancer and its clinical implications. Gigascience [Internet]. 2018;7(6). Available from: http://www.ncbi.nlm.nih.gov/pubmed/29757368

150. Bishop JL, Davies A, Ketola K, Zoubeidi A. Regulation of tumor cell plasticity by the androgen receptor in prostate cancer. Endocr Relat Cancer [Internet]. 2015/05/03. 2015;22(3):R165-82. Available from: https://www.ncbi.nlm.nih.gov/pubmed/25934687

151. Lee AR, Che N, Lovnicki JM, Dong X. Development of neuroendocrine prostate cancers by the Ser/Arg repetitive matrix 4-mediated RNA splicing network. Front Oncol. 2018;8(APR).

152. Kregel S, Kiriluk KJ, Rosen AM, Cai Y, Reyes EE, Otto KB, et al. Sox2 is an androgen receptor-repressed gene that promotes castration-resistant prostate cancer. PLoS One [Internet].

2013/01/18. 2013;8(1):e53701. Available from: https://www.ncbi.nlm.nih.gov/pubmed/23326489

153. Chen R, Li Y, Buttyan R, Dong X. Implications of PI3K / AKT inhibition on REST protein stability and neuroendocrine phenotype acquisition in prostate cancer cells. 2017;8(49):84863–76.

154. Lin TP, Chang YT, Lee SY, Campbell M, Wang TC, Shen SH, et al. REST reduction is essential for hypoxia-induced neuroendocrine differentiation of prostate cancer cells by activating autophagy signaling. Oncotarget [Internet]. 2016/04/02. 2016;7(18):26137–51. Available from: https://www.ncbi.nlm.nih.gov/pubmed/27034167

155. Cox ME, Deeble PD, Lakhani S, Parsons SJ. Acquisition of neuroendocrine characteristics by prostate tumor cells is reversible: implications for prostate cancer progression. Cancer Res [Internet]. 1999/08/14. 1999;59(15):3821–30. Available from: https://www.ncbi.nlm.nih.gov/pubmed/10447001

156. Mori S, Murakami-Mori K, Bonavida B. Interleukin-6 induces G1 arrest through induction of p27(Kip1), a cyclin-dependent kinase inhibitor, and neuron-like morphology in LNCaP prostate tumor cells. Biochem Biophys Res Commun [Internet]. 1999/04/13. 1999;257(2):609–14. Available from: https://www.ncbi.nlm.nih.gov/pubmed/10198259

157. Whitesell L, Mimnaugh EG, De Costa B, Myers CE, Neckers LM. Inhibition of heat shock protein HSP90-pp60v-src heteroprotein complex formation by benzoquinone ansamycins: essential role for stress proteins in oncogenic transformation. Proc Natl Acad Sci U S A [Internet]. 1994/08/30. 1994;91(18):8324–8. Available from: https://www.ncbi.nlm.nih.gov/pubmed/8078881

158. Svensson C, Ceder J, Iglesias-Gato D, Chuan YC, Pang ST, Bjartell A, et al. REST mediates androgen receptor actions on gene repression and predicts early recurrence of prostate cancer. Nucleic Acids Res. 2014;42(2):999–1015.

159. Liang H, Studach L, Hullinger RL, Xie J, Andrisani OM. Down-regulation of RE-1 silencing transcription factor (REST) in advanced prostate cancer by hypoxia-induced miR-106b~25. Exp Cell Res [Internet]. 2013/10/19. 2014;320(2):188–99. Available from: https://www.ncbi.nlm.nih.gov/pubmed/24135225

160. Ehrich M, Turner J, Gibbs P, Lipton L, Giovanneti M, Cantor C, et al. Cytosine methylation profiling of cancer cell lines. Proc Natl Acad Sci U S A [Internet]. 2008;105(12):4844–9. Available from: http://www.ncbi.nlm.nih.gov/pubmed/18353987

161. Massie CE, Mills IG, Lynch AG. The importance of DNA methylation in prostate cancer development. J Steroid Biochem Mol Biol [Internet]. 2017;166:1–15. Available from: http://www.ncbi.nlm.nih.gov/pubmed/27117390

162. van Bokhoven A, Varella-Garcia M, Korch C, Johannes WU, Smith EE, Miller HL, et al. Molecular characterization of human prostate carcinoma cell lines. Prostate [Internet]. 2003;57(3):205–25. Available from: http://www.ncbi.nlm.nih.gov/pubmed/14518029

163. Kleb B, Estecio MR, Zhang J, Tzelepi V, Chung W, Jelinek J, et al. Differentially methylated genes and androgen receptor re-expression in small cell prostate carcinomas. Epigenetics [Internet]. 2016;11(3):184–93. Available from: http://www.ncbi.nlm.nih.gov/pubmed/26890396

164. Cowley GS, Weir BA, Vazquez F, Tamayo P, Scott JA, Rusin S, et al. Parallel genome-scale loss of function screens in 216 cancer cell lines for the identification of context-specific genetic dependencies. Sci Data [Internet]. 2014;1:140035. Available from: http://www.ncbi.nlm.nih.gov/pubmed/25984343

165. Smith BA, Sokolov A, Uzunangelov V, Baertsch R, Newton Y, Graim K, et al. A basal stem cell signature identifies aggressive prostate cancer phenotypes. Proc Natl Acad Sci U S A [Internet]. 2015;112(47):E6544-52. Available from: http://www.ncbi.nlm.nih.gov/pubmed/26460041

166. Zhang D, Park D, Zhong Y, Lu Y, Rycaj K, Gong S, et al. Stem cell and neurogenic gene-

expression profiles link prostate basal cells to aggressive prostate cancer. Nat Commun [Internet]. 2016;7:10798. Available from: http://www.ncbi.nlm.nih.gov/pubmed/26924072

167. Aparicio A, Tzelepi V, Araujo JC, Guo CC, Liang S, Troncoso P, et al. Neuroendocrine prostate cancer xenografts with large-cell and small-cell features derived from a single patient's tumor: morphological, immunohistochemical, and gene expression profiles. Prostate [Internet]. 2011;71(8):846–56. Available from: http://www.ncbi.nlm.nih.gov/pubmed/21456067

168. Zhu Y, Liu C, Cui Y, Nadiminty N, Lou W, Gao AC. Interleukin-6 induces neuroendocrine differentiation (NED) through suppression of RE-1 silencing transcription factor (REST). Prostate [Internet]. 2014/05/14. 2014;74(11):1086–94. Available from: https://www.ncbi.nlm.nih.gov/pubmed/24819501

169. Bang YJ, Pirnia F, Fang WG, Kang WK, Sartor O, Whitesell L, et al. Terminal neuroendocrine differentiation of human prostate carcinoma cells in response to increased intracellular cyclic AMP. Proc Natl Acad Sci U S A [Internet]. 1994;91(12):5330–4. Available from: http://www.ncbi.nlm.nih.gov/pubmed/8202489

170. Lasorella A, Benezra R, Iavarone A. The ID proteins: master regulators of cancer stem cells and tumour aggressiveness. Nat Rev Cancer [Internet]. 2014;14(2):77–91. Available from: http://www.ncbi.nlm.nih.gov/pubmed/24442143

171. Mitchell L, Lambert JP, Gerdes M, Al-Madhoun AS, Skerjanc IS, Figeys D, et al. Functional dissection of the NuA4 histone acetyltransferase reveals its role as a genetic hub and that Eaf1 is essential for complex integrity. Mol Cell Biol [Internet]. 2008;28(7):2244–56. Available from: http://www.ncbi.nlm.nih.gov/pubmed/18212056

172. Ruzinova MB, Benezra R. Id proteins in development, cell cycle and cancer. Trends Cell Biol [Internet]. 2003;13(8):410–8. Available from: http://www.ncbi.nlm.nih.gov/pubmed/12888293

173. Lasorella A, Noseda M, Beyna M, Yokota Y, Iavarone A. Id2 is a retinoblastoma protein target and mediates signalling by Myc oncoproteins. Nature [Internet]. 2000;407(6804):592–8. Available from: http://www.ncbi.nlm.nih.gov/pubmed/11034201

174. Paolella BR, Havrda MC, Mantani A, Wray CM, Zhang Z, Israel MA. p53 directly represses Id2 to inhibit the proliferation of neural progenitor cells. Stem Cells [Internet]. 2011;29(7):1090–101. Available from: http://www.ncbi.nlm.nih.gov/pubmed/21608079

175. Iavarone A, Garg P, Lasorella A, Hsu J, Israel MA. The helix-loop-helix protein Id-2 enhances cell proliferation and binds to the retinoblastoma protein. Genes Dev [Internet]. 1994;8(11):1270–84. Available from: http://www.ncbi.nlm.nih.gov/pubmed/7926730

176. Chiaverotti T, Couto SS, Donjacour A, Mao JH, Nagase H, Cardiff RD, et al. Dissociation of epithelial and neuroendocrine carcinoma lineages in the transgenic adenocarcinoma of mouse prostate model of prostate cancer. Am J Pathol [Internet]. 2007/12/25. 2008;172(1):236–46. Available from: https://www.ncbi.nlm.nih.gov/pubmed/18156212

177. Ahuja D, Saenz-Robles MT, Pipas JM. SV40 large T antigen targets multiple cellular pathways to elicit cellular transformation. Oncogene [Internet]. 2005;24(52):7729–45. Available from: http://www.ncbi.nlm.nih.gov/pubmed/16299533

178. Lee AR, Li Y, Xie N, Gleave ME, Cox ME, Collins CC, et al. Alternative RNA splicing of the MEAF6 gene facilitates neuroendocrine prostate cancer progression. Oncotarget. 2017;8(17).

179. Zhou W, Li X, Premont RT. Expanding functions of GIT Arf GTPase-activating proteins, PIX Rho guanine nucleotide exchange factors and GIT-PIX complexes. J Cell Sci [Internet]. 2016;129(10):1963–74. Available from: http://www.ncbi.nlm.nih.gov/pubmed/27182061

180. Yamaguchi H, Pixley F, Condeelis J. Invadopodia and podosomes in tumor invasion. Eur J Cell Biol. 2006;

181. Weaver AM. Invadopodia: Specialized cell structures for cancer invasion. Clinical and Experimental Metastasis. 2006.

182. Petrova V, Annicchiarico-Petruzzelli M, Melino G, Amelio I. The hypoxic tumour microenvironment. Oncogenesis [Internet]. 2018;7(1):10. Available from: http://www.ncbi.nlm.nih.gov/pubmed/29362402

183. Geiger B, Spatz JP, Bershadsky AD. Environmental sensing through focal adhesions. Nat Rev Mol Cell Biol [Internet]. 2009;10(1):21–33. Available from: http://www.ncbi.nlm.nih.gov/pubmed/19197329

184. Yoo SM, Antonyak MA, Cerione RA. The adaptor protein and Arf GTPase-activating protein Cat-1/Git-1 is required for cellular transformation. J Biol Chem. 2012;

185. Peng H, Dara L, Li TWH, Zheng Y, Yang H, Tomasi ML, et al. MAT2B-GIT1 interplay activates MEK1/ERK 1 and 2 to induce growth in human liver and colon cancer. Hepatology. 2013;

186. Chen J, Yang P, Yang J, Wen Z, Zhang B, Zheng X. GIT1 is a novel prognostic biomarker and facilitates tumor progression via activating ERK/MMP9 signaling in hepatocellular carcinoma. Onco Targets Ther. 2015;

187. Huang WC, Chan SH, Jang TH, Chang JW, Ko YC, Yen TC, et al. MiRNA-491-5p and GIT1 serve as modulators and biomarkers for oral squamous cell carcinoma invasion and metastasis. Cancer Res. 2014;

188. Tsao CK, Galsky MD, Oh WK. Is metastatic prostate cancer changing, and how will we know it? it's time for standard nomenclature for nonosseous metastases in clinical trials of patients with metastatic castration resistant prostate cancer. European Urology. 2014.

189. Černohorská M, Sulimenko V, Hájková Z, Sulimenko T, Sládková V, Vinopal S, et al. GIT1/βPIX signaling proteins and PAK1 kinase regulate microtubule nucleation. Biochim Biophys Acta - Mol Cell Res. 2016;

190. Dehm SM. Androgen levels increase by intratumoral de novo steroidogenesis during progression of castration-resistant prostate cancer. Locke JA, Guns ES, Lubik AA, Adomat HH, Hendy SC, Wood CA, Ettinger SL, Gleave ME, Nelson CC, The Prostate Center at Vancouver Gen. Urologic Oncology: Seminars and Original Investigations. 2008.

191. Lindström MS, Jurada D, Bursac S, Orsolic I, Bartek J, Volarevic S. Nucleolus as an emerging hub in maintenance of genome stability and cancer pathogenesis. Oncogene. 2018.

192. Huang J, Yao JL, Zhang L, Bourne PA, Quinn AM, di Sant'Agnese PA, et al. Differential expression of interleukin-8 and its receptors in the neuroendocrine and non-neuroendocrine compartments of prostate cancer. Am J Pathol [Internet]. 2005;166(6):1807–15. Available from: http://www.ncbi.nlm.nih.gov/pubmed/15920165

193. Kim J, Jin H, Zhao JC, Yang YA, Li Y, Yang X, et al. FOXA1 inhibits prostate cancer neuroendocrine differentiation. Oncogene [Internet]. 2017/03/21. 2017;36(28):4072–80. Available from: https://www.ncbi.nlm.nih.gov/pubmed/28319070

194. Chang PC, Wang TY, Chang YT, Chu CY, Lee CL, Hsu HW, et al. Autophagy pathway is required for IL-6 induced neuroendocrine differentiation and chemoresistance of prostate cancer LNCaP cells. PLoS One [Internet]. 2014;9(2):e88556. Available from: http://www.ncbi.nlm.nih.gov/pubmed/24551118

195. Cavadas MA, Mesnieres M, Crifo B, Manresa MC, Selfridge AC, Keogh CE, et al. REST is a hypoxia-responsive transcriptional repressor. Sci Rep [Internet]. 2016;6:31355. Available from: http://www.ncbi.nlm.nih.gov/pubmed/27531581

196. Klimstra DS, Beltran H, Lilenbaum R, Bergsland E. The Spectrum of Neuroendocrine Tumors:

Histologic Classification, Unique Features and Areas of Overlap. Am Soc Clin Oncol Educ B. 2015;

197. Bates DO, Morris JC, Oltean S, Donaldson LF. Pharmacology of Modulators of Alternative Splicing. Pharmacol Rev [Internet]. 2017;69(1):63–79. Available from: http://www.ncbi.nlm.nih.gov/pubmed/28034912

198. Meijboom KE, Wood MJA, McClorey G. Splice-Switching Therapy for Spinal Muscular Atrophy. Genes (Basel) [Internet]. 2017;8(6). Available from: http://www.ncbi.nlm.nih.gov/pubmed/28604635

Appendix

Appendix A: Primers for RT-qPCR

Primer Name	Forward Primer Sequence	Reverse Primer Sequence
18S	TTGACGGAAGGGCACCACCAG	GCACCACCACCCACGGAATCG
ABII(C)	GGCTGGTTATTTCCATGCTTGA	TCACAAAATAATAGCACCTGCG
ABII(NS)	ATGCTTGGCTTTTAGCCACTT	TCACAAAATAATAGCACCTGCG
ALDH1A2	TTGCAGGGCGTCATCAAAAC	ACACTCCAATGGGTTCATGTC
AMIGO1	CTGCGTACACTGGATGAGTTC	ACCGCCATGATGTGGTTATTG
AR	TCTTGTCGTCTTCGGAAATGT	AAGCCTCTCCTTCCTCCTGTA
ASCL1	CCCAAGCAAGTCAAGCGACA	AAGCCGCTGAAGTTGAGCC
ATL2(C)	TTCCTCCATCAAATTATCACCC	TCTTGTGTAACCTTGTCATGGG
ATL2(NS)	GATGACAGTCTCTGTCGCTGTG	CTGAAACACTATGGGAACAGAG
BHC80(C)	AGTCTTTGAGCCAGAGCGTAAG	CACTGCATTGTATTTTGGAGGA
BHC80(NS)	GGAAGAGAGCCAATGAGGAAC	AGTAACTGGCCACTTTTTCTGC
CAMTA2(C)	GCTGAAATCGCTTCTGTTCATA	GTTACCGGAAGTACAAGCAGTT
CAMTA2(NS)	GCTGAAATCGCTTCTGTTCATA	GTACAAGCAGCTGACCTGGATT
CDH1	ATTTTTCCCTCGACACCCGAT	TCCCAGGCGTAGACCAAGA
CDH2	TGCGGTACAGTGTAACTGGG	GAAACCGGGCTATCTGCTCG
CDK6	CCAGATGGCTCTAACCTCAGT	AACTTCCACGAAAAAGAGGCTT
CHGA	TAAAGGGGATACCGAGGTGATG	TCGGAGTGTCTCAAAACATTCC
CHGB	CGAGGGGAAGATAGCAGTGAA	CAGCATGTGTTTCCGATCTGG
CIB1	CACGGCTTAGTGCGTCTGAG	AAAGTCTGGAGAACGGGAGAT
DYNLL2	ACCCTACCTGGCATTGTATCG	AGCCTGACTTGAAGAGGAGGA
EFNA1	TCAGGCCCATGACAATCCAC	GTGACCGATGCTATGTAGAACC
ENO2	CCGGGAACTCAGACCTCATC	CTCTGCACCTAGTCGCATGG
EPHA2	AGAGGCTGAGCGTATCTTCAT	GGTCCGACTCGGCATAGTAGA
ERGIC2(C)	GAAGATGCAGGAGCAGAAGAAT	AGCTCTGCAAGTCATGGACGT
ERGIC2(NS)	CAGATACTATTGAGCAGTGCCG	AAGCTCTGCAAGTCATGGATCT
FOCX1	TGTTCGAGTCACAGAGGATCG	ACAGTCGTAGACGAAAGCTCC
FOXD3	TCACGCACCAATTCTAACGC	CACGGCTTGCTTACTGAAGG
GAPDH	GGACCTGACCTGCCGTCTAGAA	GGTGTCGCTGTTGAAGTCAGAG
GAPDH exon7/8 (ChIP)	GGCATGGACTGTGGTCATGAG	TGCACCACCAACTGCTTAGC
GIT1 exon7/8 (ChIP)	CTGATGTGAAAAGGCGTGTG	GCACTTTTGCCGAGATCTAAGT
GIT1(C) or *GIT1-C*	TTCTACCTCTGTGGACGCAAG	AATTCGGATAAGTCAAGGCTGTC
GIT1(NS) or *GIT1-A*	CCACAGATGGCTGACAGATC	TACACGTCCATGGCGAGTT
HEY1	GTTCGGCTCTAGGTTCCATGT	CGTCGGCGCTTCTCAATTATTC
ID1	TCTGCACACCTACTAGTCACCA	GAGAAGCACCAAACGTGACC
ID3	GGAGCGAAGGACTGTGAACT	CCACGCTCTGAAGAGACCTT
ID4	GGCCACTCAAGCAGCATTTG	TCTGGTTGCCTGGTTAGGAC
IGFBP1	GGCCATCGAGAATTGTTGCAG	CCAGGGATCAGGTGAGACTG
KIT	TTGTGATTTTGGTCTAGCCAGAGA	GTGCCATCCACTTCACAGGTAG
KLK3	AGTGCGAGAAGCATTCCCAAC	CCAGCAAGATCACGCTTTTGTT
KRT8	TCCTCAGGCAGCTATATGAAGAG	GGTTGGCAATATCCTCGTACTGT
MEAF6 (ChIP)	ACCAATTCTTGCTAGGGTGGCTA	TCATAATCAAACATGCCAGACG
MEAF6 (total)	AGGAGCTGGCGGAAACATTG	TGGTTGGTCAGATACCGATCC

MEAF6(C) or *MEAF6-2*	GAATAAAAACCGGCACAGGATTG	AAGGGAAGCAGGGCTCTACA
MEAF6(NS) or *MEAF6-1*	AATAAAAACCGGCACAGCCC	AAGGGAAGCAGGGCTCTACA
MEF2D(C)	GGGGTTAATGCATCACTTGACTG	TGGCTGAGTAAACTCGGCGT
MEF2D(NS)	GGGGTTAATGCATCACTTGAACA	TGGCTGAGTAAACTCGGCGT
MON2(C)	AAATGCAAAATATAATCAGGCG	GCTTTGTGACACGCTGTTTTT
MON2(NS)	ATCCAACTATTTGCACCGGC	GCTTTGTGACACGCTGTTTTT
MSX1	GGGGCAGGGAAAACACAGAT	AGGGATGTTTGAGAGCCACAC
NKX3-1	CCCACACTCAGGTGATCGAG	GAGCTGCTTTCGCTTAGTCTT
OCT3/4	GTGTTCAGCCAAAAGACCATCT	GGCCTGCATGAGGGTTTCT
PTK2(C)	ATGTACATCTCCAAATTGGCCT	GATACTTACACCATGCCCTCAAC
PTK2(NS)	TACATCTCCAAATTGGCCTTCT	GCCCTCAAAAAGCTATGGAATA
RB1	TTGGATCACAGCGATACAAACTT	AGCGCACGCCAATAAAGACAT
REST(C)	TGCGTACTCATTCAGGTGAGA	TCTTGCATGGCGGGTTACTT
REST(NS)	GCGTACTCATTCAGTGGGGTAT	GATTAGAGGCCACATAACTGCAC
SCG3	GTCTTCATCAACTAGACGGGACT	ACAATCTTGTCAAACACGGCTC
SCGN	GGCCATTTCTGAGGCTAAACT	GGGCTCCTGTTTTACTAACATCA
SH3GLB2(C)	GAGGGCACCACAGGCATAGT	AGAAGCAGCTGGGCAGATTT
SH3GLB2(NS)	GAGGGCACCACAGGCATAGT	CAGCTCCCAGGGTGCCATAT
SIX2	AAGGCACACTACATCGAGGC	CACGCTGCGACTCTTTTCC
SNAI2	CGAACTGGACACACATACAGTG	CTGAGGATCTCTGGTTGTGGT
SNAI2	TGTGACAAGGAATATGTGAGCC	TGAGCCCTCAGATTTGACCTG
SOX2	GCCGAGTGGAAACTTTTGTCG	GGCAGCGTGTACTTATCCTTCT
SRRM4	CACAAGCGACGCAGGTCAT	CGGTGGCGGTGAGACTTTC
SYP	TTAGTTGGGGACTACTCCTCG	GGCCCTTTGTTATTCTCTCGGTA
SYT4	ATGGGATACCCTACACCCAAAT	TCCCGAGAGAGGAATTAGAACTT
TGFB2	CAGCACACTCGATATGGACCA	CCTCGGGCTCAGGATAGTCT
TGFBR3	TGGGGTCTCCAGACTGTTTTT	CTGCTCCATACTCTTTTCGGG

* C = Constitutive variant
* NS = Neuro-specific variant
* ChIP = Chromatin immunoprecipitation

Appendix B: Antibodies

Antibody	Clone ID	Cat. No.	Supplier
AR (IHC)	N-20	sc-816	Santa Cruz
B-Actin (WB)	C-11	sc-1615	Santa Cruz Biotech
c-PARP (WB)	Asp214	9541	Cell Signaling
CD56 (IHC)	MRQ-42	156R-94	Milipore Sigma
CHGA (IHC)	EP38	AC-0037	Milipore Sigma
E-Cadherin (IHC)	EP6	AC-0003	Epitomics
E-Cadherin (WB)	H-108	sc-7870	Santa Cruz
Flag (RNA-ChIP and WB)	M5	F4042	Sigma-Aldrich
GIT1 (WB & IF)	H-170	sc-13961	Santa Cruz
ID1 (WB)		Ab134163	Abcam
Ki-67 (IHC)	SP6	RM-9106	Thermo Fisher
Pan-Cytokeratin (IHC)		Z0622	Dako
PSA (IHC)	C-19	sc-7638	Santa Cruz
SOX2 (IHC)		NB110-37235	Novus Biologicals
SOX2 (WB)	D6D9	3579S	Cell Signaling
SRRM4 (WB)		Sab2107518	Sigma-Aldrich
SYP (IHC)	D-4	sc-17750	Santa Cruz
SYP (WB)	D-4	sc-17750	Santa Cruz
Vinculin (WB & IF)	hVIN-1	V9131	Sigma-Aldrich

* WB = Western blot
* IHC = Immunohistochemistry
* RNA-ChIP = RNA-chromatin immunoprecipitation
* IF = Immunofluorescence

Appendix C: Detailed *GIT1-A*, *GIT1-C*, and *SRRM4* RISH scores in CRPC TMA

Histopathology	*GIT1A*	*GIT1C*	*SRRM4*
AdPC	0	0	0
AdPC	0	1	0
AdPC	0	2	0
AdPC	0	1	0
AdPC	0	1	0
AdPC	0	1	0
AdPC	0	1	0
AdPC	0	1	0
AdPC	0	1	0
AdPC	0	2	0
AdPC	0	2	0
AdPC	0	2	0
AdPC	0	2	0
AdPC	0	2	0
AdPC	0	2	0
AdPC	0	2	0
AdPC	0	1	0
AdPC	0	1	0
AdPC	0	1	0
AdPC	0	1	0
AdPC	0	1	0
AdPC	0	2	0
AdPC	0	2	0
AdPC	0	2	0
AdPC	0	2	0
AdPC	0	2	0
AdPC	0	2	0
AdPC	0	2	0
AdPC	0	2	0
AdPC	0	2	0
AdPC	0	2	0
AdPC	0	2	0
AdPC	0	1	0
AdPC	0	2	0
AdPC	0	2	0
AdPC	0	2	0

AdPC	0	1	0
AdPC	0	1	0
AdPC	0	1	0
AdPC	0	1	0
AdPC	0	1	0
AdPC	0	1	0
AdPC	0	1	1
AdPC	1	2	0
AdPC	1	2	1
AdPC	1	2	0
AdPC	1	2	0
AdPC	1	2	1
AdPC	1	1	0
AdPC	1	1	0
AdPC	1	1	1
AdPC	1	2	1
AdNC	0	0	1
AdNC	1	1	1
AdNC	1	1	1
AdNC	1	0	1
AdNC	1	0	2
AdNC	1	0	2
SCNC	1	0	2
SCNC	2	1	2
SCNC	2	0	2
SCNC	2	0	1
SCNC	2	0	2
SCNC	2	0	2

* AdPC = Prostate adenocarcinoma

* AdNC = Prostate adenocarcinoma with neuroendocrine cells

* SCNC = Small-cell prostatic carcinoma

Appendix D: Validation of SRRM4 expressions in the SRRM4-transduced stable cell and xenograft models

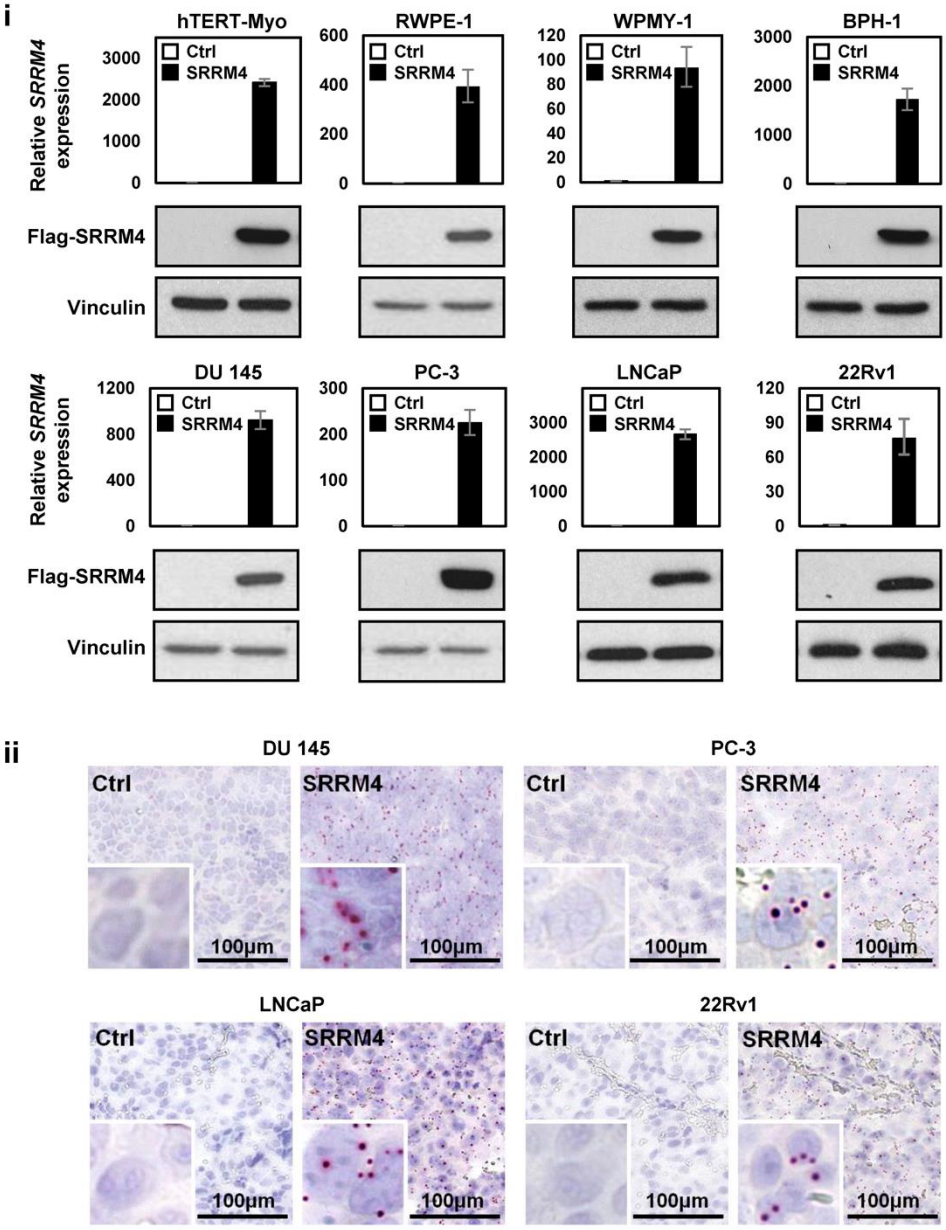

Appendix D Validation of SRRM4 expressions in the SRRM4-transduced stable cell and xenograft models. Lentiviral transduction to create SRRM4-overexpressing stable lines in hTERT-Myo, RWPE-1, WPMY-1, BPH-1, DU145, PC-3, LNCaP, and 22Rv1 parental cells were validated by **(i)** Western blot and RT-qPCR. Anti-flag antibody was used to detect against exogenous SRRM4 and anti-vinculin antibody was used to detect the loading control, vinculin. This validation was repeated three times, and only one representative repeat is presented. All results are presented as the mean ± SEM **(ii)** DU145, PC-3, LNCaP, and 22Rv1 stable cell lines overexpressing *SRRM4* or its respective control cells were inoculated in bilateral flanks subcutaneously in 6-8-week-old nude mice. Tumours were harvested, fixed in 10% paraformaldehyde, paraffin embedded, and processed for RNA *in situ* hybridization using an anti-sense probe to detect against SRRM4 mRNA. Scale bars represents 100 μm.

Appendix E: SRRM4 induces stem cell differentiation and neural fate factors in DU145 cells

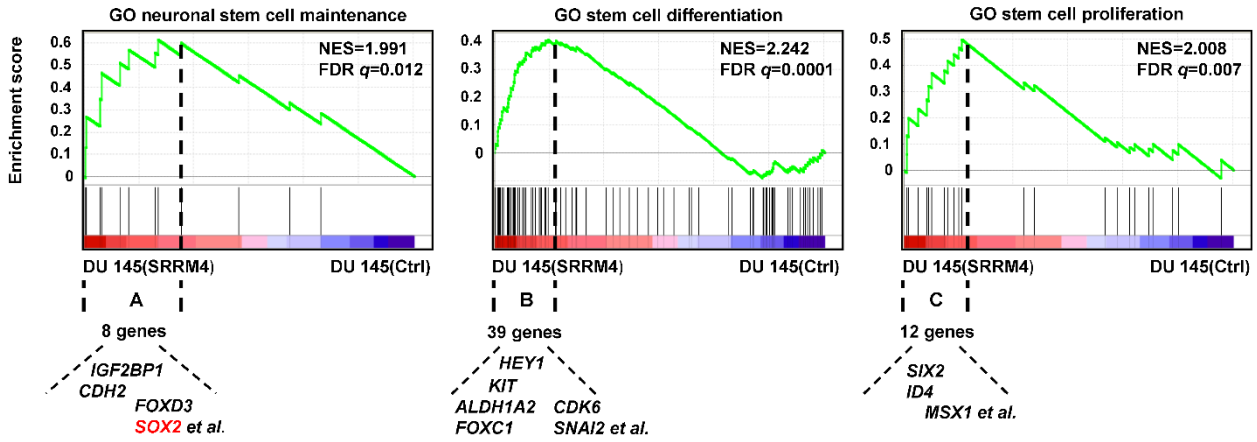

Appendix E SRRM4 induces stem cell differentiation and neural fate factors in DU145 cells. GSEA enrichment plots shows the correlations of the DU145(SRRM4), DuNE, vs DU145(Ctrl) dataset (n = 6033) with the GSEA gene sets in the 'lineage plasticity' subgroup from subfigure 4a. Thirteen stem cell marker or stem cell-related genes were selected from the leading-edge groups associated with the DuNE phenotype in the three GSEA enrichment plots to validate in subfigure 4C. GSEA, gene set enrichment analysis; GO, gene ontology; NES, normalized enrichment score; FDR, false discovery rate.

Appendix F: *SOX2* and *AR* are negatively correlated in CRPC cohorts

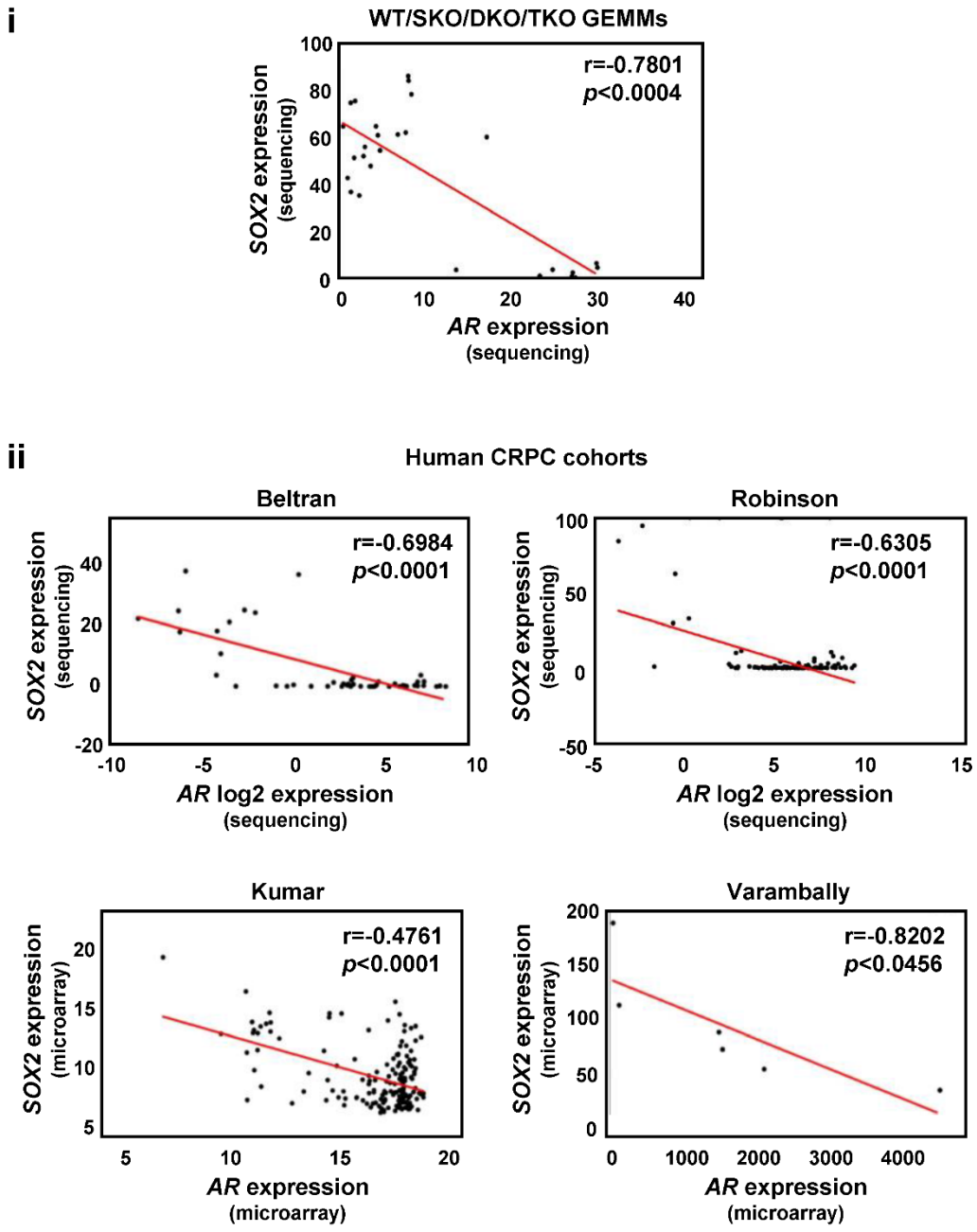

Appendix F *SOX2* and *AR* are negatively correlated in CRPC cohorts. (i-ii) Pearson's *r* correlation coefficient between *SOX2* and *AR* expressions obtained from GEMMs by Ku *et al.* (2017) **(i)**, and human CRPC cohorts by Beltran *et al.* (2016), Robinson *et al.* (2015), Kumar *et al.* (2016), and Varambally *et al.* (2005) **(ii)** are shown. GEMMs, genetically engineered mouse models; CRPC, castration-resistant prostate cancer.

Appendix G: *SRRM4* and *SOX2* are positively correlated in CRPC cohorts

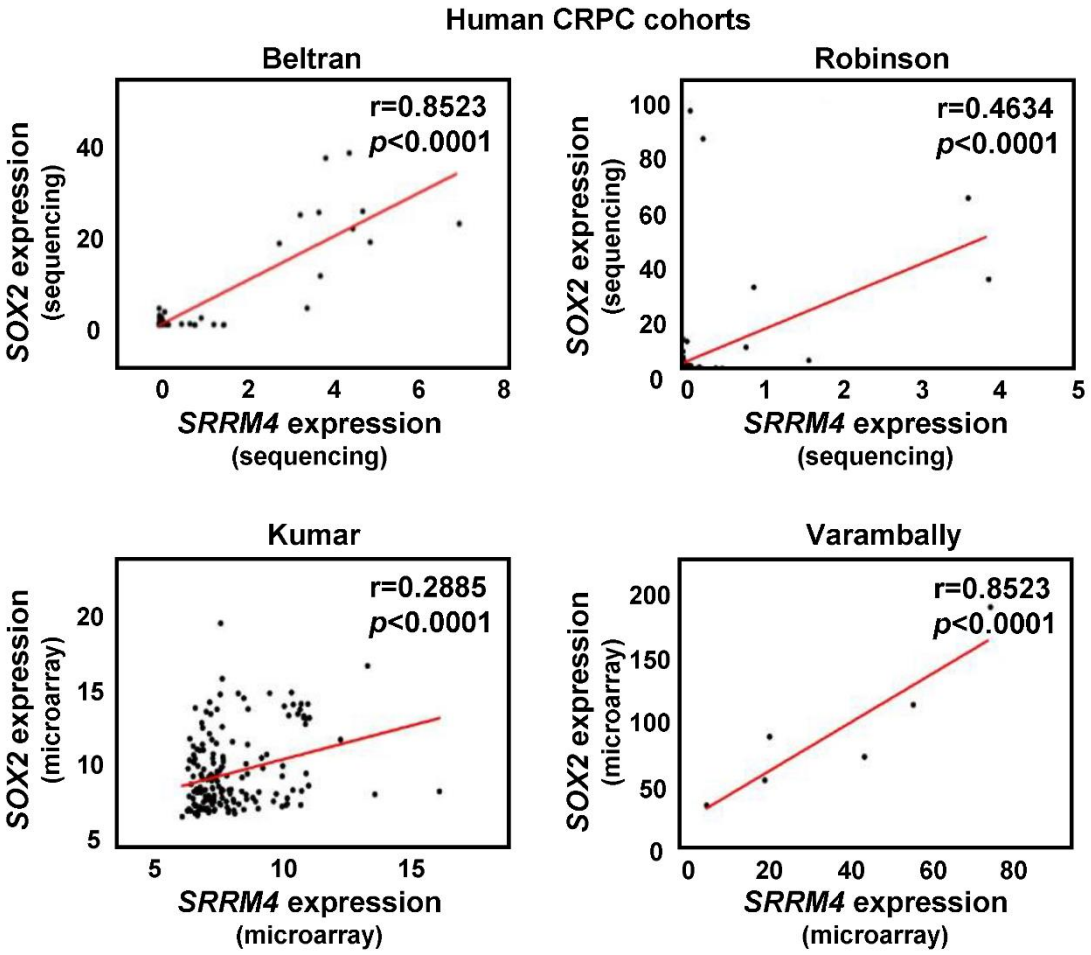

Appendix G *SRRM4* and *SOX2* are positively correlated in CRPC cohorts. Pearson's *r* correlation coefficient between *SRRM4* and *SOX2* expressions obtained from human CRPC cohorts by Beltran *et al.* (2016), Robinson *et al.* (2015), Kumar *et al.* (2016), and Varambally *et al.* (2005) are shown. CRPC, castration resistant prostate cancer.

Appendix H: *MEAF6* RNA splicing is positively correlated with *SRRM4* expression and *REST* RNA splicing

i

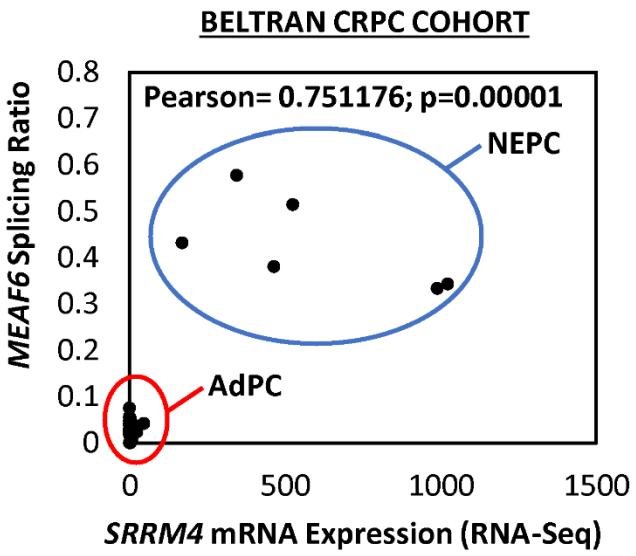

ii

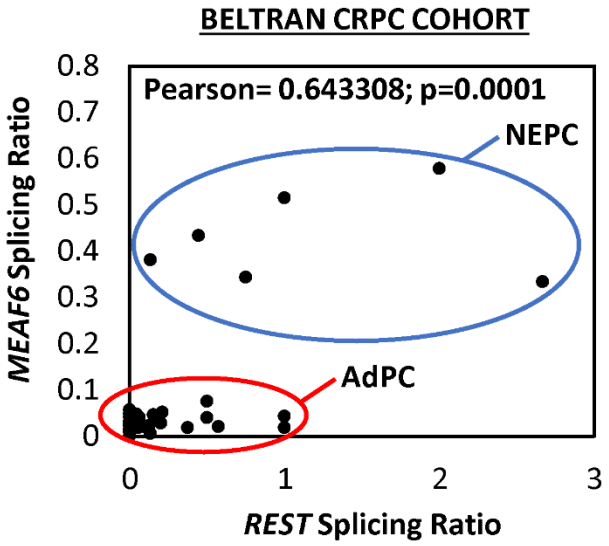

Appendix H *MEAF6* RNA splicing is positively correlated with *SRRM4* expression and *REST* RNA splicing. Pearson's *r* correlation coefficient between *MEAF6* splicing ratio (*MEAF6-1:MEAF6-2* RNA-seq reads per base-pair) and **(i)** *SRRM4* total expression or **(ii)** *REST* splicing ratio (*REST4:REST* RNA-seq reads per base-pair) obtained from the Beltran CRPC patient RNA-seq dataset (NEPC n=6 and AdPC n=32). CRPC, castration-resistant prostate cancer; NEPC, neuroendocrine prostate cancer; AdPC, prostate adenocarcinoma.

Appendix I: SRRM4 regulates RNA splicing of *MEAF6*

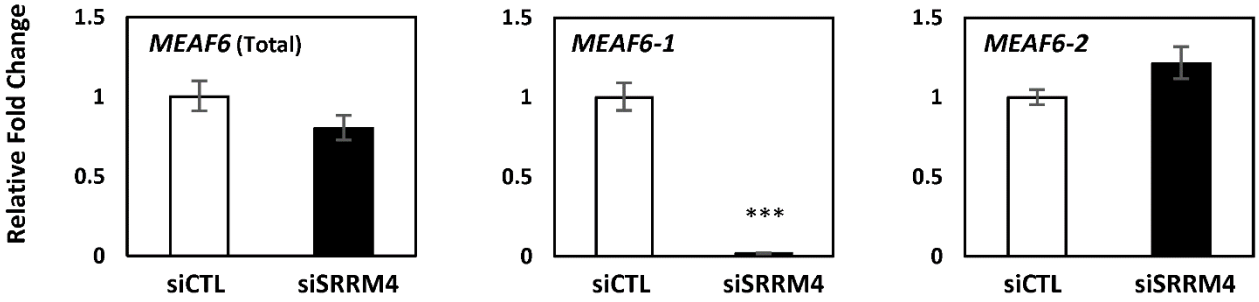

Appendix I SRRM4 regulates RNA splicing of *MEAF6*. LNCaP(SRRM4) stable cells were seeded in 6-well petri dishes in RPMI-1640 medium with 10% FBS and transfected the next day. Cells were transfected with 20 µM of control or *SRRM4*-targeted siRNA for 48 hrs and then collected for RNA extraction for RT-qPCR validation. Relative quantifications of total *MEAF6*, *MEAF6-1*, and *MEAF6-2* were compared to *18S*. FBS, fetal bovine serum; CTL, control.

Appendix J: Androgen receptor signaling does not regulate MEAF6 variant expression

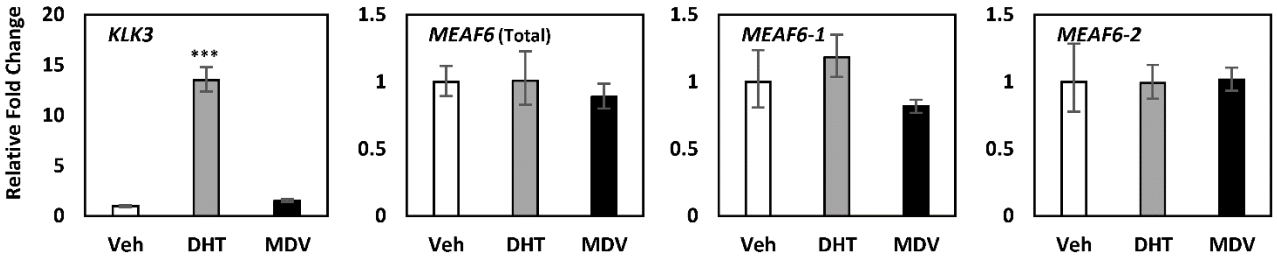

Appendix J Androgen receptor signaling does not regulate *MEAF6* variant expression. LNCaP cells were cultured in phenol red-free RPMI-1640 medium with 5% CSS for 48 hrs. Cells were then treated with DMSO (veh), 10 nM AR-agonist DHT (dihydrotestosterone), or 5 µM AR antagonist MDV3100 (Enzalutamide) for 24-hrs and subsequently collected for RNA extraction for RT-qPCR. Relative quantification of total *MEAF6*, *MEAF6-1*, *MEAF6-2*, and *KLK3* were compared to *18S*. All results are presented as the mean ± SEM (Student's 2-tailed *t*-test; n=3, *** denotes $p<0.001$). AR, androgen receptor. CSS, charcoal-stripped serum; Veh, vehicle.

Appendix K: Validation of MEAF6-1 overexpressing stable lines

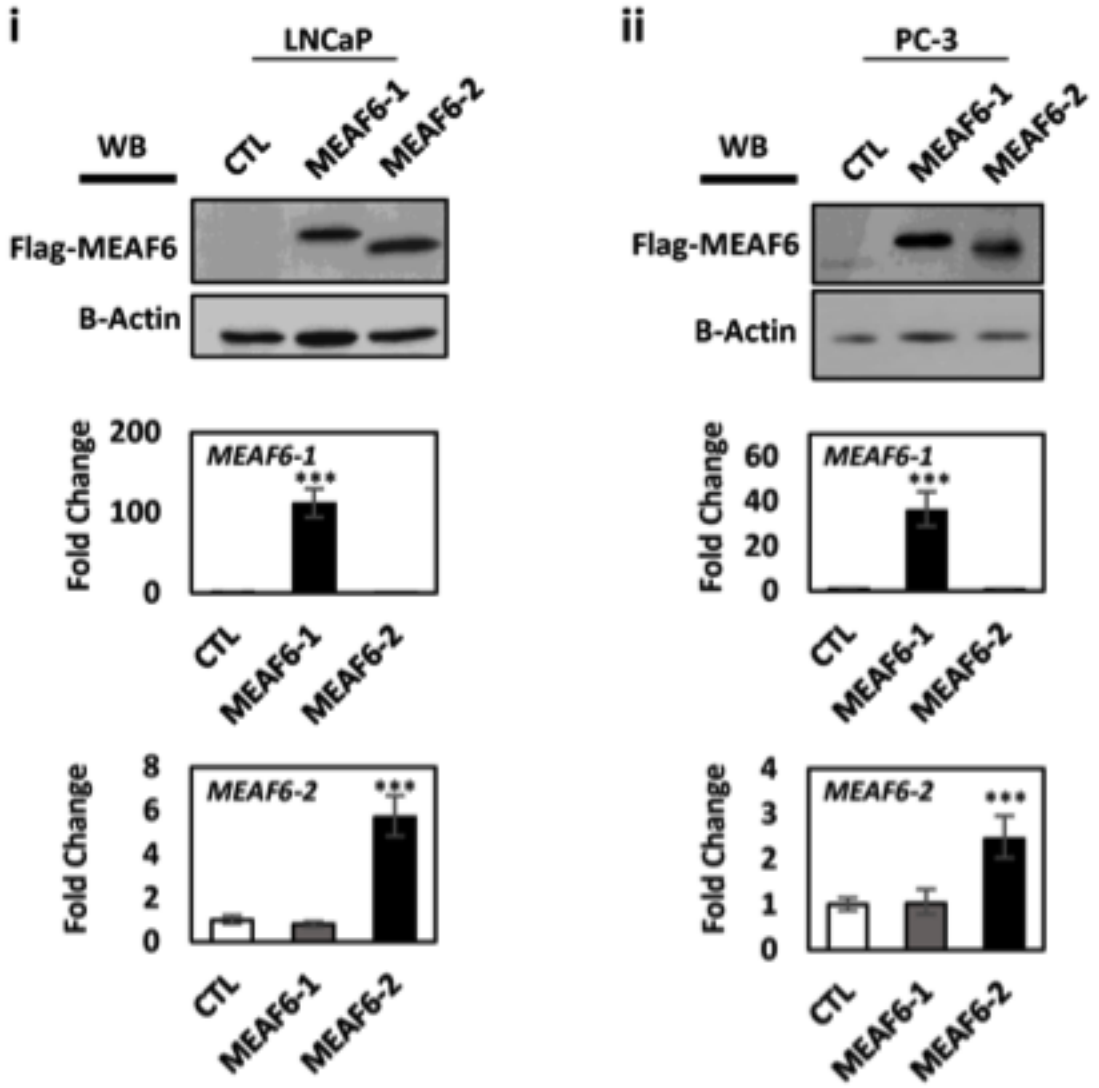

Appendix K Validation of MEAF6-1 overexpressing stable lines. Lentiviral transduction to create MEAF6-1 or MEAF6-2 overexpressing stable lines in **(i)** LNCaP and **(ii)** PC-3 parental cells were validated by Western blotting and RT-qPCR. Anti-flag antibody was used to detect exogenous MEAF6-1 and MEAF6-2 expression. Anti-beta-actin antibody was used as a loading control. CTL, control (empty vector); WB, Western blot.

Appendix L: MEAF6 does not facilitate neuroendocrine trans-differentiation

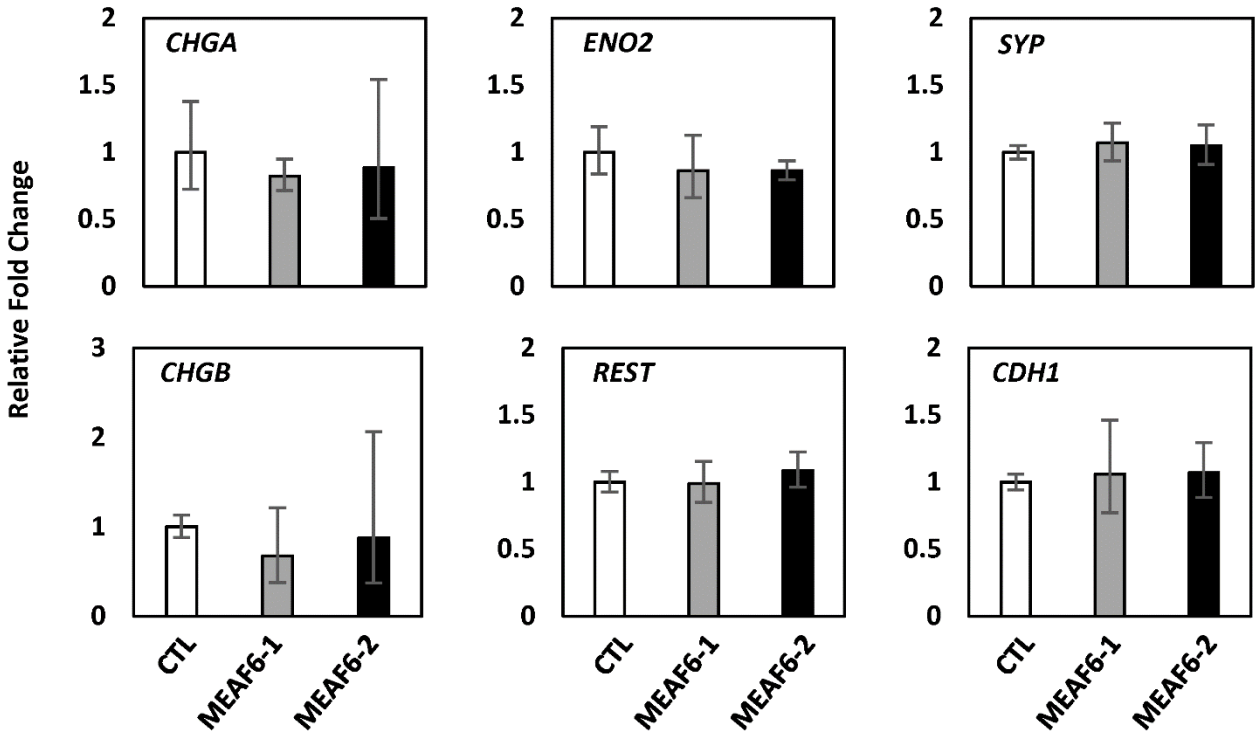

Appendix L MEAF6 does not facilitate neuroendocrine trans-differentiation. LNCaP(CTL), LNCaP(MEAF6-1), and LNCaP(MEAF6-2) cells were collected for total RNA extraction. Expression of neuroendocrine markers (i.e. *CHGA*, *CHGB*, *ENO2*, and *SYP*) and epithelial markers (i.e. *REST* and *CDH1*) were determined by RT-qPCR. Relative quantifications were compared to *18S*. CTL, control (empty vector).

Appendix M: GSEA of the GIT1-C transcriptome

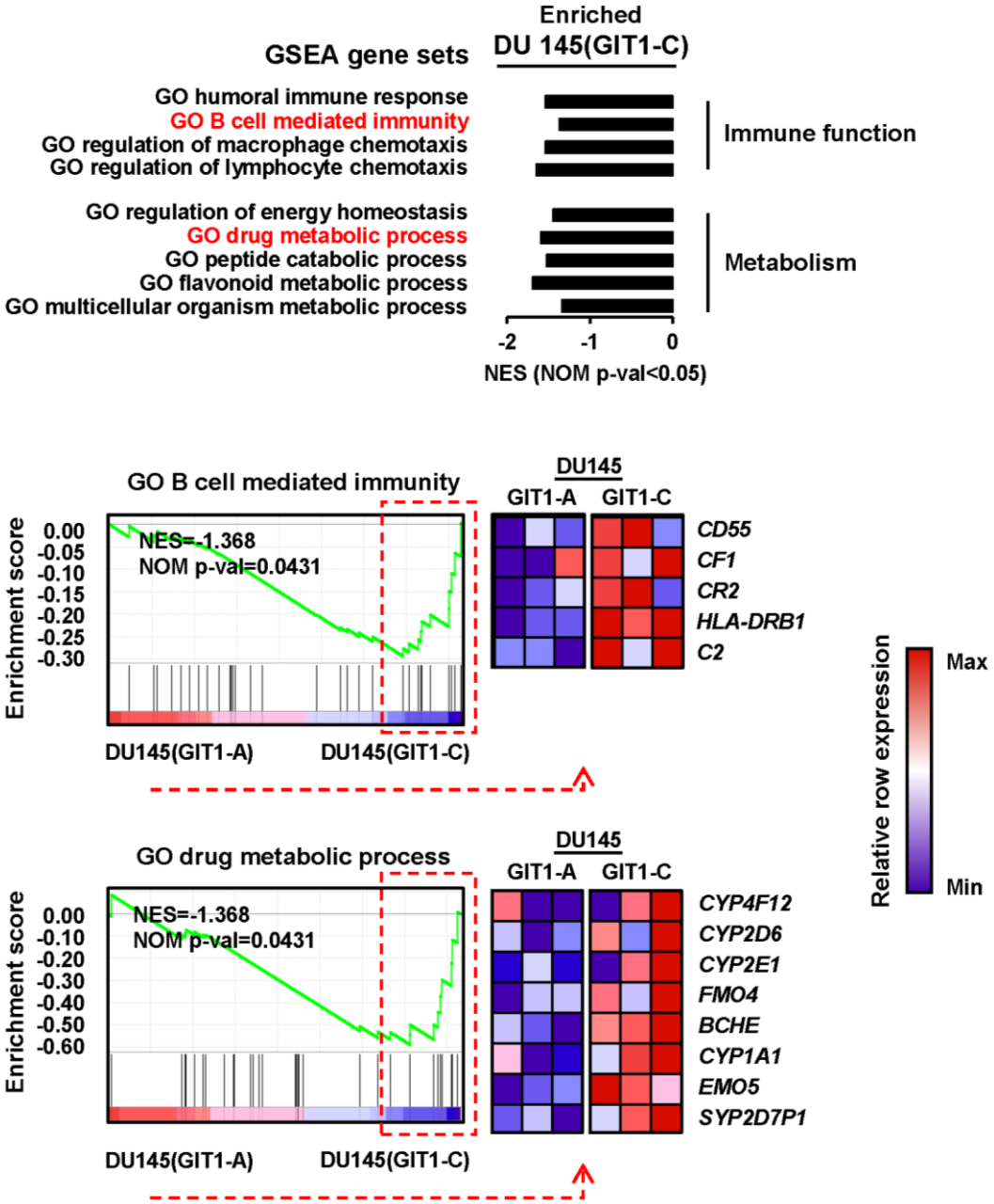

Appendix M GSEA of the GIT1-C transcriptome. The transcriptomes of GIT1-A and GIT1-C were analyzed by GSEA based on the latest MSigDB database for each collection. The GIT1-C transcriptome was enriched with gene sets associated with immune function and metabolism. GSEA enrichment plots from these categories are presented where differential expressions of the leading-edge genes are shown in the heatmaps created by the GSEA software. GSEA, gene set enrichment analysis; GO, gene ontology; NES, normalized enrichment score; NOM p-val, nominal *p*-value.

Appendix N: RB1 knockdown in the SRRM4-transduced PC-3 cell model does not induce a NEPC-specific phenotype

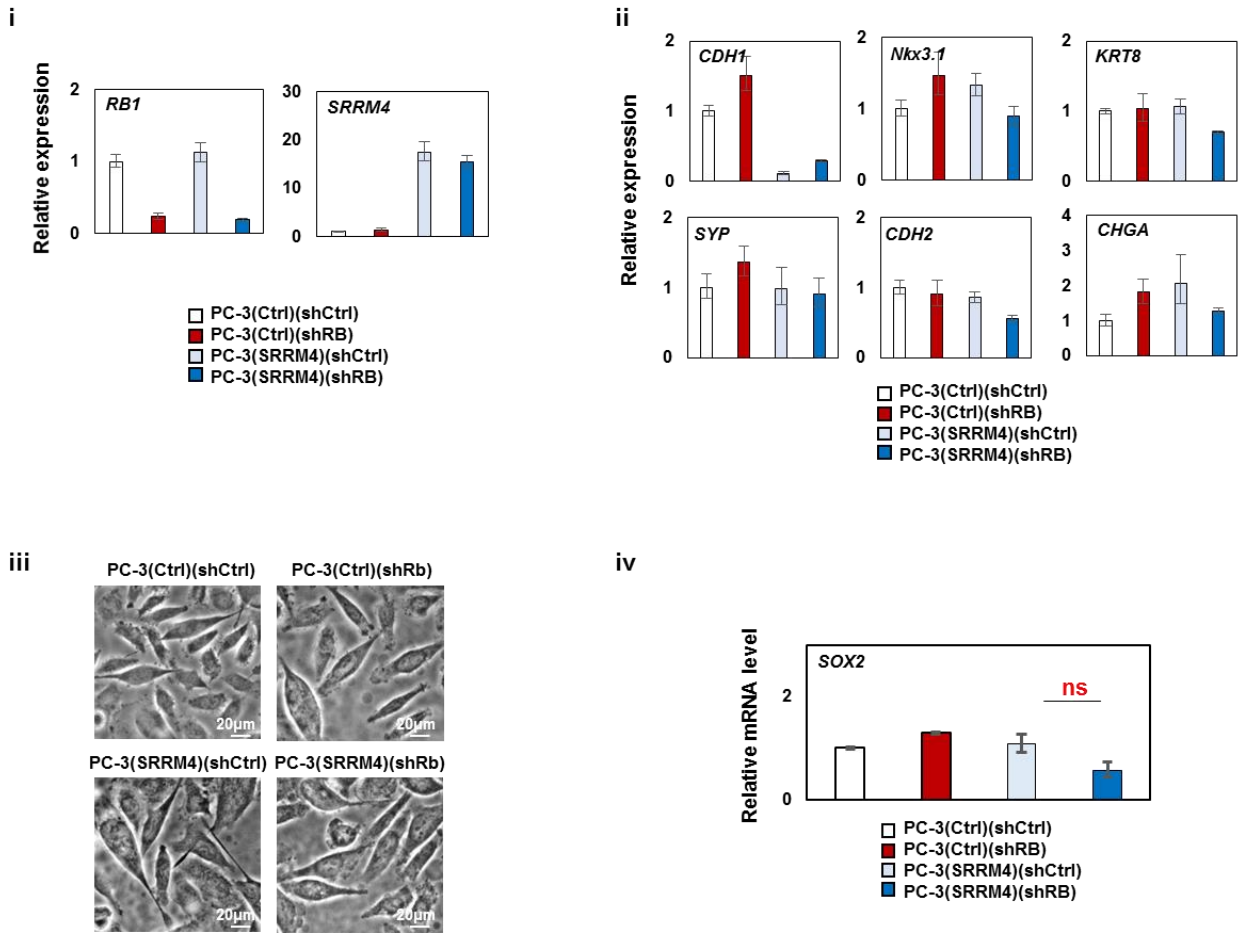

Appendix N RB1 knockdown in the SRRM4-transduced PC-3 cell model does not induce a NEPC-specific phenotype. A second round of lentiviral transduction of shRNA targeting RB1 using the PC-3(Ctrl) and PC-3(SRRM4) cell lines to establish PC-3(Ctrl)(shCtrl), PC-3(Ctrl)(shRB1), PC-3(SRRM4)(shCtrl), and PC-3(SRRM4)(shRB1) stable cell models. These cell lines were validated for *SRRM4* and *RB1* mRNA expression by **(i)** RT-qPCR. **(ii)** RNA was extracted to measure levels of luminal epithelial (i.e. *CDH1*, *Nkx3.1*, and *KRT8*) and neuroendocrine markers (i.e. *SYP*, *CDH2*, and *CHGA*) via RT-qPCR. **(iii)** The morphology of these cells was imaged by Zeiss light microscope, where the scale bars represent 20 μm. **(iv)** RNA was extracted from these cell lines to measure levels of *SOX2* mRNA via RT-qPCR. All experiments were repeated three times, and only one representative repeat is presented. All results are presented as the mean ±SEM. Ns, not significant.

Appendix O: Differential functions of GIT1 splice variants in FA stability under endogenous GIT1 depletion

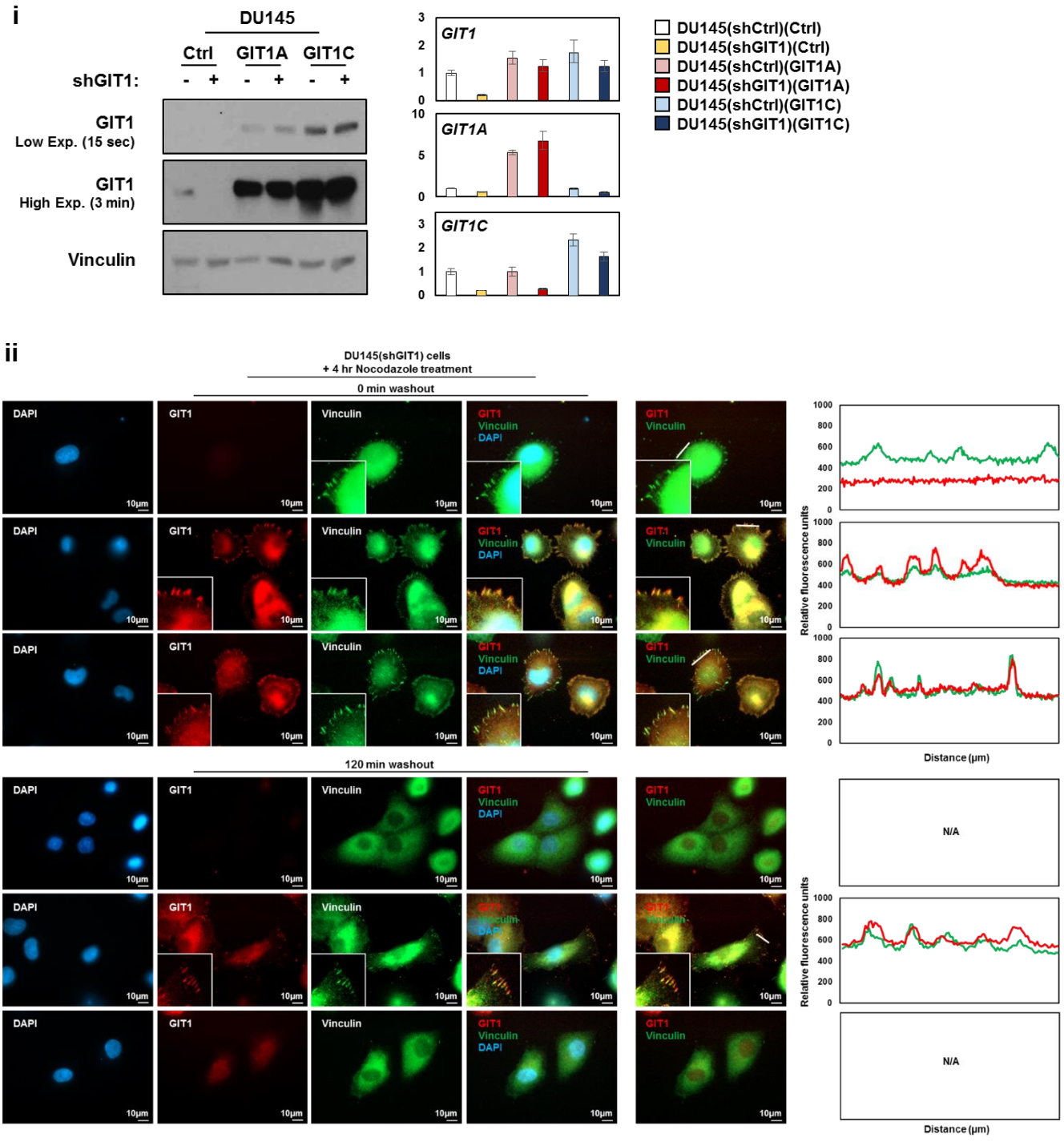

Appendix O Differential functions of GIT1 splice variants in FA stability under endogenous GIT1 depletion. (i) Lentiviral approaches were performed to create DU145 stable cell lines overexpressing GIT1-A, GIT1-C, or empty vector under GIT1 depletion via shRNA targeting the 3' UTR of the GIT1 transcript. Stable cell lines were validated by Western blot and RT-qPCR. **(ii)** These cells were seeded on coverslips and serum-starved the next day. They were treated with 10 μM Nocodazole for 4-hrs, subsequently washed away, and replaced with serum-containing medium. Cells were fixed at 0- or 120-min after the washout, co-stained against GIT1 and vinculin, and then mounted with DAPI staining mount. Cells were imaged using the ZEISS AxioObserver Z1 microscope, where the scale bar represents 10 μm. Overlapping signals between GIT1 and vinculin appear yellow. The overlapping of the two signals in a cross section (indicated by the white line) of FA complexes were profiled by the ZEN program. All experiments were repeated three times. Exp, exposure; IF, immunofluorescence; FA, focal adhesion; ZEN, ZEISS efficient navigation.

Appendix P: Differential localization of the MEAF6 splice variants

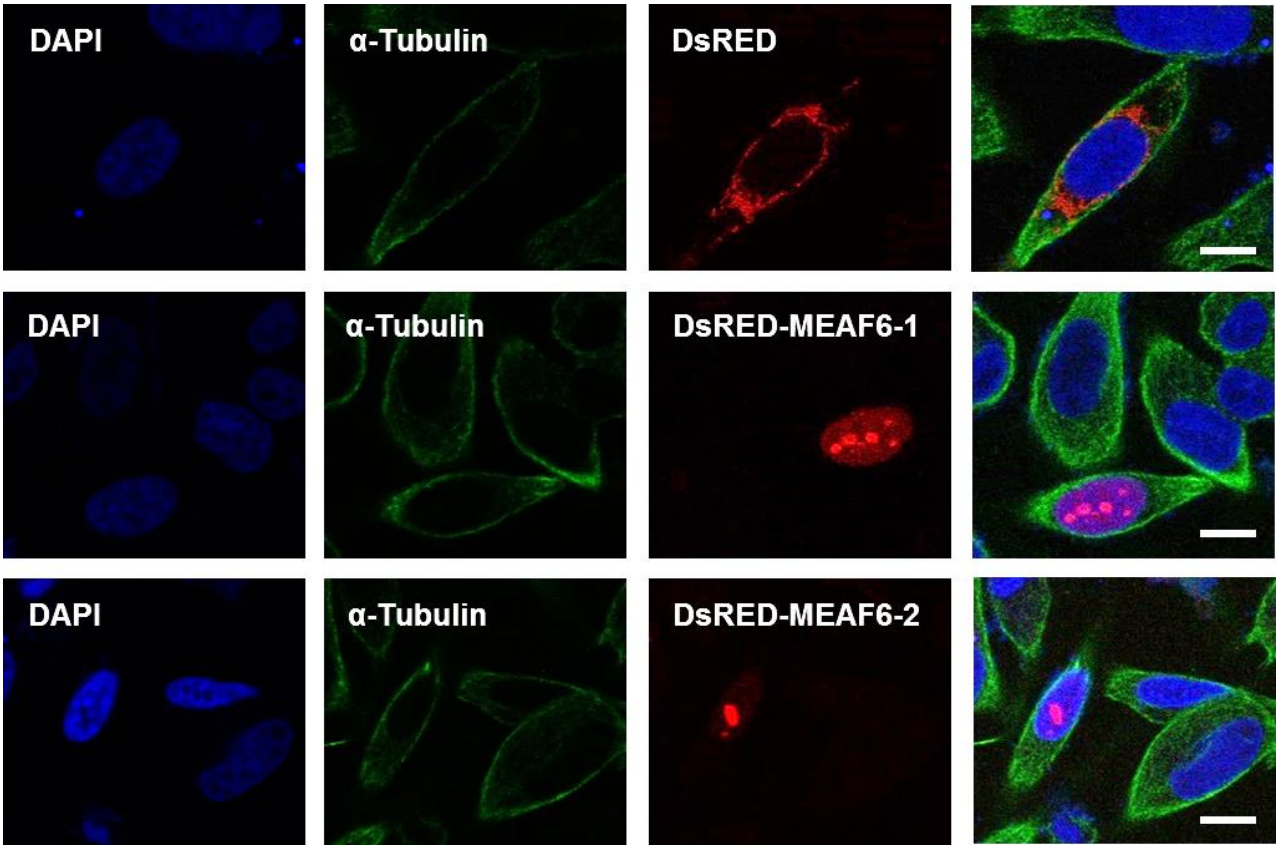

Appendix P Differential localization of the MEAF6 splice variants. PC-3 cells were transfected with 4 µg of plasmid encoding DsRED-tagged empty vector, MEAF6-1, or MEAF6-2. Cells were fixed for IF, and stained for α-tubulin, and then mounted with DAPI staining mount. Cells were imaged using the ZEISS AxioObserver Z1 microscope, where the scale bar represents 10 µm. All experiments were repeated three times. IF, immunofluorescence; ZEN, ZEISS efficient navigation.